AD-A083 332 SRI INTERNATIONAL MENLO PARK CA F/G 18/3
LABORATORY STUDIES OF CONTAINMENT IN UNDERGROUND NUCLEAR TESTS.(U)
JAN 79 J C CIZEK, A L FLORENCE DNA001-77-C-0025
UNCLASSIFIED DNA-4847F NL

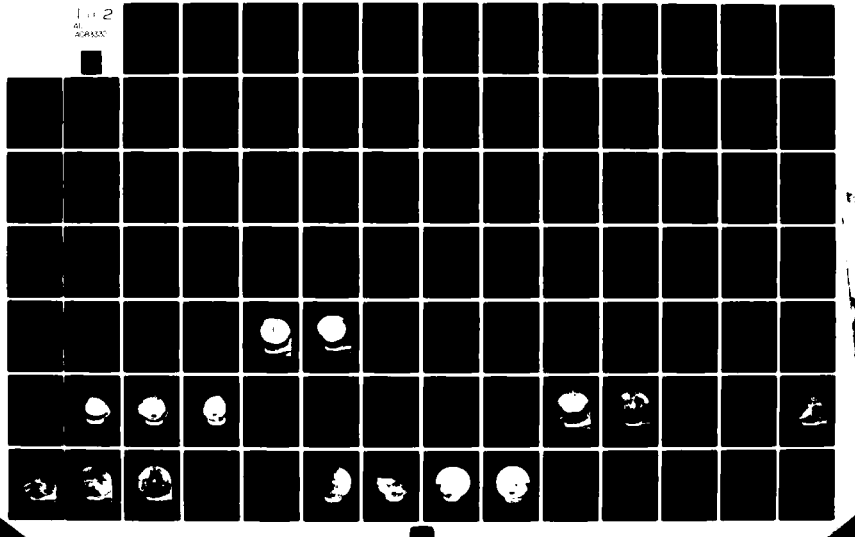

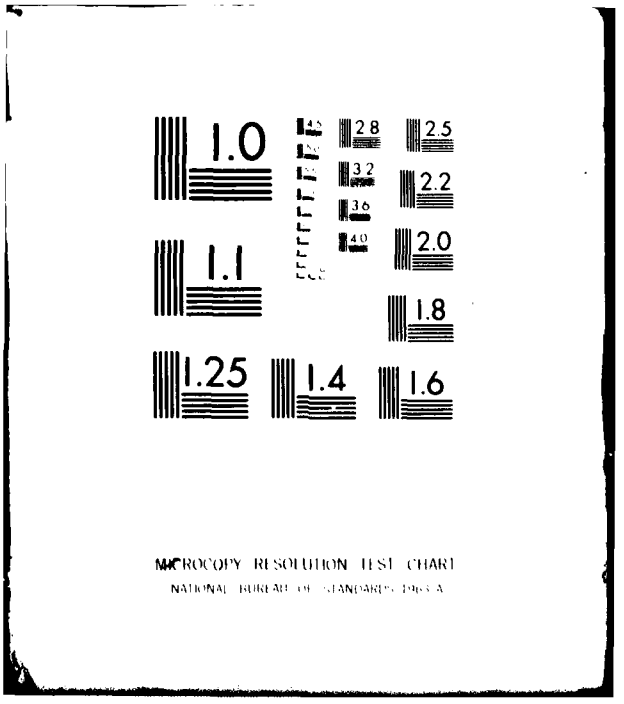
1.0
1.1
1.25
1.4
1.6
1.8
2.0
2.2
2.5
2.8
3.2
3.6
4.0
MICROCOPY RESOLUTION TEST CHART
NATIONAL BUREAU OF STANDARDS 1963-A

DNA 4847F

LABORATORY STUDIES OF CONTAINMENT IN UNDERGROUND NUCLEAR TESTS

J. C. Cizek

A. L. Florence

SRI International
333 Ravenswood Avenue
Menlo Park, California 94025

31 January 1979

Final Report for Period 16 November 1977—31 January 1979

CONTRACT No. DNA 001-77-C-0025

APPROVED FOR PUBLIC RELEASE;
DISTRIBUTION UNLIMITED.

THIS WORK SPONSORED BY THE DEFENSE NUCLEAR AGENCY
UNDER RDT&E RMSS CODE B345077462 J24AAXYX98341 H2590D.

Prepared for
Director
DEFENSE NUCLEAR AGENCY
Washington, D. C. 20305

Destroy this report when it is no longer needed. Do not return to sender.

PLEASE NOTIFY THE DEFENSE NUCLEAR AGENCY, ATTN: STTI, WASHINGTON, D.C. 20305, IF YOUR ADDRESS IS INCORRECT, IF YOU WISH TO BE DELETED FROM THE DISTRIBUTION LIST, OR IF THE ADDRESSEE IS NO LONGER EMPLOYED BY YOUR ORGANIZATION.

UNCLASSIFIED

SECURITY CLASSIFICATION OF THIS PAGE *(When Data Entered)*

REPORT DOCUMENTATION PAGE		READ INSTRUCTIONS BEFORE COMPLETING FORM
1. REPORT NUMBER DNA 4847F	2. GOVT ACCESSION NO. AD-A083332	3. RECIPIENT'S CATALOG NUMBER
4. TITLE *(and Subtitle)* LABORATORY STUDIES OF CONTAINMENT IN UNDERGROUND NUCLEAR TESTS		5. TYPE OF REPORT & PERIOD COVERED Final Report for Period 16 Nov 77—31 Jan 79
		6. PERFORMING ORG. REPORT NUMBER SRI PYU-5958
7. AUTHOR(s) J. C. Cizek A. L. Florence		8. CONTRACT OR GRANT NUMBER(s) DNA 001-77-C-0025 new
9. PERFORMING ORGANIZATION NAME AND ADDRESS SRI International 333 Ravenswood Avenue Menlo Park, California 94025		10. PROGRAM ELEMENT, PROJECT, TASK AREA & WORK UNIT NUMBERS Subtask J24AAXYX983-41
11. CONTROLLING OFFICE NAME AND ADDRESS Director Defense Nuclear Agency Washington, D.C. 20305		12. REPORT DATE 31 January 1979
		13. NUMBER OF PAGES 142
14. MONITORING AGENCY NAME & ADDRESS*(if different from Controlling Office)*		15. SECURITY CLASS *(of this report)* UNCLASSIFIED
		15a. DECLASSIFICATION DOWNGRADING SCHEDULE

16. DISTRIBUTION STATEMENT *(of this Report)*

Approved for public release; distribution unlimited.

17. DISTRIBUTION STATEMENT *(of the abstract entered in Block 20, if different from Report)*

18. SUPPLEMENTARY NOTES

This work sponsored by the Defense Nuclear Agency under RDT&E RMSS Code B345077462 J24AAXYX98341 H2590D.

19. KEY WORDS *(Continue on reverse side if necessary and identify by block number)*

Nuclear	Hydrofracture
Underground	Fracture Initiation
Explosion	Surface Fracture
Containment	Overburden
Cavity	

20. ABSTRACT *(Continue on reverse side if necessary and identify by block number)*

As part of the DNA stemming and containment program for underground nuclear testing, laboratory studies were performed to further develop and apply experimental techniques for assessing the effects on containment of the residual stress field surrounding an exploded cavity. A comparison of hydrofracture pressures for exploded and unexploded cavities revealed the existence of this stress field. Experimental parameter studies were conducted to provide an understanding of the mechanisms controlling containment. Sensors were developed

DD FORM 1 JAN 73 1473 EDITION OF 1 NOV 65 IS OBSOLETE

UNCLASSIFIED

SECURITY CLASSIFICATION OF THIS PAGE *(When Data Entered)*

20. ABSTRACT (Continued)

to generate quantitative estimates of crack growth, fluid motion, and the states of stress and strain in the region surrounding a cavity during hydrofracture. The data generated provide results suitable for development of new containment theories as well as for correlation with predictions of existing computer codes. Hydrofracture pressure records were simulated by applying classical fracture mechanics theory.

SUMMARY

The primary objective of this project is to develop and perform laboratory containment experiments in support of the DNA stemming and containment program for underground nuclear tests. Over the years, the DNA stemming and containment program has consisted of five main parts:

(1) Code development and application for ground motion, tunnel closure, and grout flow calculations.

(2) Material properties determination.

(3) Laboratory investigations.

(4) Scaled high explosive tests.

(5) Field diagnostics.

SRI has been conducting the laboratory investigations.

During this phase of the laboratory program, a previously developed experimental technique was used for further study of the residual stress surrounding an exploded cavity in a rheological material. The data generated are suitable as a basis for development of containment theories as well as for correlation with predictions of codes employed by the calculators of the DNA containment community. Classical fracture mechanics analysis was applied to interpret experimental results and to guide future tests.

In the basic containment experiment, a small spherical charge is cast in a sphere of rock-matching grout (RMG) with properties similar to those of Nevada Test Site tuff. The RMG sphere is hydraulically pressurized to represent overburden. The explosive is detonated and the residual gases are released by drilling into the cavity. (A recent development makes gas release optional.) Dyed fluid is pumped into the cavity at a constant flow rate to initiate and propagate a crack. Pumping continues until the fracture plane reaches the surface and a steady-state

flow of fluid is established. The internal pressure is removed, and then the external pressure is removed. The cracked sphere is drained and tapped into two parts by use of a chisel, and the exposed fracture plane is photographed. The effect of the explosively generated residual stress field is assessed by conducting a separate hydrofracture test on a sphere with an unexploded cavity equal in size to the exploded cavity.

Hydrofracture tests were performed with 12-inch-diameter RMG spheres to establish reproducibility of the basic experimental technique. Overburden, flow rate, and fluid viscosity were fixed. Because of the potential perturbing effects of embedded sensors, only surface gages were used to monitor fracture and fluid arrival. In the unexploded cavity tests, a smooth and unlined cavity of 3/4-inch (1.90-cm) diameter was used. In the exploded cavity tests, a 3/8-gram charge was used and the residual gases were released. Results of the reproducibility tests provide comparison data for investigating the effects on containment of the following features:

- Overburden. Hydrofracture tests were performed on unexploded cavities subjected to three different external pressures.
- Cavity size. Hydrofracture tests were performed on unexploded cavities of three different sizes.
- Cavity lining. Hydrofracture tests were performed on unexploded cavities that were lined with an impermeable membrane.
- Unvented cavity. Gas pressure was measured and hydrofracture performed without venting an exploded cavity.
- Creep. Three distinct periods of residual stress relaxation were permitted prior to hydrofracture.

Additional investigations include the following:

- Reproducibility of the explosive source was assessed.
- Techniques were developed and applied to monitor crack growth and fluid arrival during hydrofracture.

- Changes in stress and strain due to overburden, charge detonation, hydrofracture, and creep were measured.

- Fracture mechanics analysis was applied to unexploded and exploded cavity hydrofracture tests.

The principal findings of the above studies are:

- Reproducibility of the unexploded cavity tests is very good.

- Reproducibility of the explosive source is good.

- Reproducibility of vented exploded cavity tests, measured in terms of fracture initiation and final steady-state pressures is good. However, a range of maximum cavity pressures is generated that may be influenced by a random development of multiple fracture planes and the pressure gradient in the crushed region surrounding an exploded cavity. Fracture initiation pressures in vented cavity tests are slightly lower than in corresponding unexploded cavity tests.

- Increased overburden results in higher fracture initiation pressures for unexploded cavities.

- Hydrofracture records for unexploded cavities are unaffected by small changes in cavity size.

- Lining an unexploded cavity results in higher fracture initiation and final steady-state pressures.

- Unvented exploded cavities result in higher fracture initiation pressures than the corresponding unexploded cavities.

- Creep appears to cause a relaxation of the residual stress field surrounding an exploded cavity resulting in pressures at the low end of the spectrum of hydrofracture records.

- Crack growth in exploded cavity tests appears to be initially stable, but subsequent growth is unstable. Crack growth in unexploded cavity tests is unstable.

- Reproducibility tests indicate that a greater volume of hydrofracture fluid is required to initiate surface fracture in exploded cavity tests. Relaxation of the residual stress field and use of embedded gages tend to reduce this volume in exploded cavity tests.

- The embedded fracture gages used were too strong and caused an increase in final steady-state pressures.

- Near the surface of a sphere, fluid follows the crack tip more closely in unexploded than in exploded cavity tests.

- Hydrofracture pressures produce strain gage outputs that are larger than elasticity theory predictions.

- Qualitative features of the pressure records can be explained in terms of classical fracture mechanics theory.

By comparing hydrofracture pressures that are generated in tests on unexploded and exploded cavities before surface cracking of the sphere is detected, it appears that the residual stress field is beneficial to containment after fracture initiation. Hydrofracture from unexploded cavities generates the maximum pressure at fracture initiation (Figure 3.1) whereas hydrofracture from exploded cavities generates higher pressures after fracture initiation (Figures 3.14 and 3.17) and reaches values higher than the fracture initiation pressures of unexploded cavities.

Conversion factors for U.S. customary to metric (SI) units of measurement

To Convert From	To	Multiply By
angstrom	meters (m)	1.000 000 X E -10
atmosphere (normal)	kilo pascal (kPa)	1.013 25 X E +2
bar	kilo pascal (kPa)	1.000 000 X E +2
barn	meter^2 (m^2)	1.000 000 X E -28
British thermal unit (thermochemical)	joule (J)	1.054 350 X E +3
calorie (thermochemical)	joule (J)	4.184 000
cal (thermochemical)/cm^2	mega joule/m^2 (MJ/m^2)	4.184 000 X E -2
curie	*giga becquerel (GBq)	3.700 000 X E +1
degree (angle)	radian (rad)	1.745 329 X E -2
degree Fahrenheit	degree kelvin (K)	$t_K = (t°f + 459.67)/1.8$
electron volt	joule (J)	1.602 19 X E -19
erg	joule (J)	1.000 000 X E -7
erg/second	watt (W)	1 000 000 X E -7
foot	meter (m)	3.048 000 X E -1
foot-pound-force	joule (J)	1.355 818
gallon (U.S. liquid)	meter^3 (m^3)	3.785 412 X E -3
inch	meter (m)	2.540 000 X E -2
jerk	joule (J)	1.000 000 X E +9
joule/kilogram (J/kg) (radiation dose absorbed)	Gray (Gy)	1.000 000
kilotons	terajoules	4.183
kip (1000 lbf)	newton (N)	4.448 222 X E +3
kip/inch^2 (ksi)	kilo pascal (kPa)	6.894 757 X E +3
ktap	newton-second/m^2 ($N-s/m^2$)	1.000 000 X E +2
micron	meter (m)	1 000 000 X E -6
mil	meter (m)	2.540 000 X E -5
mile (international)	meter (m)	1.609 344 X E +3
ounce	kilogram (kg)	2.834 952 X E -2
pound-force (lbs avoirdupois)	newton (N)	4.448 222
pound-force inch	newton-meter (N·m)	1.129 848 X E -1
pound-force/inch	newton/meter (N/m)	1.751 268 X E +2
pound-force/foot^2	kilo pascal (kPa)	4.788 026 X E -2
pound-force/inch^2 (psi)	kilo pascal (kPa)	6.894 757
pound-mass (lbm avoirdupois)	kilogram (kg)	4.535 924 X E -1
pound-mass-foot^2 (moment of inertia)	kilogram-meter^2 ($kg·m^2$)	4.214 011 X E -2
pound-mass/foot^3	kilogram/meter^3 (kg/m^3)	1.601 846 X E +1
rad (radiation dose absorbed)	**Gray (Gy)	1.000 000 X E -2
roentgen	coulomb/kilogram (C/kg)	2.579 760 X E -4
shake	second (s)	1.000 000 X E -8
slug	kilogram (kg)	1.459 390 X E +1
torr (mm Hg, 0° C)	kilo pascal (kPa)	1.333 22 X E -1

*The becquerel (Bq) is the SI unit of radioactivity; 1 Bq = 1 event/s.
**The Gray (Gy) is the SI unit of absorbed radiation.

PREFACE

This research was conducted under Contract DNA001-77-C-0025 in support of the DNA stemming and containment program for underground nuclear tests.

The authors are indebted to the technical monitor, Mr. Carl Keller (FCDNA), for insights, suggestions, and continued overall guidance. In addition, the insights provided by the theoretical work of Pacifica Technology and Systems, Science and Software are appreciated.

The authors are also indebted to G. R. Greenfield for the design and fabrication of instrumentation, to J. K. Gran and T. C. Goodale for generating computer code results, to L. J. Dary for performing the experiments and suggesting improvements, and to G. R. Abrahamson for overall supervision.

CONTENTS

ILLUSTRATIONS

TABLES

SECTION 1

INTRODUCTION

A requirement of underground nuclear testing is that radioactive gases be prevented from entering the atmosphere. In general, this requirement will be met if experimental tunnels leading from the nuclear device cavity are stemmed successfully and if the cavity gases are contained by the adjacent surrounding medium. The residual stress field generated in this surrounding medium by the explosion probably aids containment. Although containment has been achieved for many years and stemming has generally been successful in recent nuclear tests, reliability is uncertain and planned tests still require extensive containment evaluation.

Over the years, the DNA stemming and containment (SAC) program has consisted of five main parts: code development for ground motion, tunnel closure, and grout flow calculations; material properties determination; laboratory investigations; scaled high explosive tests; and field diagnostics. Over the past several years SRI has been conducting the laboratory investigations.[1-5]

Laboratory investigations during the last year have focused mainly on containment. One purpose of the experimental program has been to compare the containment capability of cavities generated under a variety of conditions. Another purpose is to validate calculations[6,7] of the residual stress field as a major containment feature of underground nuclear tests. The data generated in the laboratory are suitable for correlation with the predictions of existing codes. The experimental technique has also been used to determine the influence of major geological and test site features. Although our basic containment experiment may not be regarded as a small-scale version of an explosively

simulated underground nuclear test, simulation is close enough to provide the correct important mechanisms required in a study of containment.

In our basic containment experiment, a small spherical charge is cast in a sphere of rock-matching grout (RMG) with properties similar to those of Nevada Test Site tuff. The RMG sphere is hydraulically pressurized to represent overburden. The explosive is detonated and the residual gases are released by drilling into the cavity. (In an alternative version of the test, the gases are not released.) Dyed fluid is pumped into the cavity at a constant flow rate until fracture occurs and a steady radial pressure gradient is established. The internal pressure is removed, and then the external pressure is removed. The cracked sphere is drained and tapped into two parts by use of a chisel, and the exposed fracture plane is photographed. The effect of the explosively generated residual stress field on containment is assessed by conducting a separate hydrofracture test on a sphere with an unexploded cavity equal in size to the exploded cavity.

Hydrofracture tests were performed on RMG spheres of 12-inch (10.48-cm) diameter to establish reproducibility of the basic experimental technique. The fixed parameters were overburden pressure, rate of fluid flow into the cavity, and viscosity of the hydrofracture fluid. Surface gages monitored fracture and fluid arrival. Embedded gages were not used in the reproducibility tests because of their potential perturbing effects on fracture initiation and growth. In unexploded cavity tests, a smooth and unlined cavity of 3/4-inch (1.90-cm) diameter was chosen. In exploded cavity tests, a 3/8-gram charge of PETN* was chosen and the cavity was vented. Results of the reproducibility tests provide comparison data for assessing the effects on containment of the following features:

- Overburden. External pressures of 0, 1000, and 2000 psi (0, 6.9, and 13.8 MPa) were applied to unexploded cavity spheres.

*Pentaerythritol tetranitrate ($C_5H_8O_{12}N_4$).

- Cavity size. Unexploded cavities with 11/16, 3/4, and 1-inch (1.75, 1.90, and 2.54-cm) diameters were hydrofractured.

- Cavity lining. Unexploded cavities were lined with an impermeable membrane before hydrofracture.

- Unvented cavity. Gas pressure in an exploded cavity was measured and hydrofracture performed without venting the detonation products.

- Creep. Stress relaxation periods of 3, 4, and 17 hours were permitted in vented exploded cavity tests before hydrofracture.

In addition, reproducibility of the 3/8-gram explosive source was assessed through a series of charge calibration tests. Embedded and surface gages monitored the crack growth and fluid motion produced by hydrofracture. A transparent model permitted direct observation of crack growth and fluid motion. Changes in stress and strain associated with overburden, charge detonation, hydrofracture, and creep were measured. Finally, a fracture mechanics analysis was applied to unexploded and exploded cavity tests.

The principal findings of the investigations form the latter part of the Summary.

The next phase of the experimental program will include application of the techniques for monitoring crack arrival, fluid arrival, stress, and strain with the objective of determining the extent to which a residual field around an exploded cavity is beneficial to containment. Such an investigation will include

- Hydrofracture of unvented exploded cavities immediately after charge detonation to prevent excessive unloading and to minimize the creep duration prior to hydrofracture.

- Hydrofracture of lined cavities to obtain pressures without allowing fluid into the cracks.

- Use of a residual stress caused by plastic deformation instead of body forces in the plastic analysis

- Application of the technique to examine the effects of geological and man-made features on containment.

An organized list of tests performed during the current phase of this program is given in Section 3.1 (Table 3.1). The extensive variety of tests limited the maximum number in most categories to three. Section 2 describes the experimental techniques, Section 3 presents and discusses the results, and Section 4 outlines the fracture mechanics theory. The appendix collects the grout material properties.

SECTION 2

EXPERIMENTAL DEVELOPMENT

2.1 CONCEPT

The experiment shown schematically in Figure 2.1 was devised[4] to simulate in the laboratory the conditions in an underground nuclear test. A small spherical explosive charge representing the device is sealed in a thin Lucite container and cast in a much larger sphere of rock-matching grout (RMG) with properties similar to those of Nevada Test Site tuff [Figure 2.1(a)]. The grout surface is sealed and hydraulically pressurized to represent overburden [Figure 2.1(b)]. The explosive is detonated and the residual gases are released [Figure 2.1(c)]. An alternative version of this experiment was developed to allow hydrofracture without venting. Fluid is pumped into the cavity at a constant flow rate until fracture occurs and a steady flow develops along the fracture surface [Figure 2.1(d)].

The final stages of gas release and cavity pressurization are included to determine the effect of the residual stress field by comparing the cavity pressures required to crack the RMG sphere with and without residual stresses. In the experiments without a residual stress field, spherical cavities are cast in the grout sphere; these unexploded cavities are the same size as the exploded cavities.

2.2 EXPERIMENTAL APPARATUS

Figure 2.2 shows the experimental apparatus. A 12-inch-diameter RMG sphere is shown inside a steel vessel containing water that can be pressurized to the desired overburden. The sphere is suspended from the lid by a steel tube cast in the grout. In a vented exploded cavity test, this tube provides a means for positioning the charge, potting in the detonator cables, and drilling into the cavity after detonation. The water in the vessel is maintained at a constant pressure throughout

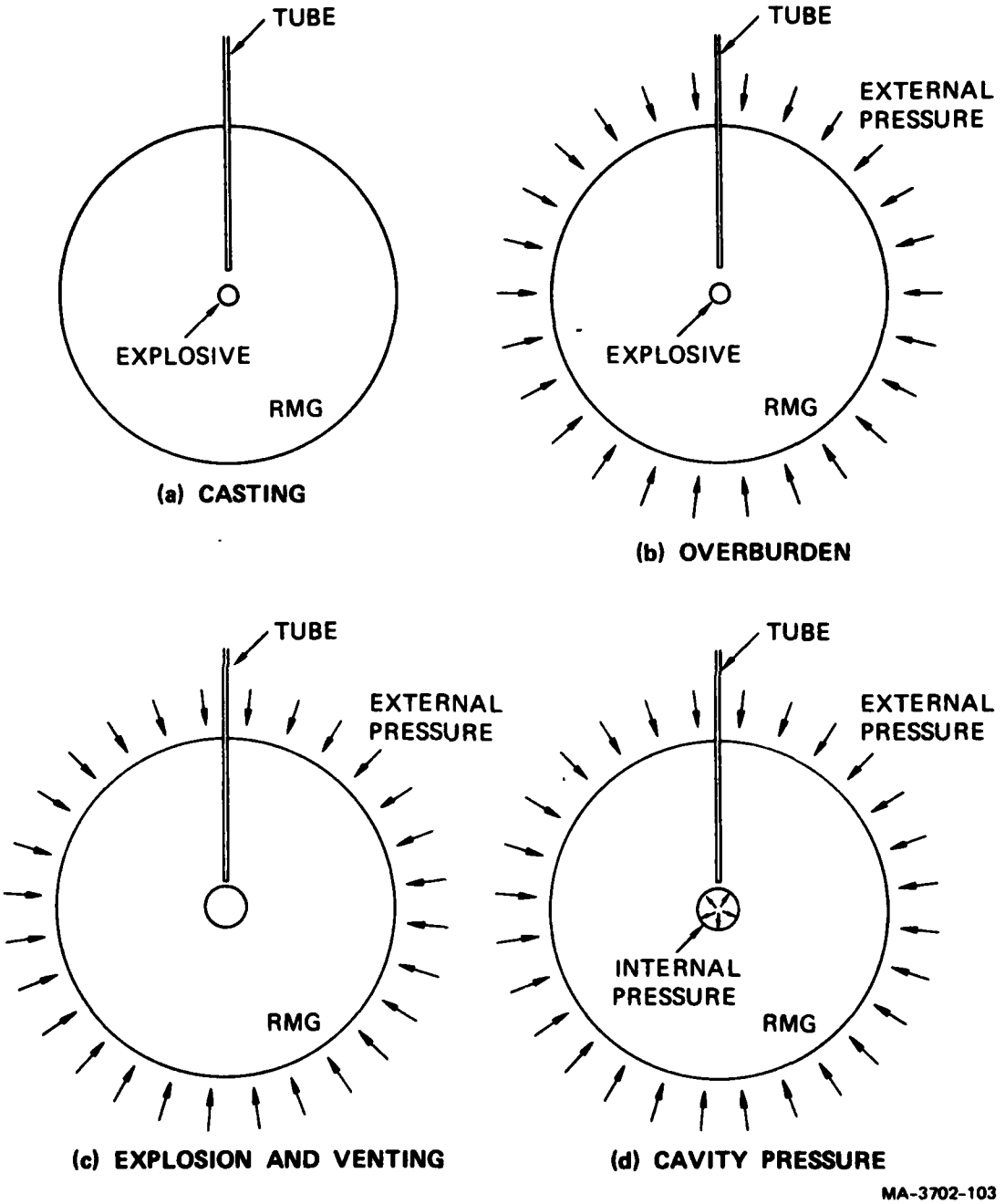

FIGURE 2.1 SEQUENCE OF OPERATIONS IN CONTAINMENT EXPERIMENTS
(Vented Exploded Cavity)

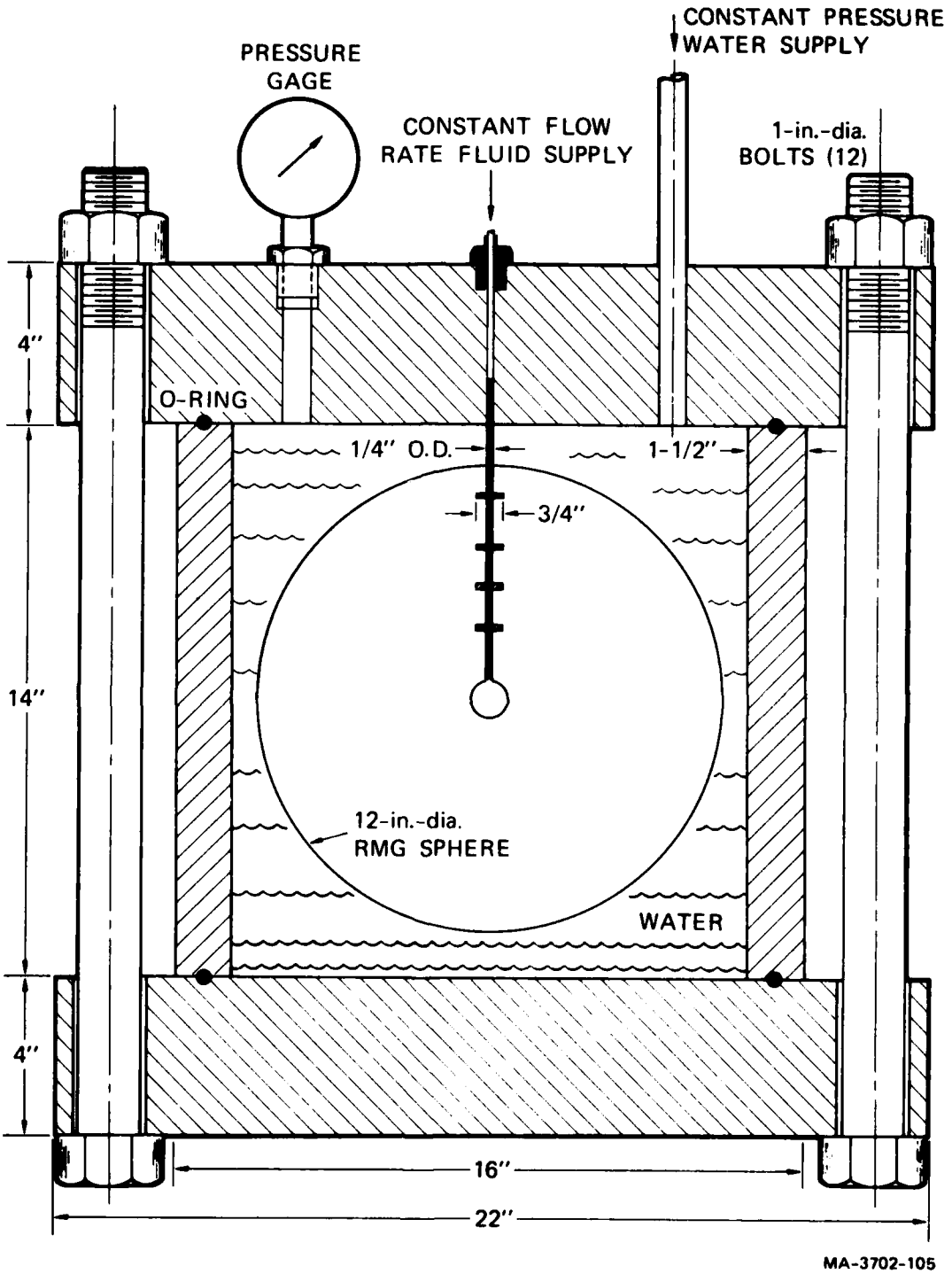

FIGURE 2.2 CONTAINMENT EXPERIMENT APPARATUS

the test by incorporating a high-pressure gas reservoir and valve in the water supply line.

The constant flow rate system shown schematically in Figure 2.3 conforms with standard hydrofracture practice. The specifications of this system are as follows:

Motor:	Dayton Gear motor Model 5K933, 1/4 hp, 6 rpm, 600 in-lb torque
Pump:	High Pressure Equipment Co. Model 87-6-5 60-cm^3 capacity, 5000-psi maximum pressure 4.26-cm^3/min flow rate (0.71-cm^3/revolution)
System:	Fluid: dyed glycerin Volume (excluding pump): 31.33 cm^3

The motor shaft rotates at a constant angular velocity of 6 rpm. A slotted tubular coupling allows an extension of the shaft to translate as well as rotate. The shaft extension is threaded and rotates in a fixed threaded bearing, resulting in a constant velocity translation of the pump piston. Hence, fluid is driven at a constant rate of 4.25 cm^3/min into the cavity supply line (Figure 2.2). Fluid flow is recorded automatically with pen and chart by measuring the voltage change across an angular potentiometer geared to the rotating shaft; a constant chart speed introduces time, and calibration test results relate flow to voltage change. Similarly, pressure is recorded by measuring the voltage change across a calibrated resistance pressure transducer. Faster or slower flow rates are possible through a modification of the gear system.

Compliance of the hydrofracture system is measured by performing a pressure test in which the cavity is replaced by a rigid vessel of equivalent volume. The pressure-volume curve for this test is then used to compensate for the effects of system compliance on the hydrofracture records.

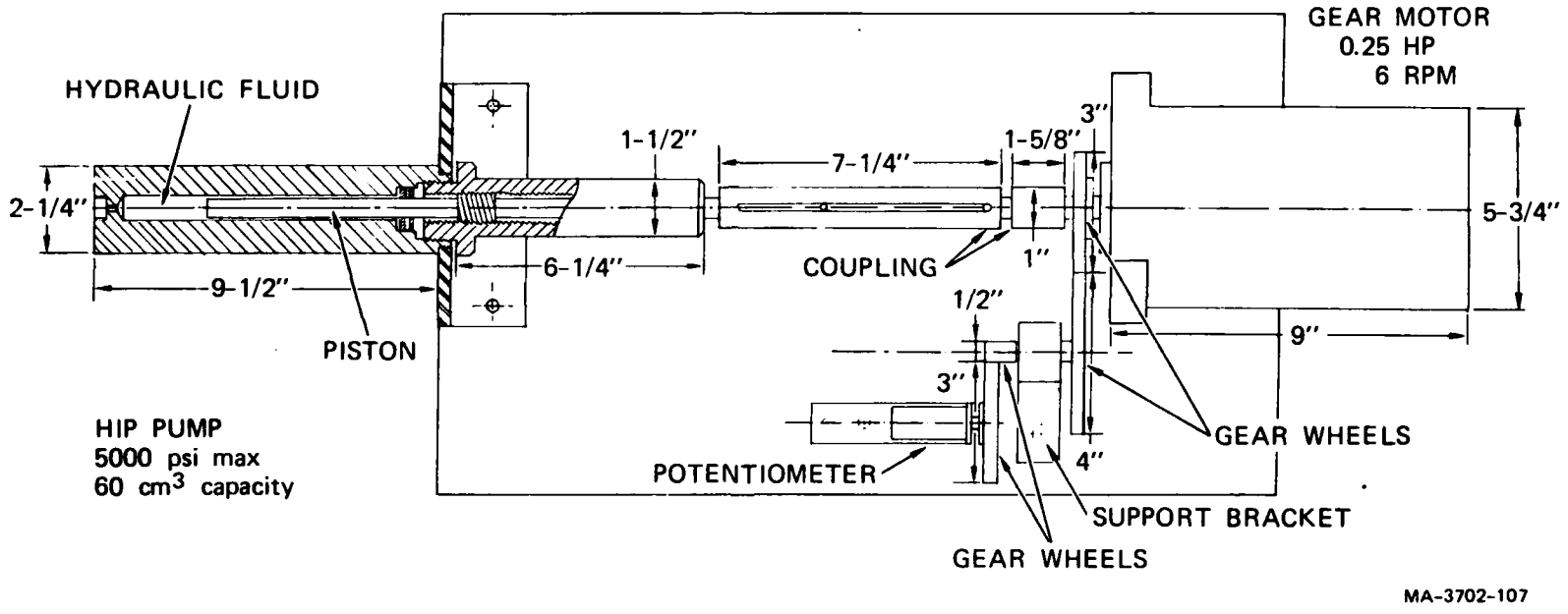

FIGURE 2.3 CONSTANT FLOW-RATE HYDROFRACTURE SYSTEM

Vented Cavity

The basic configuration for vented exploded cavity hydrofracture tests is shown in Figure 2.4. Figure 2.5 shows the charge design, which consists of 3/8-gram of PETN in a 3/8-inch-OD (9.52-mm) Lucite case with a wall thickness of 34 mils (0.864 mm). A constant explosive density of 1 g/cm^3 is desired for reproducibility; achievable machining accuracy results in slight variation of PETN weight from charge to charge. Hence 3/8-gram is the nominal weight of explosive. The charges are assembled by pressing PETN to a density of 1 g/cm^3 into a pair of mating Lucite hemispheres. The bridgewire assembly is then positioned as shown in Figure 2.5, using a notch in one of the hemispheres as a guide, and the hemispheres are snapped together and sealed with Homalite.* A wide-angle ferrule is attached near the end of the access tube to compress the grout around the tube as the cavity expands and prevent a leak path to the overburden from developing. The charge is positioned by drawing the lead wires through the access tube and filling the space between charge holder and tube with epoxy. The access tube is filled with epoxy. Venting occurs when the tube is drilled out following charge detonation.

Unvented Cavity

The basic configuration for unvented exploded cavity hydrofracture tests is shown in Figure 2.6. The charge is positioned by gluing the charge holder to the steel ball that acts as a valve; the lead wires are brought out of the sphere along the plane of the equator. Cavity gas pressure is measured and hydrofracture performed by following the sequence of steps shown in Figure 2.7. Before charge detonation, the entire system is filled with hydrofracture fluid. The steel ball attached to a valve stem seals the end of the access tube [Figure 2.7(a)]. Charge detonation expands the cavity past the end of the tube

*Homalite Corporation, Wilmington, Delaware.

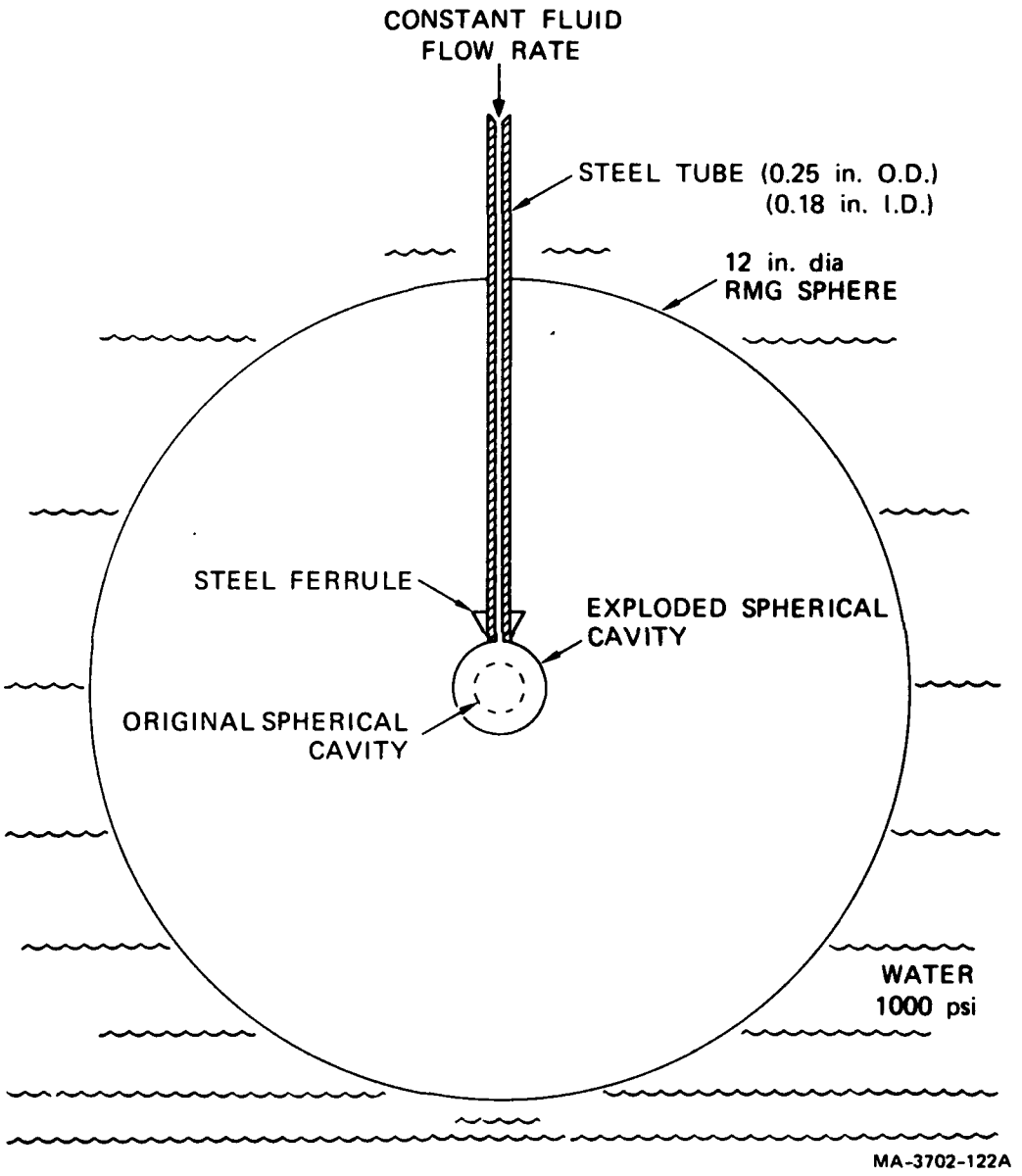

FIGURE 2.4 BASIC CONFIGURATION FOR VENTED EXPLODED CAVITY TESTS

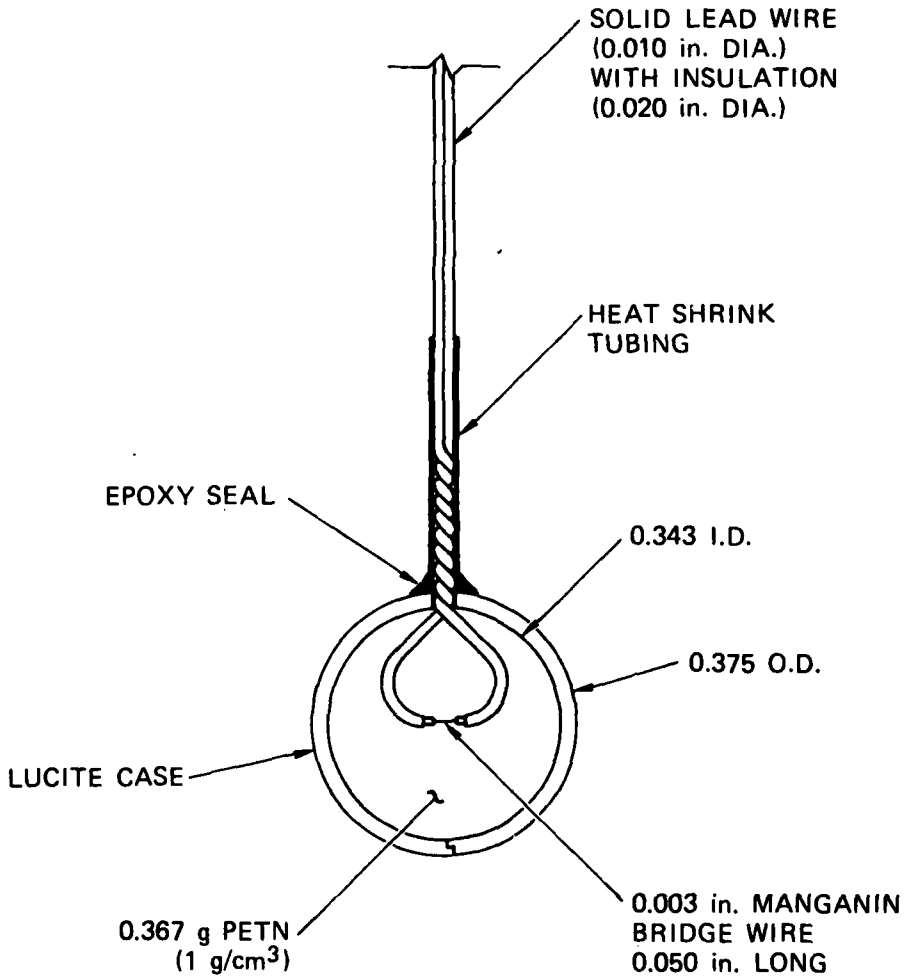

FIGURE 2.5 EXPLOSIVE CHARGE

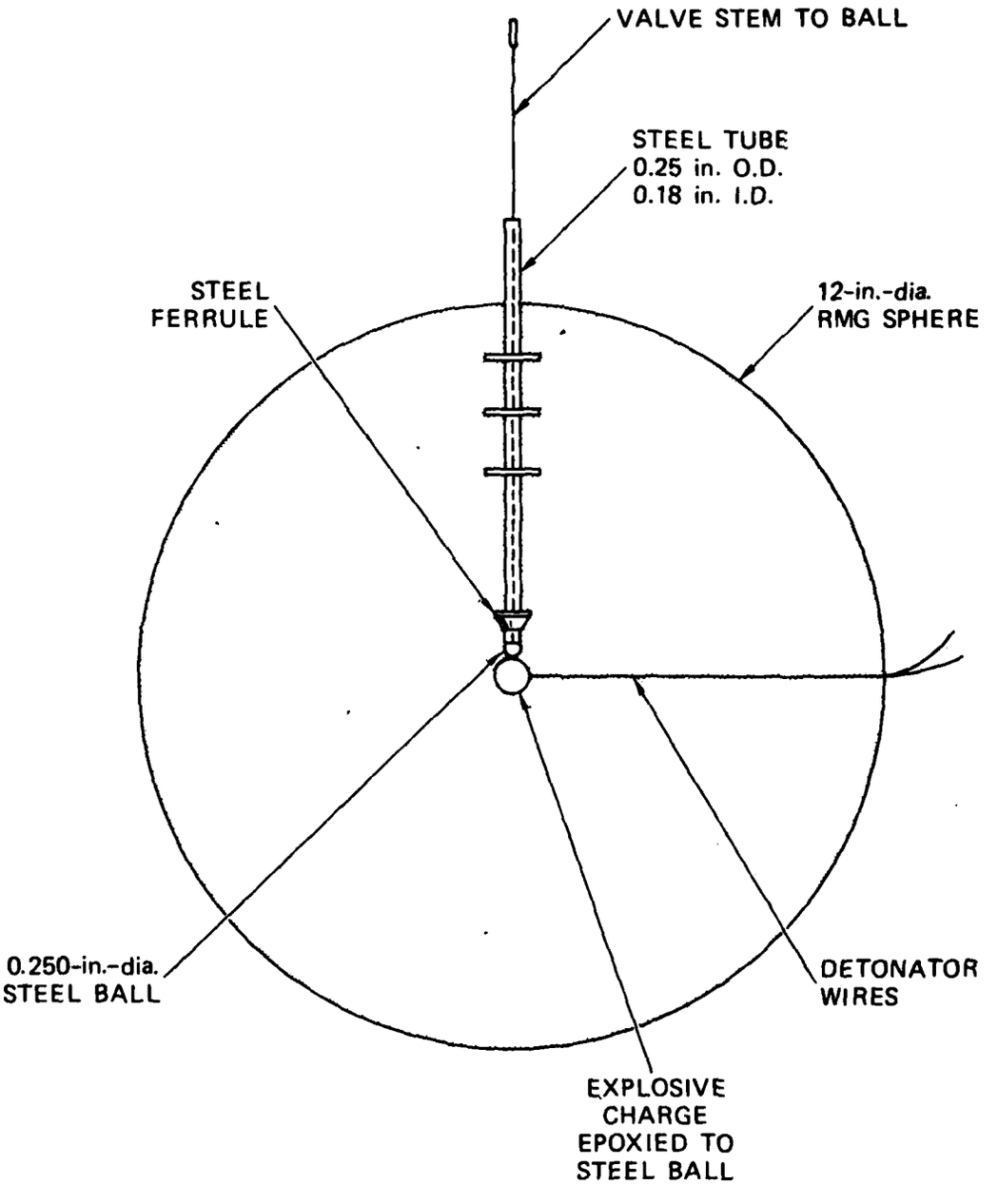

FIGURE 2.6 OVERALL CONFIGURATION FOR UNVENTED EXPLODED CAVITY TEST

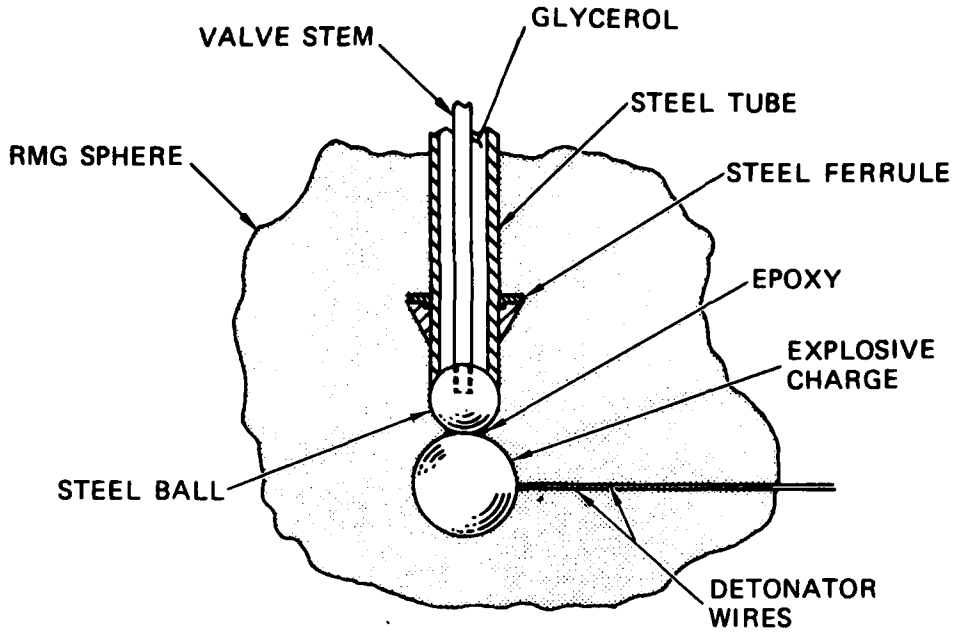

(a) INITIAL CONFIGURATION

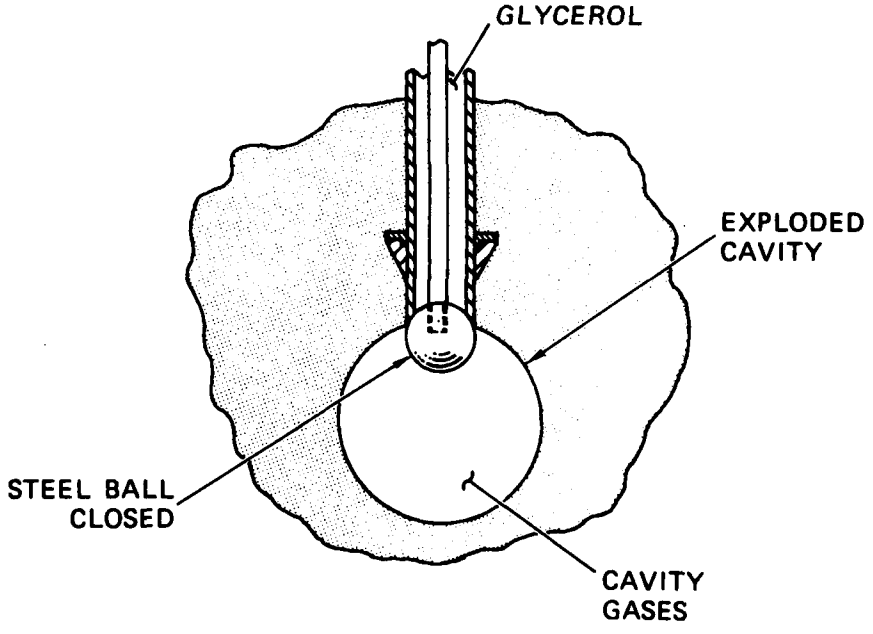

(b) CHARGE EXPLODED

MA-5958-96

FIGURE 2.7 SEQUENCE OF OPERATIONS FOR UNVENTED EXPLODED CAVITY TESTS

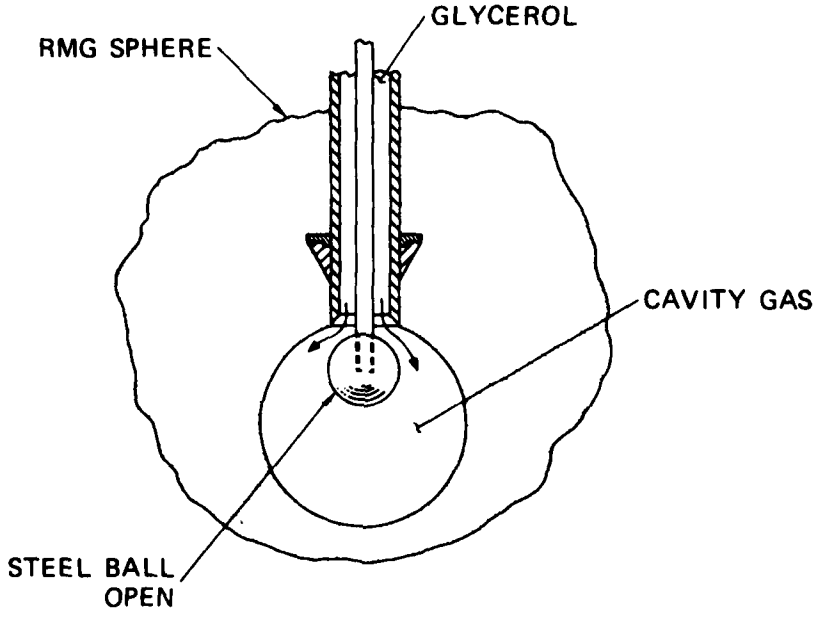

(c) START OF HYDROFRACTURE PROCESS

MA-5958-97

FIGURE 2.7 SEQUENCE OF OPERATIONS FOR UNVENTED EXPLODED CAVITY TESTS (Concluded)

[Figure 2.7(b)], and when the ball valve is lowered [Figure 2.7(c)], cavity gases pressurize the hydrofracture fluid. Pumping may begin immediately. Cavity gas and hydrofracture pressures are measured by the pressure transducer located in the fluid supply line.

Accuracy of the cavity gas pressure measurement was assessed by performing a calibration test. In this test the exploded cavity and gases are replaced by a rigid vessel containing an equivalent volume of nitrogen at a known pressure. When the ball valve was lowered, the compliance of the hydrofracture system allowed the nitrogen to expand and drop in pressure. To eliminate the pressure drop due to compliance, the hydrofracture system was pressurized to 300 psi (2.1 MPa). This prepressurizing technique was incorporated into the unvented exploded cavity tests.

Unexploded Cavity

The basic configuration for unexploded cavity hydrofracture tests is shown in Figure 2.8. The method of forming the central cavity is determined by the choice of a lined or unlined cavity.

An unlined cavity is formed by first inserting a rubber membrane (balloon) through the access tube and expanding the tip with water to the desired diameter. A spherical shape is maintained by means of a wire cage, which is temporarily fastened to the end of the tube. After 48 hours, the membrane has assumed a permanent shape and the cage is removed. The membrane and tube are then positioned in a Lucite mold and the grout is cast around them. After the grout has cured, the membrane is removed, leaving a smooth unlined cavity.

A lined cavity is formed by first stretching a rubber membrane over the end of the access tube and holding the membrane in place by means of a Teflon ferrule and epoxy seal. The procedure for expanding the membrane and positioning the access tube is the same as that described

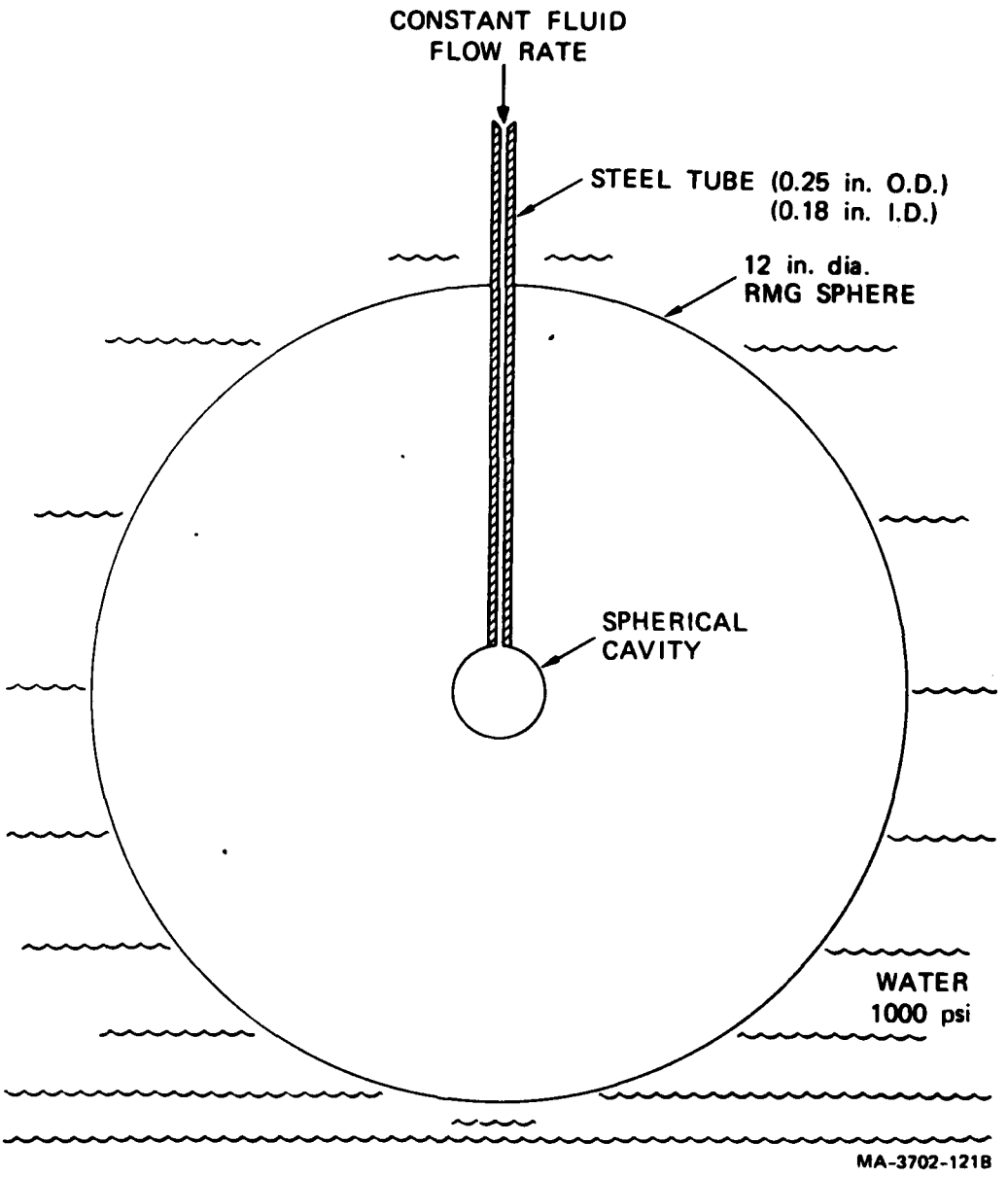

FIGURE 2.8 BASIC CONFIGURATION FOR UNEXPLODED CAVITY TESTS

above for an unlined cavity. After the grout is cured and water removed from the cavity, the membrane remains in place to act as a cavity lining during hydrofracture.

2.3 MEASUREMENT TECHNIQUES

Crack growth, fluid motion, and the states of stress and strain associated with hydrofracture are monitored by the following sensors:

- Surface fracture gage (Figure 2.9)
- Embedded fracture gage
- Surface fluid arrival gage (Figure 2.9)
- Embedded fluid arrival gage (Figure 2.10)
- Embedded strain gage (Figure 2.11)
- Embedded stress gage (Figure 2.12)

In addition, observations of crack growth and fluid motion for examining gage response were made with transparent models.

Surface Fracture Gage

Surface fracture of a grout sphere is detected by means of a 1/16-inch-wide (1.59-mm) stripe of electrically conductive silver-based paint. Two copper tabs are first embedded in the surface of the sphere during casting. After the grout is cured, the paint stripe connects the tabs to cover a desired region. During hydrofracture the resistance from tab to tab is monitored. Visual inspection of the surface of the sphere during hydrofracture has shown that a hairline crack in the grout is sufficient to break the paint and produce a noticeable resistance change in the gage. Typical regions of surface covered by the gage are shown in Figure 2.9. Initial gage resistance, which is a function of length, is 100 to 200 ohms for the gage shown. Final resistance, which is a measure of electrical conductivity through the grout, is 40,000 ohms.

Embedded Fracture Gage

One method of detecting internal fracture in a grout sphere is to embed thin brittle rods of an electrically conductive material and then monitor the resistance of the gage during the test. A propagating crack intersects the gage and results in a change in resistance. Gage length and orientation are chosen so that a convenient region of interest is covered. If a 1/32-inch-diameter (0.79-mm) graphite rod is used, initial resistance is typically 5 ohms for a 9-inch (22.86-cm) gage length. Final resistance of the fractured gage is 40,000 ohms. Although bond strength between the graphite and grout is good, sensitivity of the rod to a propagating crack is low; that is, a substantial crack width is required to change the gage resistance.

An alternative method for detecting internal fracture consists of replacing the graphite rods with 3/8-inch-diameter (9.53-mm) rods of grout coated with a stripe of conductive paint. The technique has the advantage of eliminating any possible mismatch in material properties between the embedded gage and the surrounding grout. Tests have shown that the eventual bond between cured grout rods and freshly poured grout is adequate. Also, sensitivity of the painted grout rod to a propagating crack is excellent.

Surface Fluid Arrival Gage

Arrival of hydrofracture fluid at the surface of a sphere is detected by means of a 20-mil (0.51-mm) copper wire taped to the grout. The resistance between access tube and gage is monitored during a test. Conductive hydrofracture fluid flows from the cavity, along a crack, and to the gage, resulting in a decrease in the measured resistance. The portion of the sphere in contact with the gage is coated with a brittle, electrically insulating material to provide a high initial resistance from access tube to copper wire. With this technique, the resistance decreases from 1500 to 700 ohms as fluid reaches the surface. Each copper wire may be positioned adjacent to a surface paint stripe, as shown in Figure 2.9, to allow for a correlation of surface fracture and fluid arrival. The

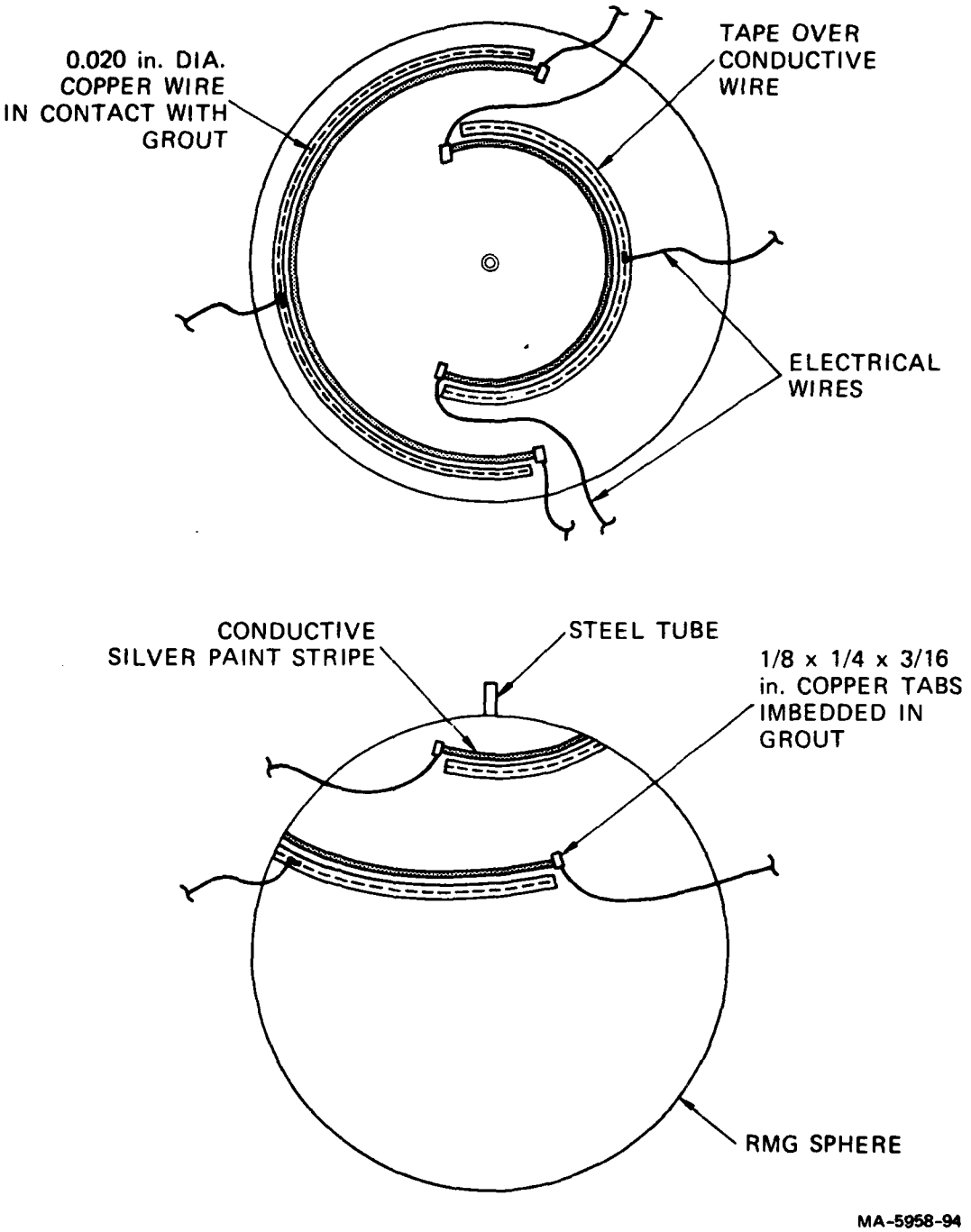

FIGURE 2.9 SURFACE CRACK AND FLUID ARRIVAL GAGES

conductive hydrofracture fluid is a mixture of dyed glycerol and copper sulface. Water is added to reduce the viscosity to that of dyed glycerol (660 centipoise), which is the normal hydrofracture fluid.

Embedded Fluid Arrival Gage

Arrival of hydrofracture fluid at some interior point of a grout sphere is detected by means of an embedded circular ring of 20-mil (0.51-mm) copper wire. The technique is similar to that of the surface fluid arrival gage described above. Conductive hydrofracture fluid flows along a crack and changes the resistance between the access tube and the ring. By adjusting the diameter and orientation of the ring, we can detect fluid arrival at any point in the sphere. A typical configuration is shown in Figure 2.10.

Embedded Strain Gage

Radial strain in a grout sphere is measured by means of a standard Constantan foil strain gage. The gage is first potted in a dog-bone-shaped holder of Castall 300 (RT-1 hardener) epoxy, which has elastic properties similar to that of grout. The entire unit is then cast in grout. Positioning is maintained by means of supporting threads and lead wires as shown in Figure 2.11. The Castall protects the gage from particles of sand and assures that the foil remains flat. An active gage length of 1/32 inch (0.79 mm) allows for reasonably accurate strain measurements even at a distance of two cavity radii from the center of the sphere where strain gradients are steep. Calibration tests performed on axially loaded cylinders show strains from an embedded gage to be in good agreement with strains from an extensometer attached to the cylinder.

Embedded Stress Gage

Static stress in a grout sphere is measured by means of the specially designed flat jack gage shown in Figure 2.12. The stress component normal to the surface of the 5/8-inch-diameter (1.59-cm) discs is

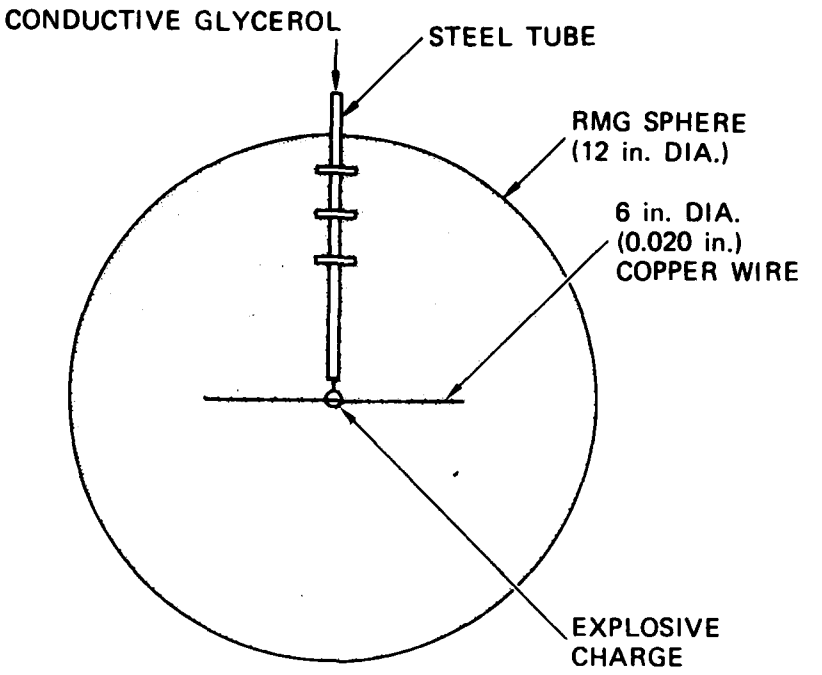

(a) CROSS SECTIONAL VIEW

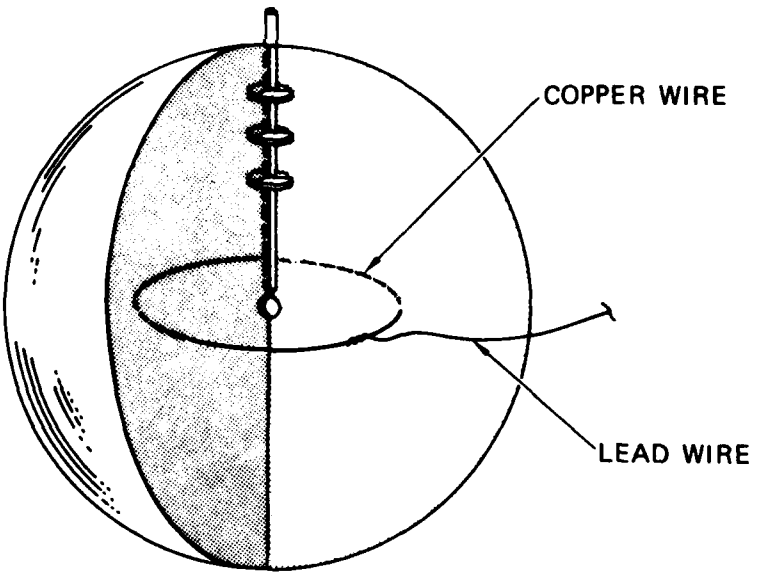

(b) CUT-AWAY VIEW

MA-5958-98

FIGURE 2.10 INTERNAL FLUID ARRIVAL GAGE

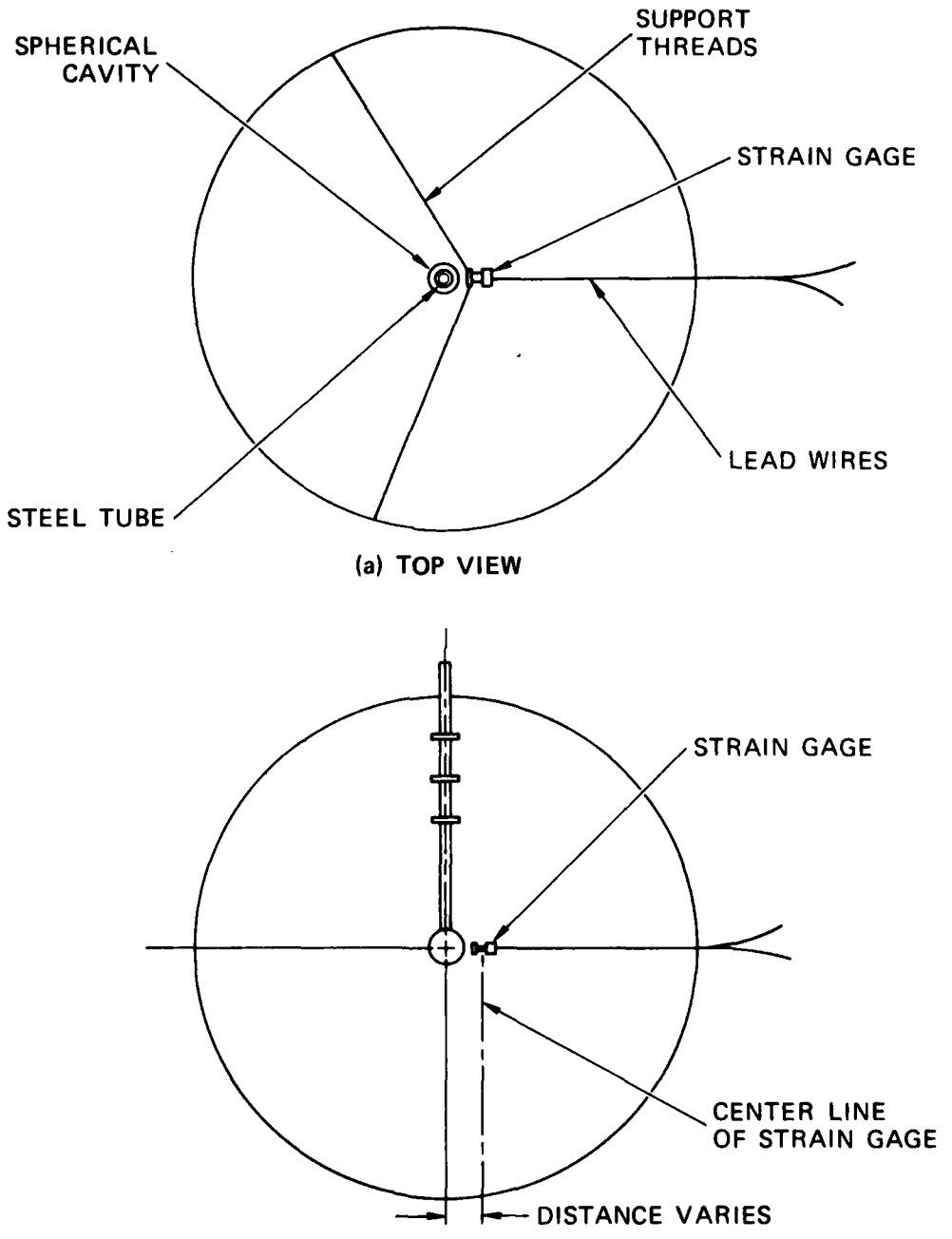

FIGURE 2.11 EMBEDDED STRAIN GAGE

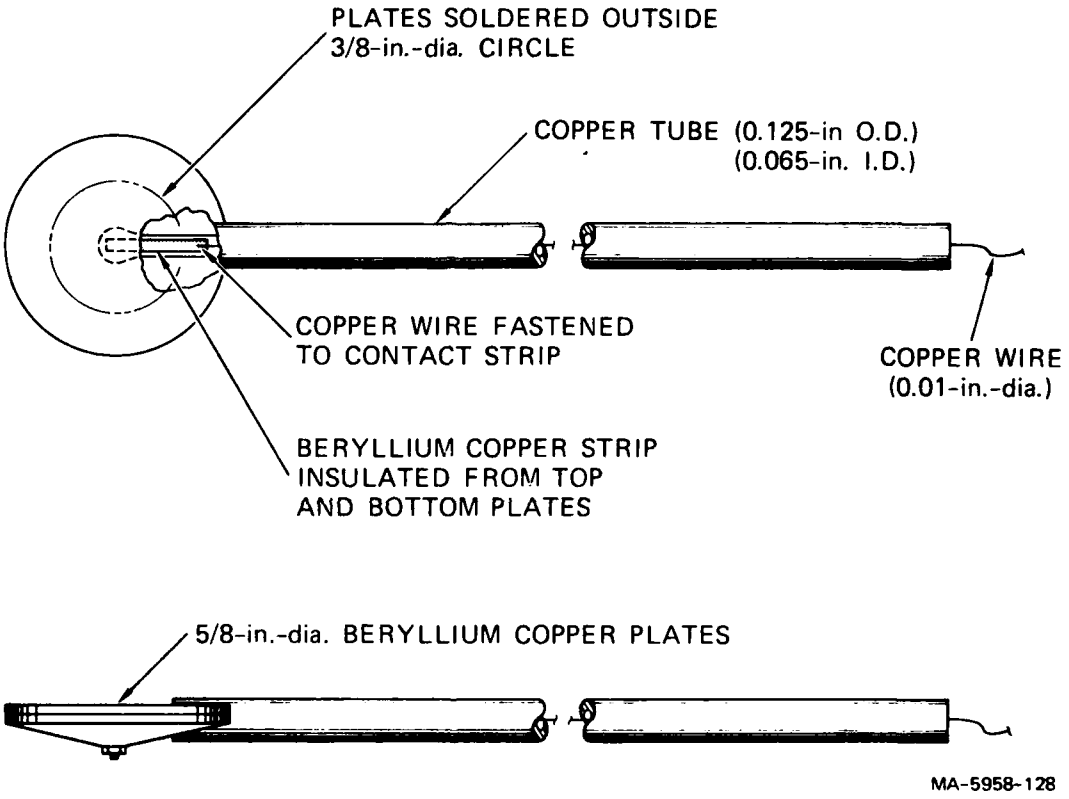

FIGURE 2.12 FLAT JACK STRESS GAGE

theoretically equal to the gas pressure required to separate the discs and open an electric circuit. However, calibration tests in water have shown that the opening pressure is 800 psi (5.5 MPa) before a hydrostatic load is applied. Subsequent increases in water pressure do result in corresponding increases in opening pressure. The gage has been designed to measure dynamically generated residual stresses, stress relaxation due to creep, and the quasi-static stresses produced by overburden and hydrofracture.

Transparent Model

Hydrofracture tests were conducted on 6-inch-diameter (15.24-cm) polyester spheres to allow for a visual check of embedded gage performance. The response of the embedded copper ring to the arrival of conductive hydrofracture fluid was instantaneous and pronounced. In one test, however, this gage served as a crack arrester. Use of a thinner wire may reduce this perturbing characteristic without affecting gage response. Alternative methods for detecting internal fluid arrival are being developed.

The newly developed embedded fracture gage, which consists of a stripe of conductive paint on a brittle rod, responded instantaneously to the arrival of the crack tip. The sensitivity of this gage is superior to that of embedded graphite rods. Hence this new technique will be incorporated in future hydrofracture tests on grout spheres.

2.4 CHARGE CALIBRATION

Reproducibility of the explosive source is a basic requirement of exploded cavity tests. To assess reproducibility, we performed a series of calibration tests on 1/4- and 3/8-gram charges. Details of the 3/8-gram charge are shown in Figure 2.5. The 1/4-gram charge, which is similar in design, has a Lucite case with a 7/16-inch (11.1-mm) OD and a nominal 54-mil (1.37-mm) wall thickness. The test configuration consisted of an explosive source epoxied to the end of a stainless steel tube and suspended in a water-filled pressure vessel as shown in

Figure 2.13. The detonation wires were guided through the tube and epoxied in place. Source output was monitored by the specially designed piezoresistive ytterbium foil stress gage shown in Figure 2.14 and by a standard piezoelectric quartz pressure transducer. The ytterbium gage was suspended near the charge by means of flexible supports that allowed the gage to follow the motion of the water. This resulted in a direct measurement of the incident shock wave pressure. The quartz transducer was rigidly and centrally mounted in the bottom of the vessel and thus measured reflected pressures. Oscilloscopes served as the recording devices.

A typical quartz gage record for á 3/8-gram charge is shown in Figure 2.15. Since the rise time was limited by the frequency response of the gage, the actual pulse probably had a shorter rise time and resulted in considerable overshoot of the gage. An estimate of the actual peak pressure is provided by the exponential fit, also shown in Figure 2.15. The parameters in this approximation are chosen by equating the impulse from the exponential to the impulse from the experiment at two arbitrary times.

The distance from the center of the explosive source to the ytterbium gage was varied from 5/16 to 5/8 inch (7.9 to 15.9 mm). The distance between source and quartz gage was fixed at 6-5/8 inches (16.8 cm). Since the amplitude of the pulse measured by the quartz gage was in the acoustic range, incident pressure is one-half the reflected value.

Results for the 3/8-gram charges are summarized in Table 2.1. Incident pressure and impulse are listed, the total impulse being obtained from an intergration of the quartz gage pressure records. Results for the 1/4-gram charges are summarized in Table 2.2.

Peak pressure from a 3/8-gram charge decays with increasing distance from the charge as shown in Figure 2.16. The pressure profile generated by the SRI PUFF 8 computer code. The portion of the experimental curve that connects ytterbium and quartz gage data was obtained from the decay law for a spherically acoustic wave. This law

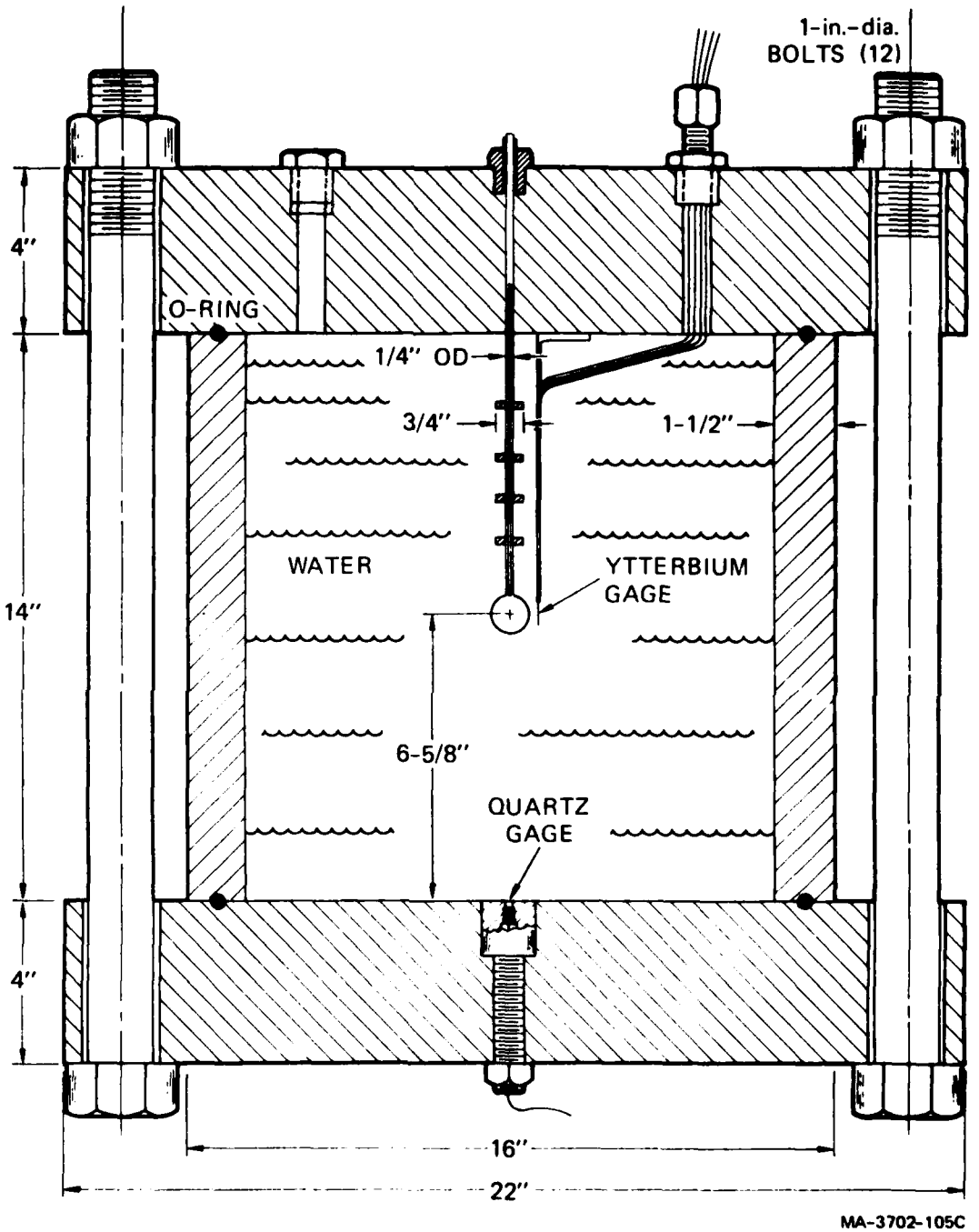

FIGURE 2.13 CHARGE CALIBRATION APPARATUS

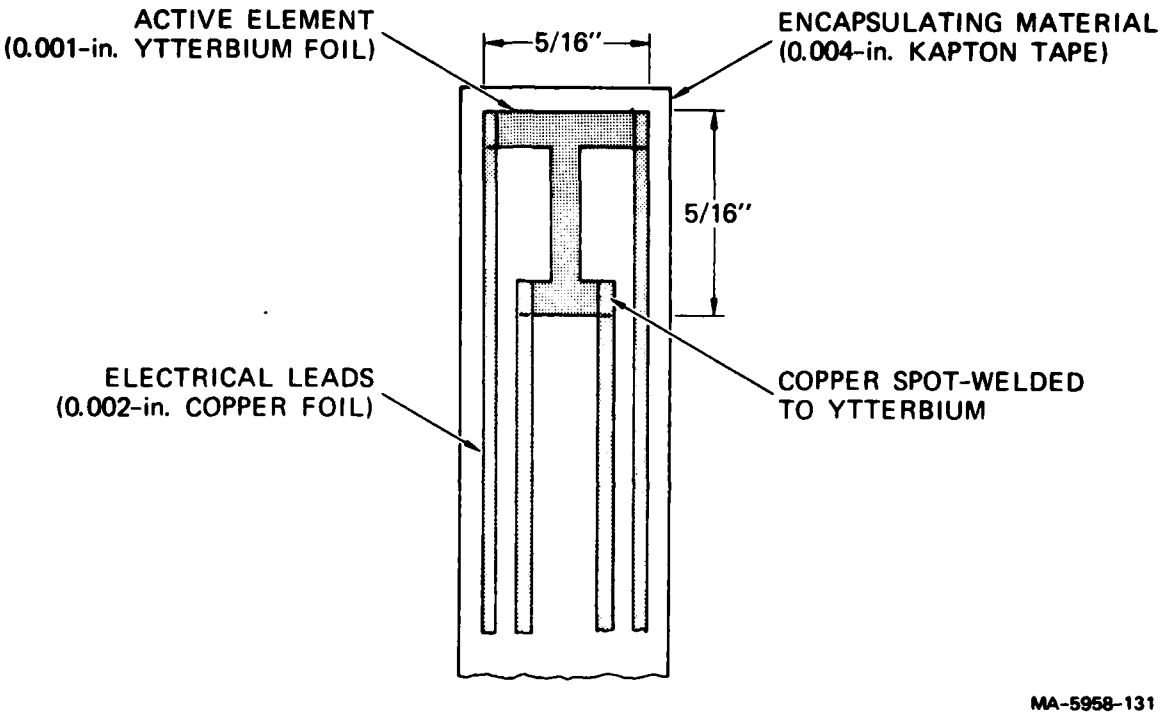

FIGURE 2.14 PIEZORESISTIVE YTTERBIUM FOIL STRESS GAGE

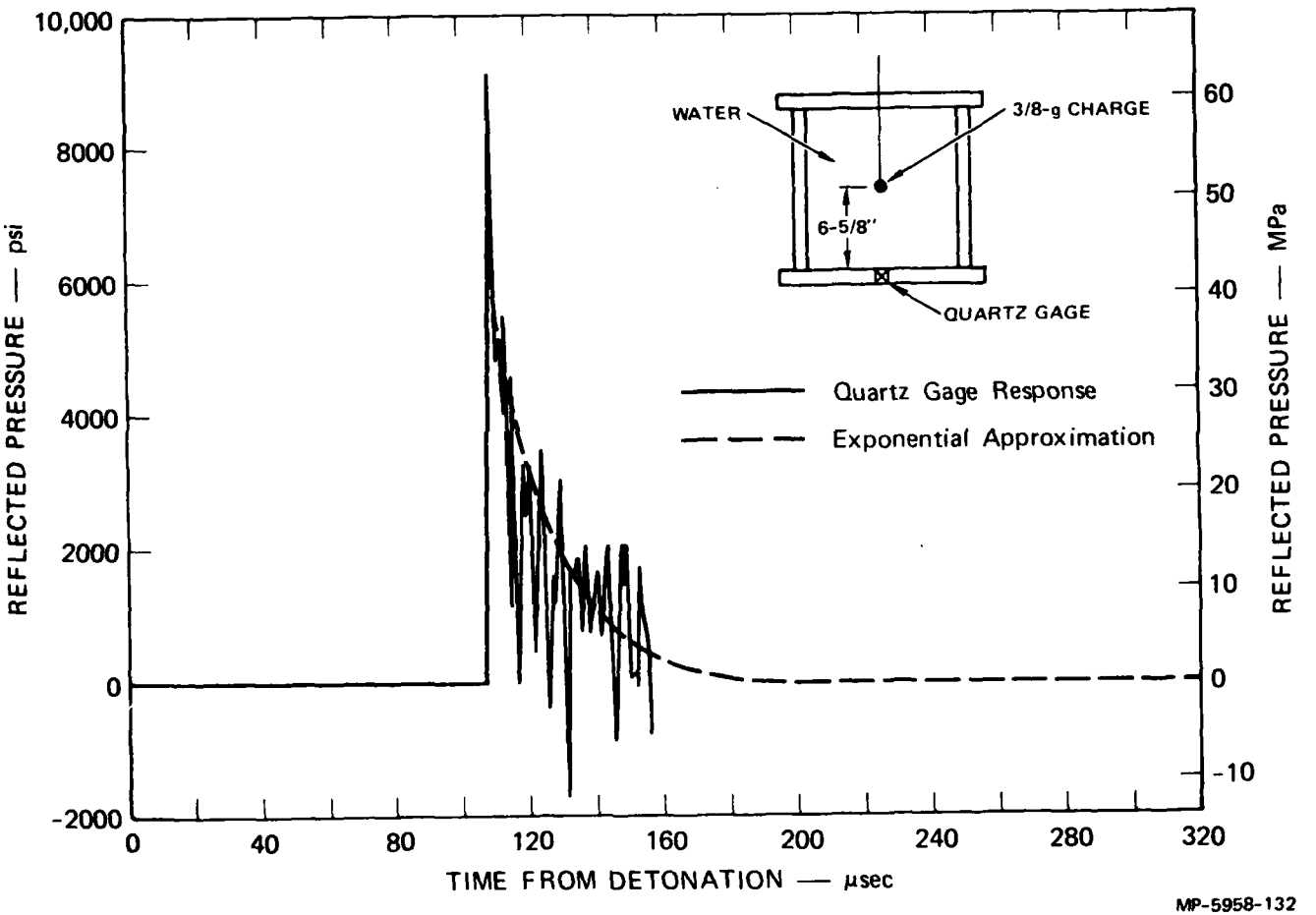

FIGURE 2.15 REFLECTED PRESSURE PULSE GENERATED BY DETONATION OF 3/8-GRAM CHARGE IN WATER

Table 2.1

SUMMARY OF RESULTS FOR 3/8-GRAM CHARGE CALIBRATION TESTS

	Quartz Gage				Ytterbium Gage	
Weight of PETN (g)	Distance of gage from center of charge (in.)	Peak incident pressure (psi)		Maximum incident impulse (psi msec)	Distance of gage from center of charge (in.)	Peak incident pressure (psi)
		From gage record	From equivalent exponential			
0.3656	6 5/8	3350	-	-	5/8	62,250
0.3630	↓	3500	-	-	↓	-
0.3644	↓	4750	-	-	↓	-
0.3634	↓	3125	3270	55.5	↓	54,100
0.3566	↓	4125	3990	55.8	↓	-
0.3586	↓	4000	3360	54.5	↓	56,600
0.3672	↓	4125	2620	53.9	↓	55,900
0.3587	↓	2875	3040	54.5	↓	55,800
0.3619	↓	3375	3190	51.0	↓	50,750
0.3701	↓	3250	3260	53.5	7/16	130,500
0.3679	↓	4500	2800	55.0	↓	102,600
0.3674	↓	4875	3360	62.0	↓	137,800
0.3794	↓	4625	3240	59.5	5/16	144,700

Table 2.2

SUMMARY OF RESULTS FOR 1/4-GRAM CHARGE CALIBRATION TESTS

	Quartz Gage				Ytterbium Gage	
Weight of PETN (g)	Distance of gage from center of charge (in.)	Peak incident pressure (psi)		Maximum incident impulse (psi msec)	Distance of gage from center of charge (in.)	Peak incident pressure (psi)
		From gage record	From equivalent exponential			
0.247	6 5/8	3120	2460	42.6	5/8	42,000
0.231	6 5/8	4000	2550	37.8	5/8	44,900

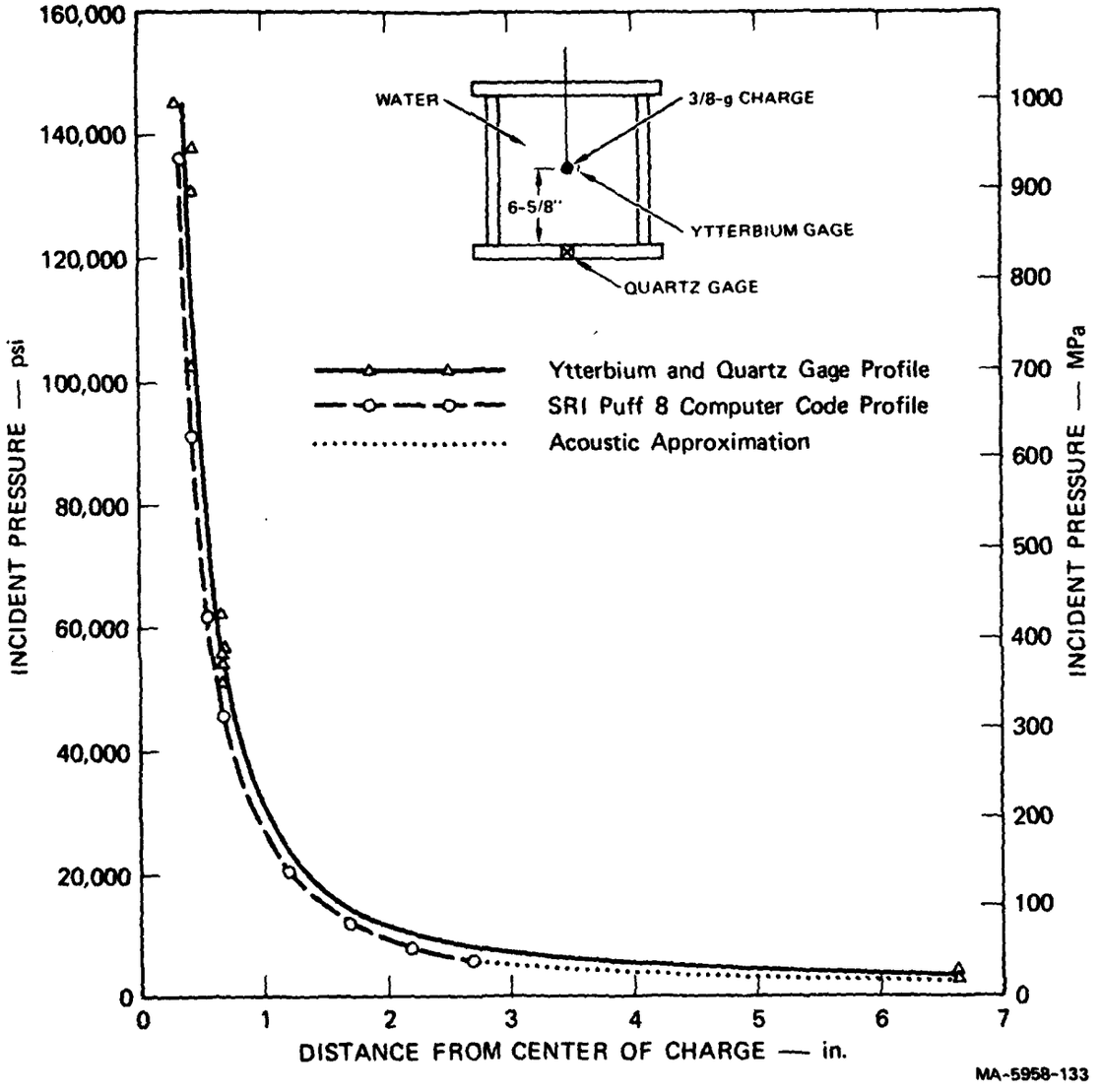

FIGURE 2.16 PRESSURE PROFILE GENERATED BY DETONATION OF 3/8-GRAM CHARGE IN WATER

was also used to extend the computer code data out to the location of the quartz gage.

The exponential fit of quartz gage data provides peak incident pressure in the range 2620 to 3990 psi (18.1 to 27.5 MPa), with an average of 3213 psi (22.2 MPa). The PUFF code predicts a peak pressure of 2430 psi (16.8 MPa). Calculations performed at Systems, Science and Software[8] (S^3) predict a peak pressure of 2320 psi (16.0 MPa). Hence measured pressures at the low end of the range are in close agreement with the calculations. Owing to the shape of the pressure pulse, variations in peak pressure do not contribute significantly to the total impulse from the charge. Measured incident impulse, which is considered an accurate measure of charge reproducibility, ranged from 51.0 to 62.0 psi·msec (352 to 427 MPa·μsec). Maximum deviation from the 55.5 psi·msec (383 MPa·μsec) average was less than 11.9%. The S^3 calculations are in excellent agreement with the integrated quartz pressure history. Hence, based on impulse data, the charges are considered adequately reproducible for use as the explosive source in exploded cavity tests.

Two tests of the 1/4-gram charge produced incident impulses of 37.8 and 42.6 psi·msec (261 and 294 MPa·μsec). These results suggest that the 1/4-gram charge is also adequately reproducible.

As an additional means of assessing charge reproducibility, quartz gage measurements were made of the pressure pulse generated in the overburden water during exploded cavity tests 139 and 148. Incident pulses are shown in Figure 2.17, where the pulse shapes are seen to be strikingly similar. Peak incident pressures measured relative to the 1000-psi (6.9-MPa) overburden were 520 and 550 psi (3.6 and 3.8 MPa). The corresponding incident impulses were 5.97 and 6.50 psi·msec (41.2 and 44.8 MPa·μsec). For calculating impulses, the pressure pulse was assumed to end when the pressure dropped to overburden as shown in Figure 2.17.

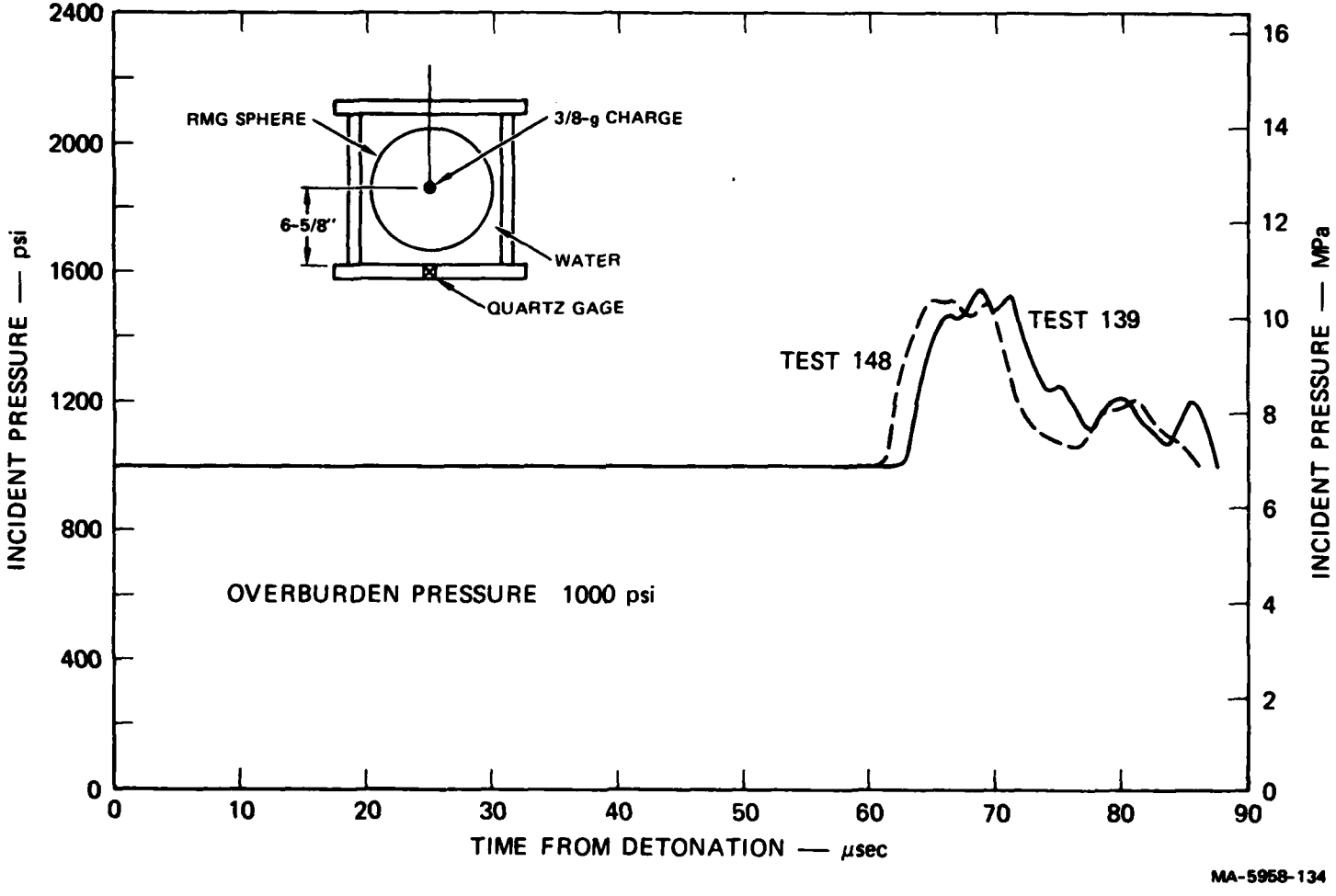

FIGURE 2.17 INCIDENT PRESSURE PULSE GENERATED DURING VENTED EXPLODED CAVITY TESTS 139 AND 148

SECTION 3

EXPERIMENTAL RESULTS

3.1 HYDROFRACTURE TEST SERIES

Table 3.1 summarizes the hydrofracture experiments. Series 1 through 8 are unexploded cavity tests, and series 9 through 17 are exploded cavity tests. Reproducibility tests, series 1 and 9, were performed to provide confidence in the basic experimental techniques and to generate comparison data for the parameter studies. The remaining tests are grouped according to the following areas of investigation:

- Overburden (series 2). In unexploded cavity tests, overburden provides a useful parameter for the study of fracture initiation. A pressure of 1000 psi (6.895 MPa), which simulates the in-situ stress environment in a typical underground nuclear test, was applied in the reproducibility tests. Pressures in the range 0-2000 psi (0-13.790 MPa) are experimentally convenient and allow for adequate testing.

- Cavity size (series 3). Since the standard 3/8-gram charge produces an explosively enlarged cavity with a 3/4-inch (1.905-cm) diameter, an unexploded cavity of the same size is chosen as the standard. For the parameter study, cavity diameters of 11/16 and 1 inch (1.746 and 2.54 cm) were chosen because they correspond to exploded cavity diameters produced by $\frac{1}{4}$- and $\frac{1}{2}$-gram charges. These cavities all closely approximate a spherical void in an infinite medium.

- Internal fracture (series 4 and 12). Attempts were made to determine the position of the leading edge of a propagating crack during hydrofracture in both exploded and unexploded cavity spheres.

- Surface fracture (series 5 and 13). Because a grout sphere may no longer be treated as infinite in extent after a surface crack develops, attempts were made to record the arrival of a propagating fracture plane at the surface of unexploded and exploded cavity spheres.

Table 3.1

SUMMARY OF CONTAINMENT INVESTIGATIONS

Series	Purpose or Parameter	Hydrofracture Pressures (Figure)	Overburden Pressure (psi)	Cavity Diameter (in.)	Number of Tests	Observations
Unexploded Cavity Experiments						
1	Reproducibility	3.1 3.2	1000	3/4	5	Excellent reproducibility for imperfection-free, unlined cavities; fracture initiation pressures are within 3% of 2800-psi average.
2	Overburden	3.4	0 1000 2000	3/4	1 4 1	Containment capability significantly improves with increased overburden.
3	Cavity size	3.6	1000	11/16 3/4 1	2 4 1	Small changes in cavity diameter have no effect on containment.
4	Internal fracture	3.7	1000	3/4	2	Fracture growth appears to be slow, but unstable.
5	Surface fracture	All tests	0 1000 2000	3/4 11/16 3/4 1 3/4	1 2 11 1	Less than 4 cm^2 of fluid is required to produce surface cracking.
6	Surface fluid	3.7	1000	3/4	3	Fluid arrives at the surface soon after the propagating crack tip.
7	Internal strain measurement	3.7	1000	3/4	5	Compressive radial strain near the cavity is larger than predicted by the theory of elasticity.
8	Cavity lining	3.12	1000	1	3	Membrane lining with pin-hole size leak yields higher fracture initiation and steady-state pressures than unlined cavity.

Table 3.1 (concluded)

SUMMARY OF CONTAINMENT INVESTIGATIONS

Series	Purpose or Parameter	Hydrofracture Pressures (Figure)	Overburden Pressure (psi)	Cavity Diameter (in.)	Number of Tests	Observations
Exploded Cavity Experiments						
9	Reproducibility	3.14	1000	3/8	4	Fracture initiation and steady-state pressures are reasonably reproducible. A spectrum of maximum cavity pressures is generated.
10	Unvented cavities	3.17	1000	3/8	2	Unvented cavities require higher fracture initiation pressures than unvented cavities. A spectrum of hydrofracture records is generated.
11	Creep	3.22	1000	3/8	3	Stress relaxation leads to hydrofracture records at the lower end of the vented cavity spectrum.
12	Internal fracture	3.22	1000	3/8	2	Initial crack growth appears to be sudden and unstable. Subsequent growth is slower and possibly stable.
13	Surface fracture	All tests	1000	3/8	9	Surface cracking occurred after 11 cm^3 of fluid flow.
14	Internal fluid arrival	3.24	1000	3/8	3	Initial fluid motion appears to be sudden and widespread.
15	Surface fluid arrival	3.24	1000	3/8	3	Fluid arrives at the surface soon after the propagating crack tip.
16	Internal strain measurement	3.22	1000	3/8	1	Dynamic strain record suggests crushing of grout near the exploded cavity.
17	Internal stress measurement	3.22	1000	3/8	1	Dynamically generated residual stress relaxes with time.

- Internal fluid arrival (series 14). Fluid flow along a fracture plane influences crack propagation. Hence fluid arrival was monitored so that it could be related to the arrival of the leading edge of the crack.

- Surface fluid arrival (series 6 and 15).

- Internal strain measurement (series 7 and 16). Charge detonation results in a large dynamic cavity expansion followed by a small contraction. The associated plastic strains in the surrounding medium produce the residual stresses. The radial component of strain near a dynamically expanding cavity was measured. The static radial strains associated with hydrofracture of exploded and unexploded cavity spheres were also measured.

- Cavity lining (series 8). Hydrofracture of a lined cavity has been limited to unexploded cavities. The objective of this testing was to initiate and propagate a fracture without the hydrofracture fluid acting directly on the wall of the cavity or entering the plane of the crack. The influence of the fluid was then assessed by comparing the results with those of unlined cavity tests.

- Unvented cavity (series 10). Since containment is a primary objective of nuclear testing, an unvented exploded cavity provides a more realistic model of a successful experiment than the vented cavity. Also, when the detonation products are contained, cavity gas pressure may be measured and hydrofracture begun immediately after charge detonation.

- Creep (series 11). Relaxation of the dynamically produced residual stress field surrounding an exploded cavity may have an adverse effect on containment. To assess the significance of this material property effect, we performed vented exploded cavity tests in which various lengths of time elapsed between charge detonation and hydrofracture.

- Internal stress measurement (series 17). An embedded stress gage was used to monitor the radial component of the decaying residual stress field near an exploded cavity. Such measurements are important in directly establishing the existence of residual stresses and the creep properties of rock-matching grout. Further applications of the embedded stress gage include a direct measurement of the stress fields associated with curing, overburden, and hydrofracture

3.2 UNEXPLODED CAVITY TESTS

Series 1 - Reproducibility

Unexploded cavity hydrofracture tests were performed to assess the reproducibility of the basic experimental technique and to provide reference data for the parameter studies. The configuration for these tests consisted of the smooth unlined cavity (Figure 2.8). A cavity of 3/4-inch (1.90-cm) diameter was chosen because it corresponds to the exploded cavity produced by a standard 3/8-gram charge. External pressure on the RMG 2C4 sphere was fixed at 1000 psi (6.895 MPa) because this represents the hydrostatic pressure in nuclear tests typically conducted at a depth of 1100 feet (335 m) in tuff with a density of 2.1 g/cm^3. Dyed glycerol, with a viscosity of 660 centipoise, was pumped into the cavity at a constant rate of 4.26 cm^3/min until the sphere fractured to the outside and a steady-state flow developed. After each test, the internal pressure was relieved before the overburden pressure. The sphere was then removed from the pressure vessel, examined for surface cracks, and wedged apart with a chisel to reveal the dyed fracture surface.

Hydrofracture pressure records for tests 123, 124, and 125 are shown in Figure 3.1. The records for tests 122 and 137 are shown in Figure 3.2. The results are typical of unexploded cavity tests in that pressure increased smoothly to a well-defined peak, dropped sharply, and then decayed slowly to a plateau well above overburden. Previous fracture initiation studies have shown that the pronounced pressure spike represents initiation of a macroscopic crack in the wall of the cavity and that the subsequent sharp pressure drop indicates crack propagation. Calibration tests, in which the cavity was replaced by a rigid vessel of equivalent volume, resulted in pressure records with an initial slope equal to those shown in Figure 3.1. Hence the 1.5 cm^3 required for fracture initiation of the grout sphere can be attributed to the combination of fluid compressibility and system compliance.

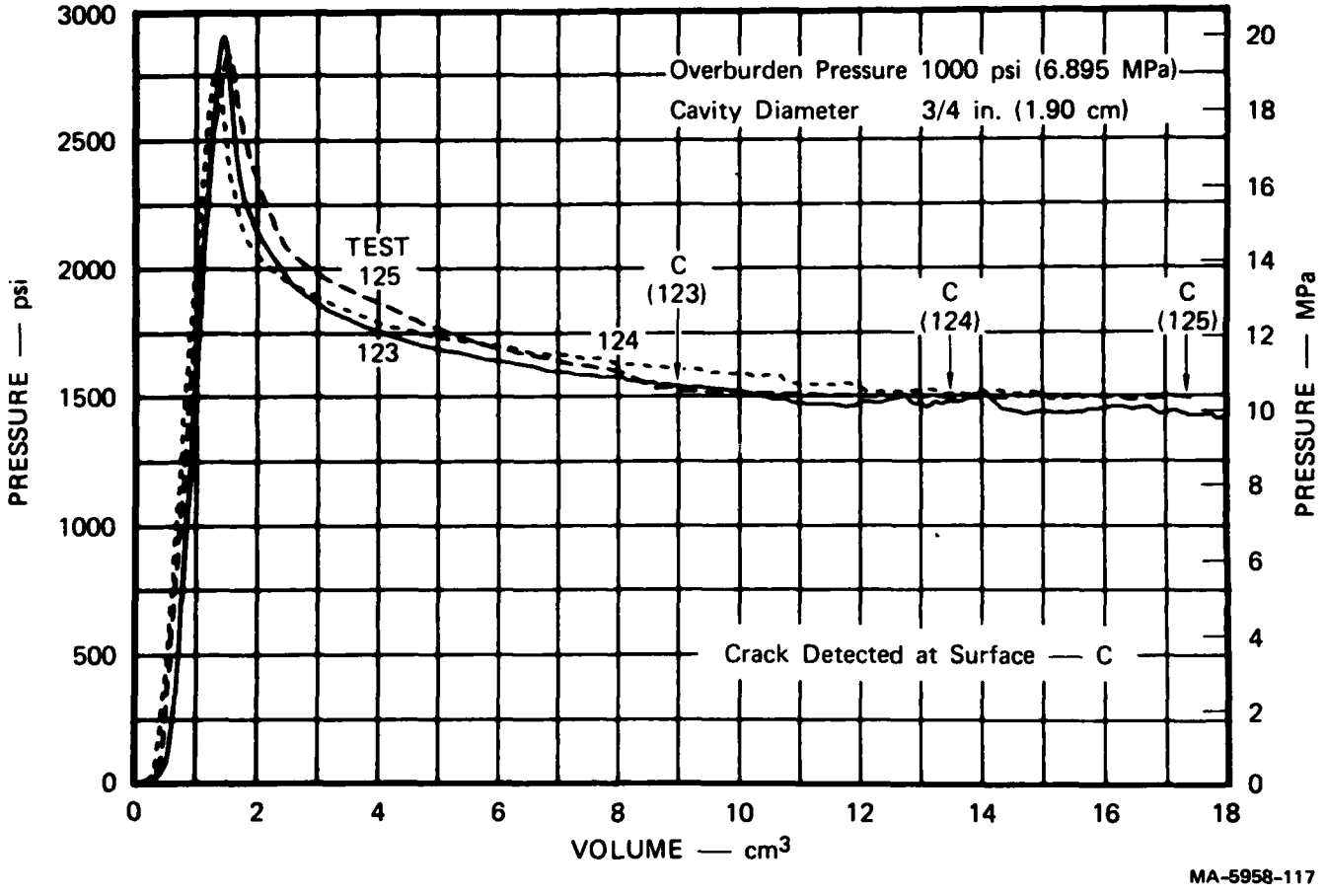

FIGURE 3.1 HYDROFRACTURE PRESSURES FOR UNEXPLODED CAVITY TESTS 123, 124, AND 125 — REPRODUCIBILITY

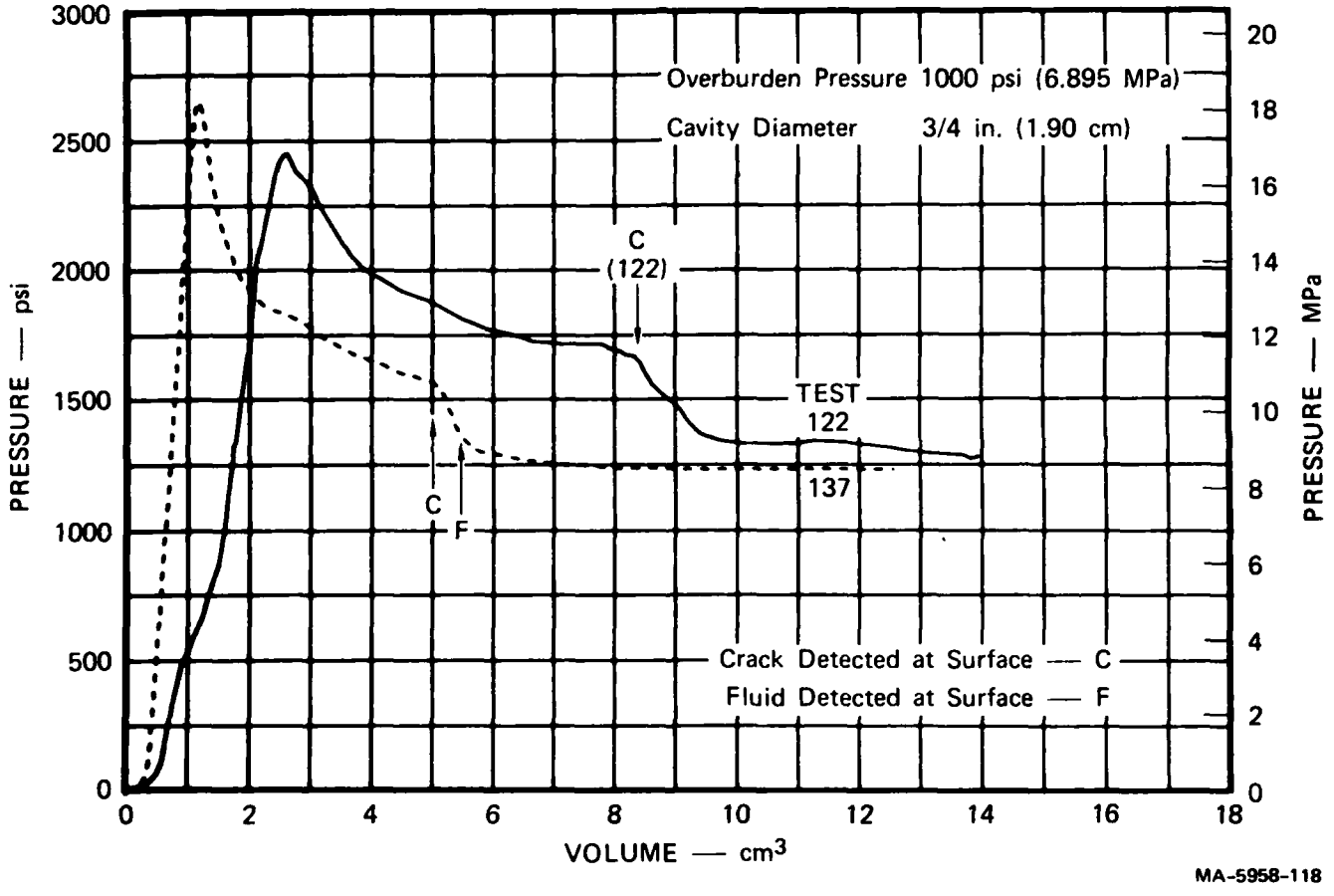

FIGURE 3.2 HYDROFRACTURE PRESSURES FOR UNEXPLODED CAVITY TESTS 122 AND 137—REPRODUCIBILITY

Peak cavity pressures, which serve as the primary measure of reproducibility, were 2910, 2780, 2860, 2470, and 2650 psi (20.1, 19.2, 19.7, 17.0, and 18.3 MPa). If the low value of test 122 is ignored, reproducibility is seen to be excellent, with a maximum deviation of only 5.4% from the 2800-psi (19.3 MPa) average.

Two unusual features in the hydrofracture record of test 122 are the initial erratic rise in cavity pressure and the low fracture initiation pressure. In view of the calibration tests, it appears that fluid escaping from the cavity accounts for the first of these anomalies. Previous hydrofracture tests with notched cavities[1] have shown that cavity imperfections reduce fracture initiation pressure. Hence, loss of fluid and a reduction in fracture initiation pressure are consistent with an irregularity such as a small void near the cavity.

Examination of the surface of each sphere following the tests revealed a single surface crack centered near the access tube and extending over an arc of approximately 120°. Wedging each sphere apart revealed a partially dyed planar fracture surface as shown in Figure 3.3 for test 124. Subsequent slices taken parallel to this plane failed to reveal additional cracking.

Examination of the fracture plane in test 122 revealed two voids near the cavity. Air trapped in the grout mixture during casting is responsible. Closer examination revealed that the voids propagated past the cavity, leaving a filament passage in their wake. These irregularities could reasonably account for the unusual character of the initial portion of the pressure record in test 122.

A second measure of reproducibility is the cavity pressure associated with steady flow along a fully developed crack. This pressure, which is determined by the flow resistance along the fracture plane, is related to crack width and the sectorial extent of the fracture in the plane of the crack. Figures 3.1 and 3.2 show that reproducibility is good, with steady-state pressures in the range 1250 to 1500 psi (8.6 to 10.3 MPa). A comparison of the dyed fracture surface in each test indicates that

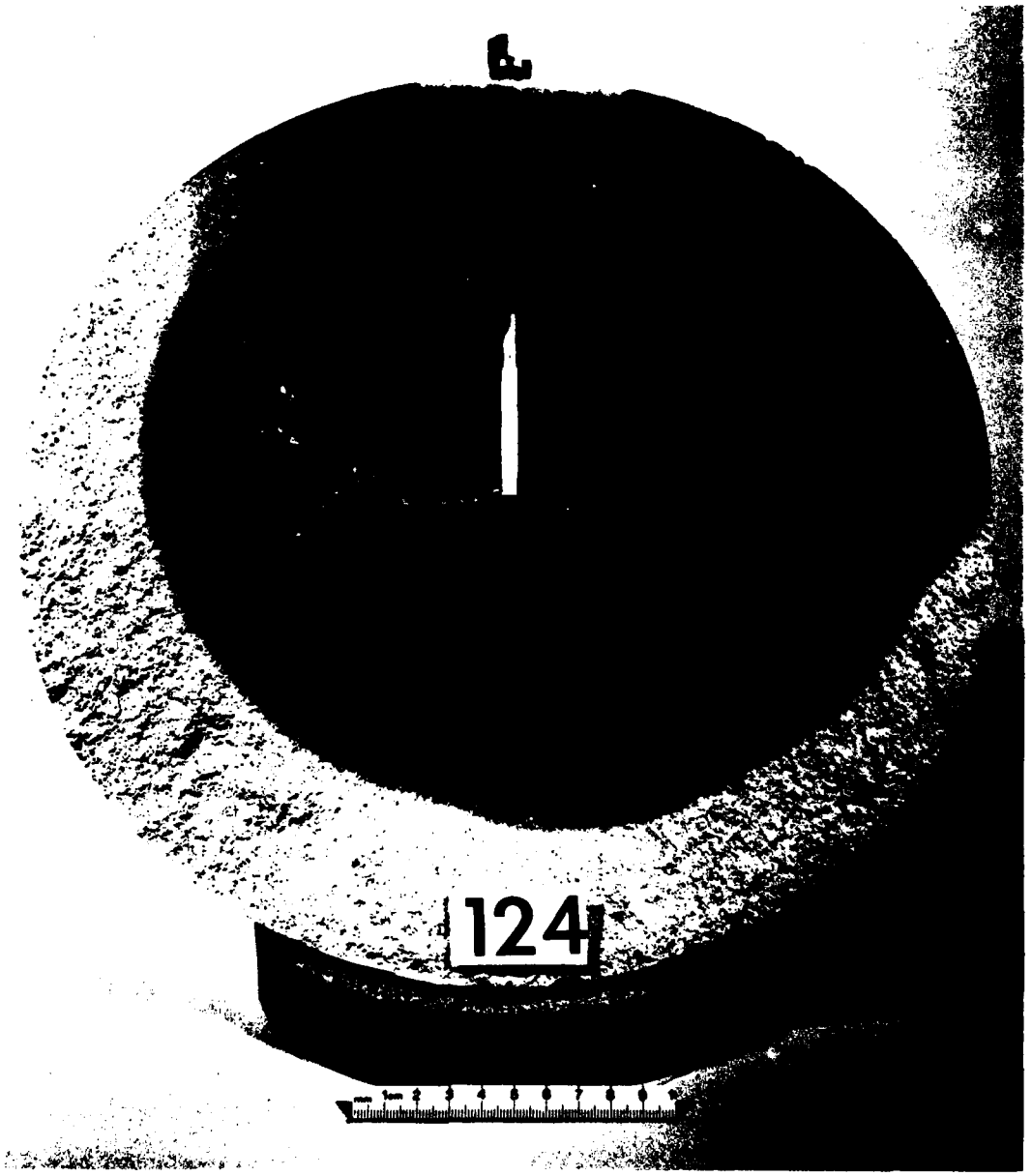

MP-5958-103

FIGURE 3.3 HYDROFRACTURE FROM UNEXPLODED CAVITY TEST 124

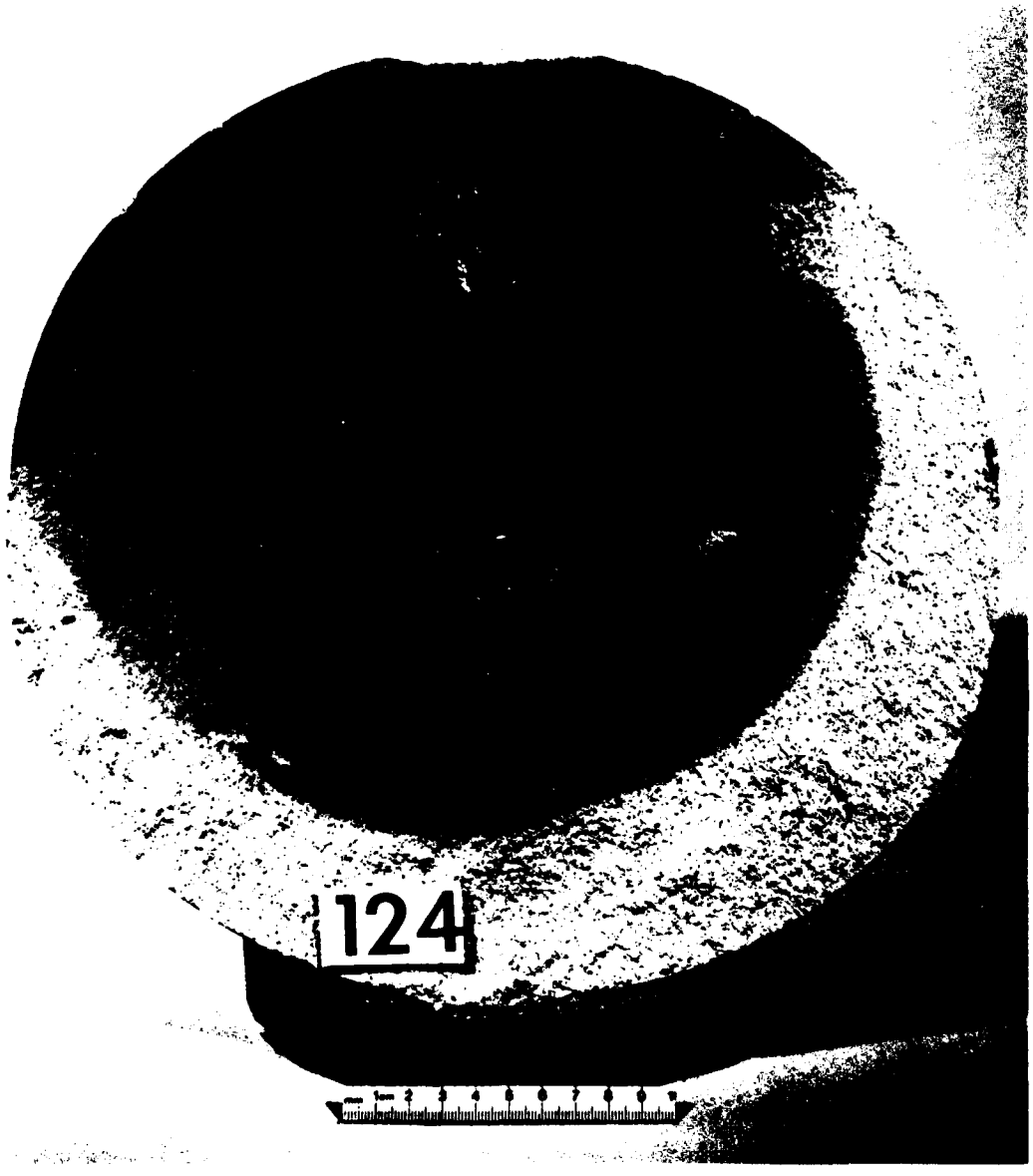

MP-5958-104

FIGURE 3.3 HYDROFRACTURE FROM UNEXPLODED CAVITY TEST 124 (Concluded)

lower steady-state pressures correspond to slightly more extensive fractured regions.

Series 2 - Overburden

Overburden tests are the hydrofracture of similar spheres subjected to a range of external pressures. The reproducibility tests of series 1 provide the results for an external pressure of 1000 psi (6.9 MPa). Tests 134 and 136 were performed at 0 and 2000 psi (0 and 13.8 MPa), respectively. Hydrofracture records are shown in Figure 3.4, where test 124 has been chosen as the typical result for 1000 psi (6.9 MPa). The records show that an increase in overburden benefits containment by increasing both the fracture initiation pressure and the subsequent steady-state pressure.

Overburden tests also provide data for establishing fracture criteria. For example, fracture initiation pressures may be plotted against overburden and compared with criteria based on tangential stress and strain at the cavity wall, as in Figure 3.5. The condition that the tangential stress equal the tensile strength of the grout is seen to be an accurate indicator of fracture initiation at zero overburden, but overestimates for higher overburden pressures. The zero tangential strain criteria, on the other hand, underestimates the fracture initiation pressure for the entire range of overburdens tested.

Series 3 - Cavity Size

Cavity size tests are the hydrofracture of spheres that are similar in all respects except for the diameter of the central cavity. The reproducibility tests of series 1 provide results for a 3/4-inch-diameter (1.90-cm) cavity. Tests 114 and 115 were performed on spheres with an 11/16-inch-diameter (1.75-cm) cavity. Test 113 was performed on a sphere with a 1-inch-diameter (2.54-cm) cavity. Hydrofracture records are shown in Figure 3.6, where test 124 has been chosen as representative of the reproducibility tests. Fracture initiation pressures are within the scatter of the reproducibility tests.

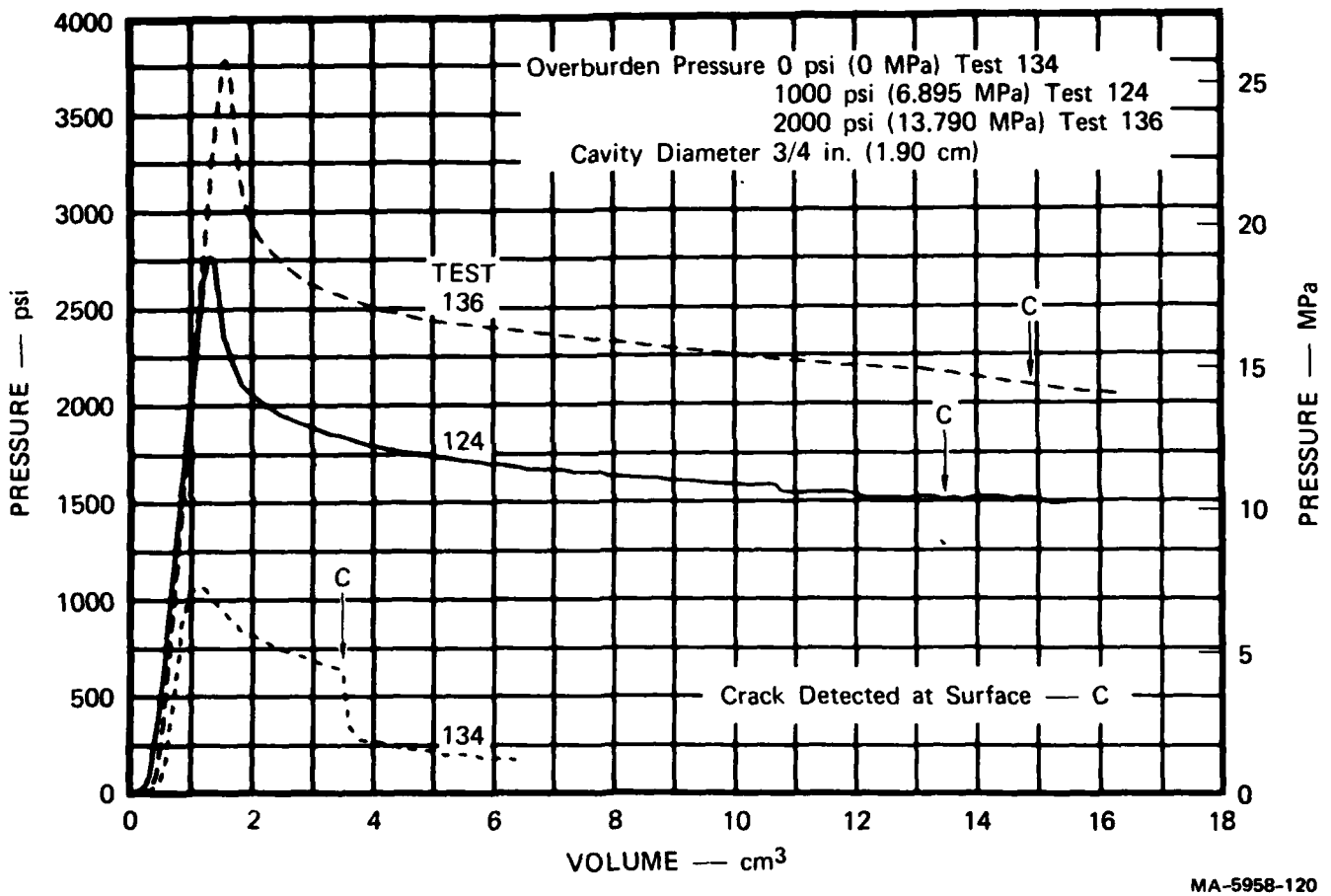

FIGURE 3.4 HYDROFRACTURE PRESSURES FOR UNEXPLODED CAVITY TESTS 124, 134, AND 136—OVERBURDEN EFFECT

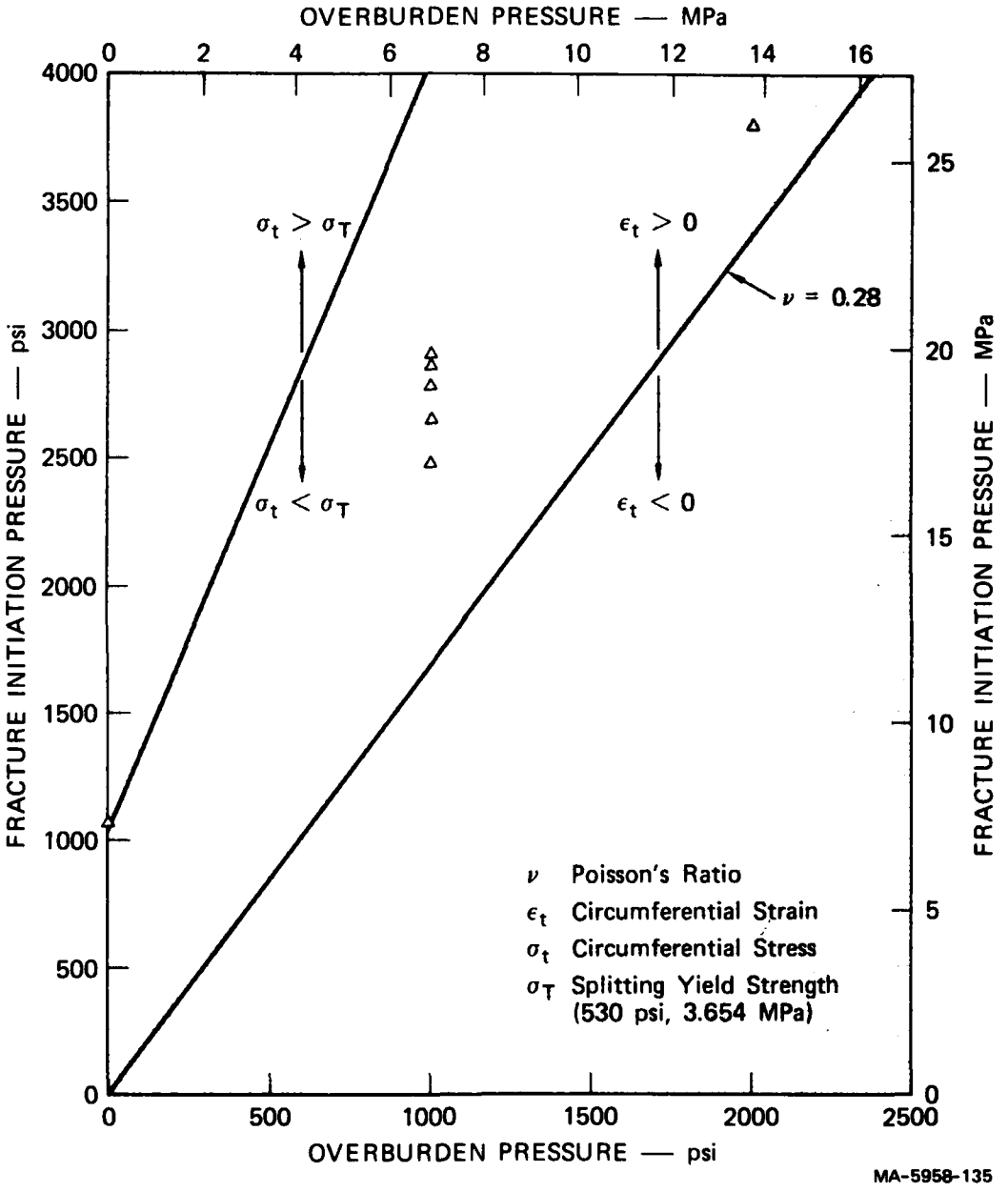

FIGURE 3.5 FRACTURE INITIATION PRESSURE VERSUS OVERBURDEN FOR UNEXPLODED CAVITY TESTS

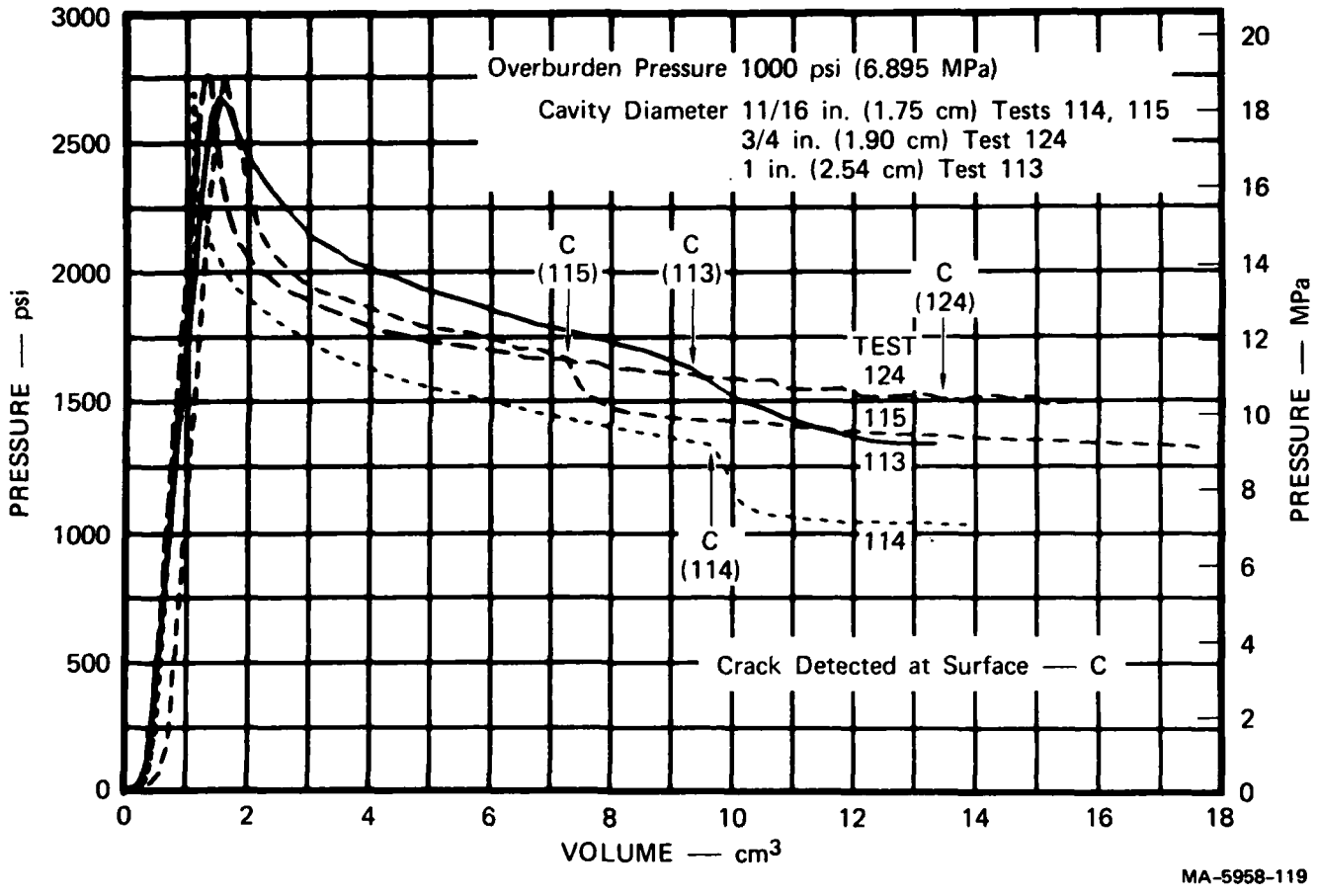

FIGURE 3.6 HYDROFRACTURE PRESSURES FOR UNEXPLODED CAVITY TESTS 113, 114, 115, AND 124—CAVITY SIZE EFFECT

Examination of each sphere following the tests shows that the variations in steady-state pressure may be attributed to the sectorial extent of cracking in the fracture plane, with lower pressures corresponding to larger fractured regions. Hence, a small change in cavity size appears to have negligible effect on the pressure records. This result is valid only for smooth cavities, whereas previous tests with notched cavities[5] have shown that an increase in size tends to reduce fracture initiation pressure.

Series 4 - Internal Fracture

Tests 144 and 147 were conducted to provide data for determining the motion of a propagating crack tip during hydrofracture. An array of brittle graphite rods described in Section 2.3 was embedded in a sphere with a 3/4-inch-diameter (1.90-cm) cavity. The rods were positioned in the equitorial plane at distances of 1.5, 3, and 4.5 inches (3.81, 7.62, and 11.43 cm) from the center of the sphere. Ideally, arrival of the crack would break a rod and produce a change in resistance. However, surface fracture was detected and a steady fluid flow developed before any of the rods broke; that is, the embedded gages lacked the sensitivity to detect the leading edge of a crack. Furthermore, the rods, even though weak in tension, apparently acted as reinforcing bars in restricting separation of the fracture surfaces. This effect is shown in Figure 3.7. The average steady-state pressure for tests 144 and 147 was 1750 psi (12.1 MPa). For the reproducibility tests of series 1, where no embedded gage was used, steady-state pressures averaged 1300 psi (9.0 MPa); the record for reproducibility test 137 is shown in Figure 3.7 as a representative example. Also, the irregularities in the pressure records for tests 144 and 147 suggest a flow restriction. Breaking of the graphite required more than 18 cm^3 of fluid and had no apparent effect on the pressure record.

As described in Section 2.3, grout rods striped with conductive paint provide a more sensitive and less perturbing stress gage. Use of such a gage is planned in future hydrofracture tests.

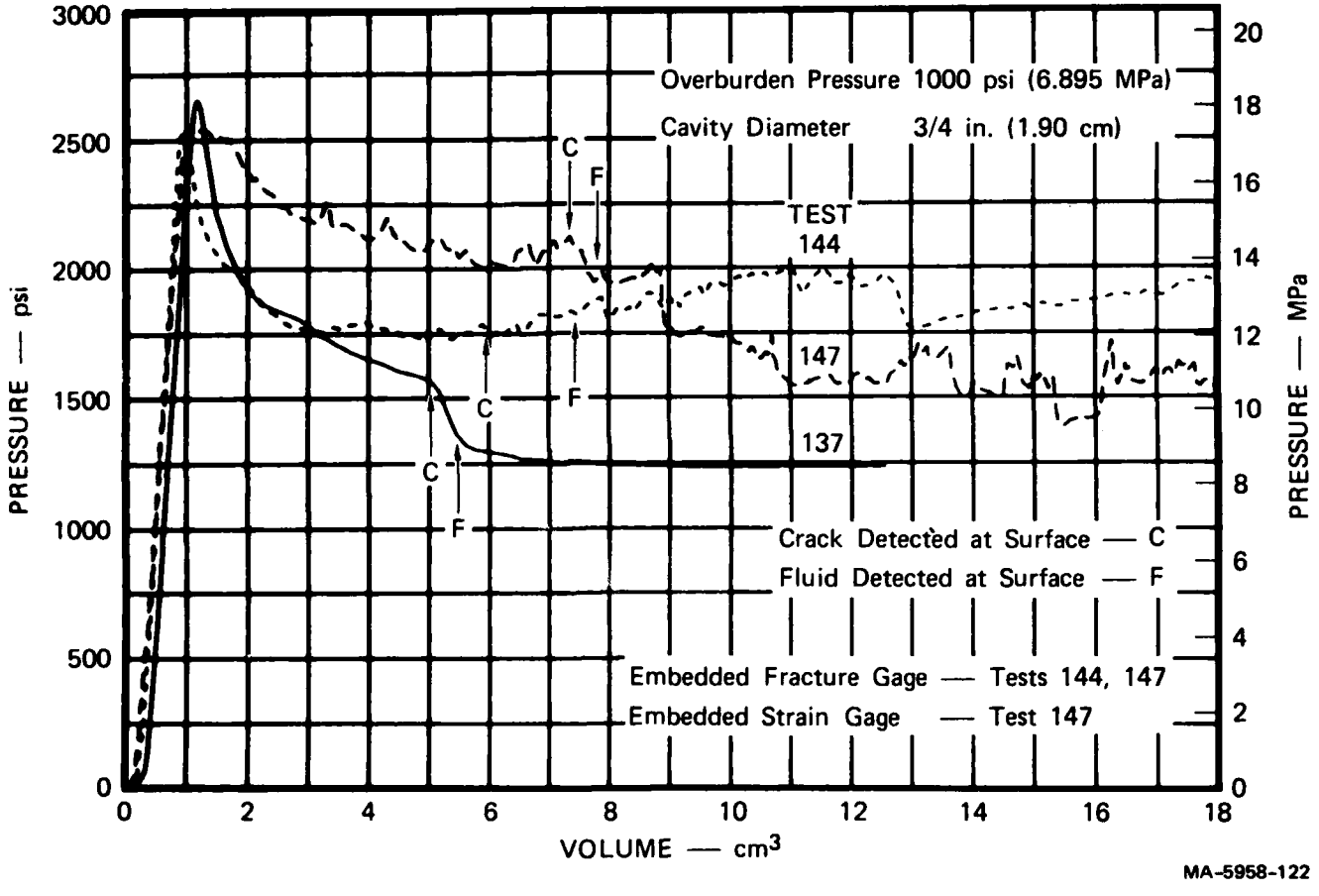

FIGURE 3.7 HYDROFRACTURE PRESSURES FOR UNEXPLODED CAVITY TESTS 137, 144, AND 147—SURFACE FLUID AND FRACTURE ARRIVAL

Series 5 - Surface Fracture

Surface fracture of spheres during hydrofracture was detected by means of the paint stripe gages described in Section 2.3. The fracture plane associated with an unexploded cavity is invariably oriented in the vertical direction (parallel to tube). Hence gages were used as a series of horizontal strips in an attempt to detect the first appearance of the crack tip. Since the gages covered only a small portion of the total surface area of a given sphere, the volume of hydrofracture fluid associated with the detection of a surface fracture is an upper bound estimate of the actual volume required to initiate surface cracking. Also, the volumes quoted below are measured from the point of fracture initiation, since, as discussed for the series 1 test for reproducibility, no actual flow occurs before then. For the reproducibility tests of series 1, Figures 3.1 and 3.2 show that the minimum fluid volume required to initiate a surface fracture was 3.8 cm^3 in test 137. The sudden change in slope of the pressure record is a strong indication that a surface fracture did suddenly occur at this time. Also, steady-state flow was then quickly established.

Test 134, the zero overburden test, was conducted in a transparent vessel and provided an opportunity for a visual check on the performance of the surface fracture gage. Figure 3.4 shows that a dramatic change in slope of the pressure recorded coincided with the detection of surface fracture. Visual inspection confirmed that a fracture plane reached the surface at this time and spread rapidly. Steady-state flow was soon established. The 2.3 cm^3 of flow required to propagate the crack to the surface was less than the 3.8 cm^3 minimum required for the 1000-psi (6.9 MPa) tests. Hence increased overburden apparently retards the rate of crack growth.

Pressure records for the 11/16- and 1-inch-diameter (1.75- and 2.54-cm) cavity tests shown in Figure 3.6 reveal that slope changes and surface crack detection coincide after 5.6, 5.8, and 8.5 cm^3 of flow. Hence the minimum volume of fluid required for surface cracking appears to be less reproducible than fracture initiation pressure, presumably because of dependence on asymmetry of crack growth.

Results of the surface fracture studies on the remaining unexploded cavity spheres give no indication of a surface crack occurring with less than the 3.8 cm^3 of flow found in test 137.

Series 6 - Surface Fluid Arrival

Arrival of hydrofracture fluid at the surface of a sphere was detected by means of the copper wires described in Section 2.3. Each wire was positioned adjacent to a fracture gage, as shown in Figure 2.9, so that the volumes of fluid required to initiate surface fracture and fluid arrival could be compared. An estimate of the distance between fluid and crack tip at an arbitrary radial position requires that at least two pairs of fracture and fluid arrival gages be used.

Surface fracture and fluid arrival for tests 137, 144, and 147 are shown in Figure 3.7. The flow between surface cracking and fluid arrival was 0.5, 0.4, and 1.5 cm^3 for the respective tests.

Series 7 - Internal Strain Measurements

Radial strain near an unexploded cavity was measured by means of the encapsulated strain gage described in Section 2.3. In each sphere the gage was cast in the plane of the equator two cavity radii from the center. The method of suspension during the casting process ranged from an attached flexible tube to the guide wires shown in Figure 2.11. Strains were generated by overburden and hydrofracture pressures.

Pressure records for strain gage tests 128, 129, and 132 are shown in Figure 3.8. A comparison of these results with those of the reproducibility tests in Figure 3.1 shows that the strain gage had no significant effect on hydrofracture pressures. In tests 128 and 129 the fracture plane bypassed the gage. However, as shown in Figure 3.9, two distinct fracture planes developed in test 132, and one of them intersected the gage.

The pressure record for test 147, which also included a strain gage, is shown in Figure 3.7. This test also had an embedded fracture gage.

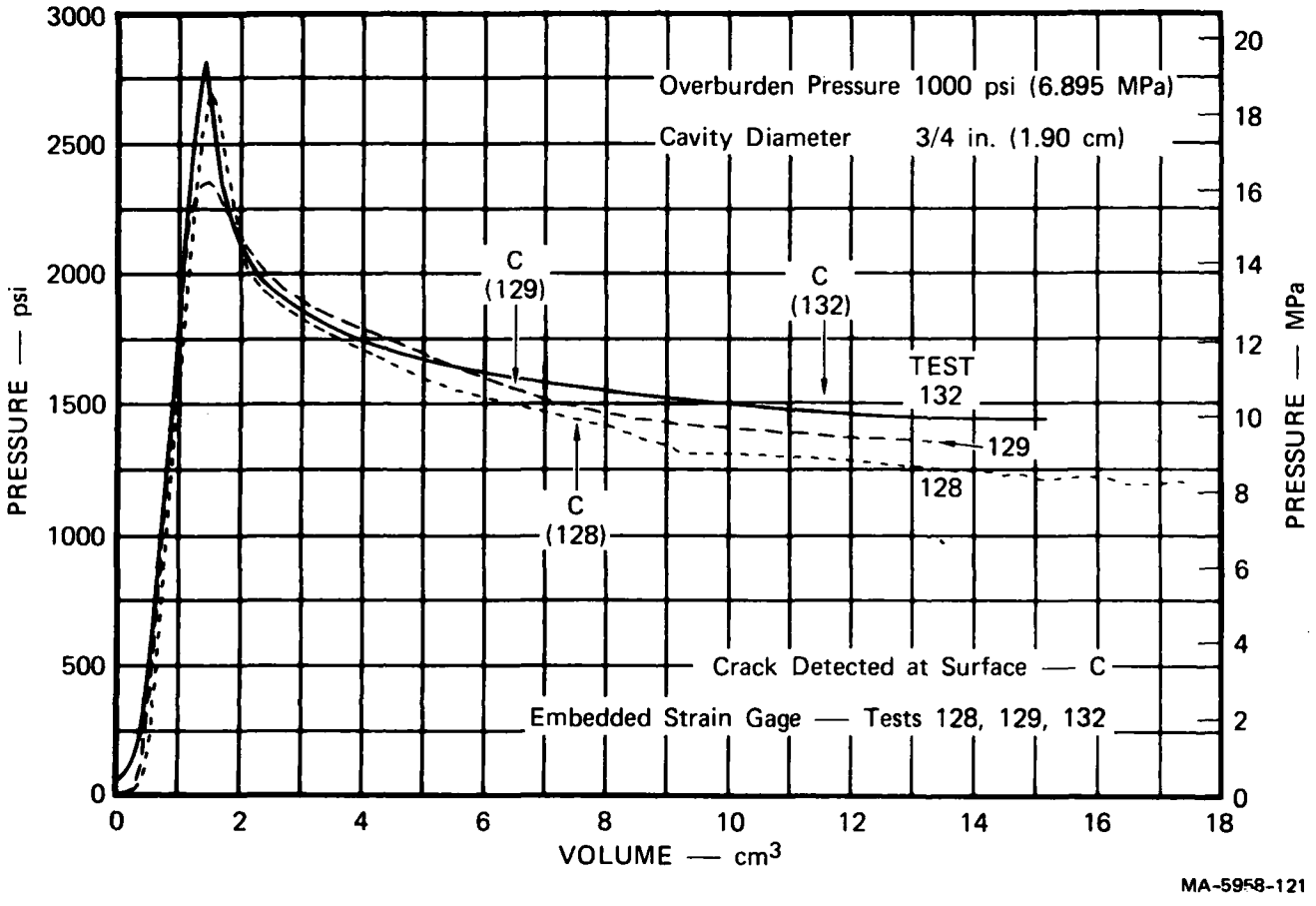

FIGURE 3.8 HYDROFRACTURE PRESSURES FOR UNEXPLODED CAVITY TESTS 128, 129, AND 132—INTERNAL STRAIN MEASUREMENT

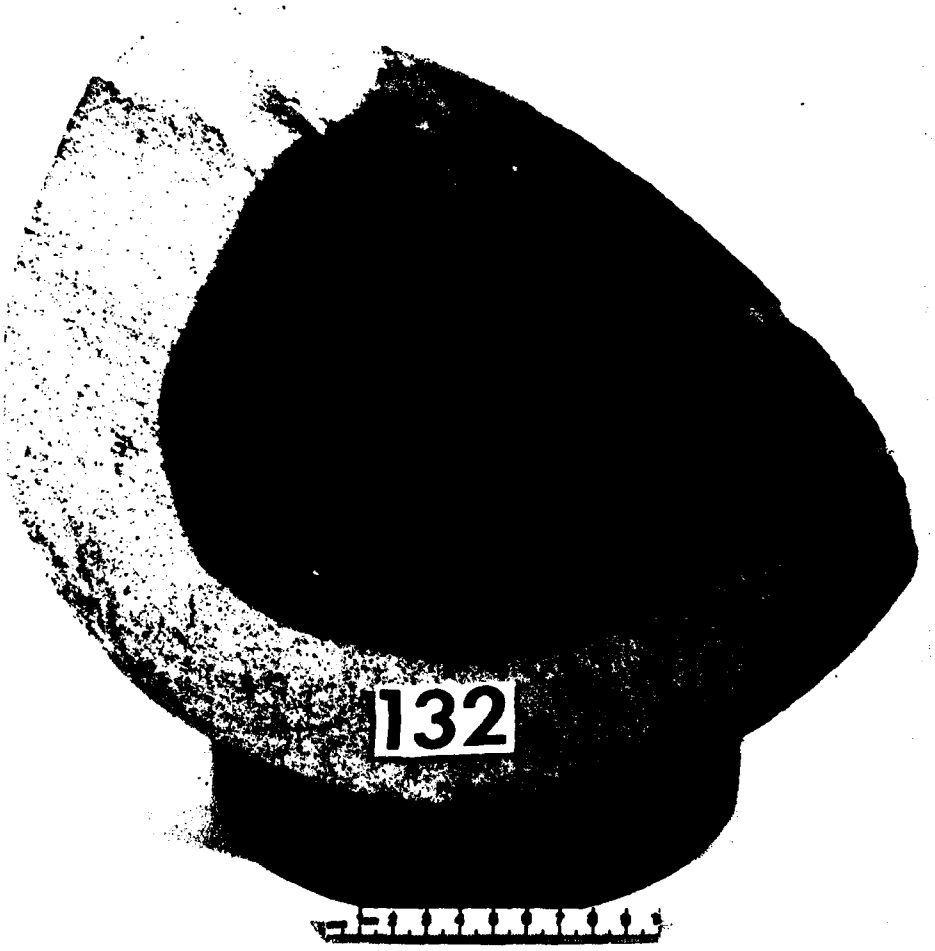

MP-5958-109

FIGURE 3.9 HYDROFRACTURE FROM UNEXPLODED CAVITY TEST 132

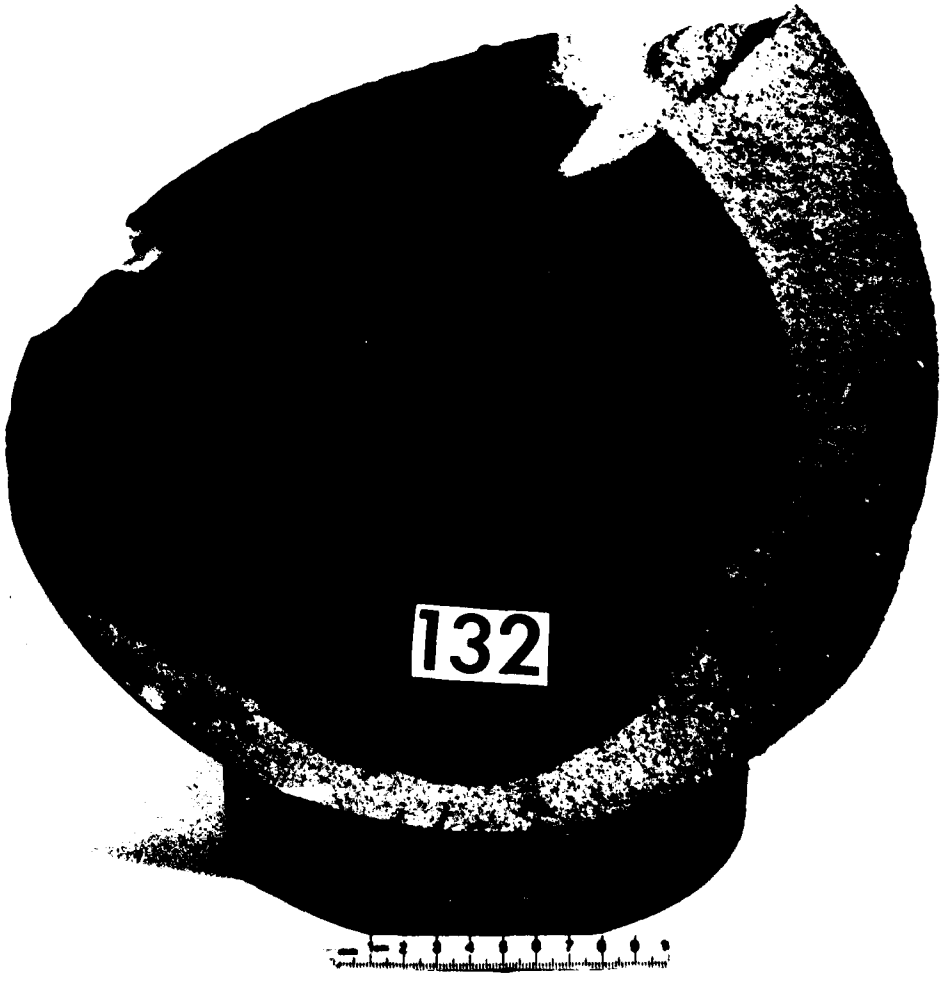

MP-5958-110

FIGURE 3.9 HYDROFRACTURE FROM UNEXPLODED CAVITY TEST 132 (Continued)

MP-5958-111

FIGURE 3.9 HYDROFRACTURE FROM UNEXPLODED CAVITY TEST 132 (Concluded)

The high late-time steady-state pressure is attributed to the presence of the fracture gage.

Experimental strain records are shown in Figure 3.10. Since the maximum strains are elastic (less than 1500 μ-strain), an elasticity theory prediction based on a typical pressure record is included. The theory, which neglects the effects of cracking and subsequent fluid flow, predicts a radial strain of 105 μ-strain for 1000 psi (6.9 MPa) overburden and zero cavity pressure. The corresponding experimental values ranged from 106 to 317 μ-strain. Since the theory also neglects the effects of creep, higher experimental values are expected. However, the effects of creep do not account for the spread of the results. The lack of reproducibility is currently attributed to variable grout properties under initial loading at small stress. In Figure 3.11 the strain records of Figure 3.10 have been shifted to agree with the theoretical overburden strain. Even with this shifting, a spectrum of experimental strain records is produced, with the theoretical curve at the low end of the spectrum.

Several features of the strain records are noteworthy. For example, the discontinuities in the record of test 132 reflect the arrival of a fracture plane at the gage and the subsequent arrival of hydrofracture fluid. Also, the large steady-state strains in test 147 reflect the large steady-state pressures.

Series 8 - Cavity Lining

Attempts were made to jacket an unexploded cavity with an impermeable rubber membrane using the technique described in Section 2.3. A successful lining prevents hydrofracture fluid from acting directly on the walls of the cavity and from entering the fracture plane following fracture initiation. A comparison of pressure records for lined and unlined cavities then allows assessment of the effects of hydrofracture fluid on the fracture initiation pressure and stability of subsequent crack growth.

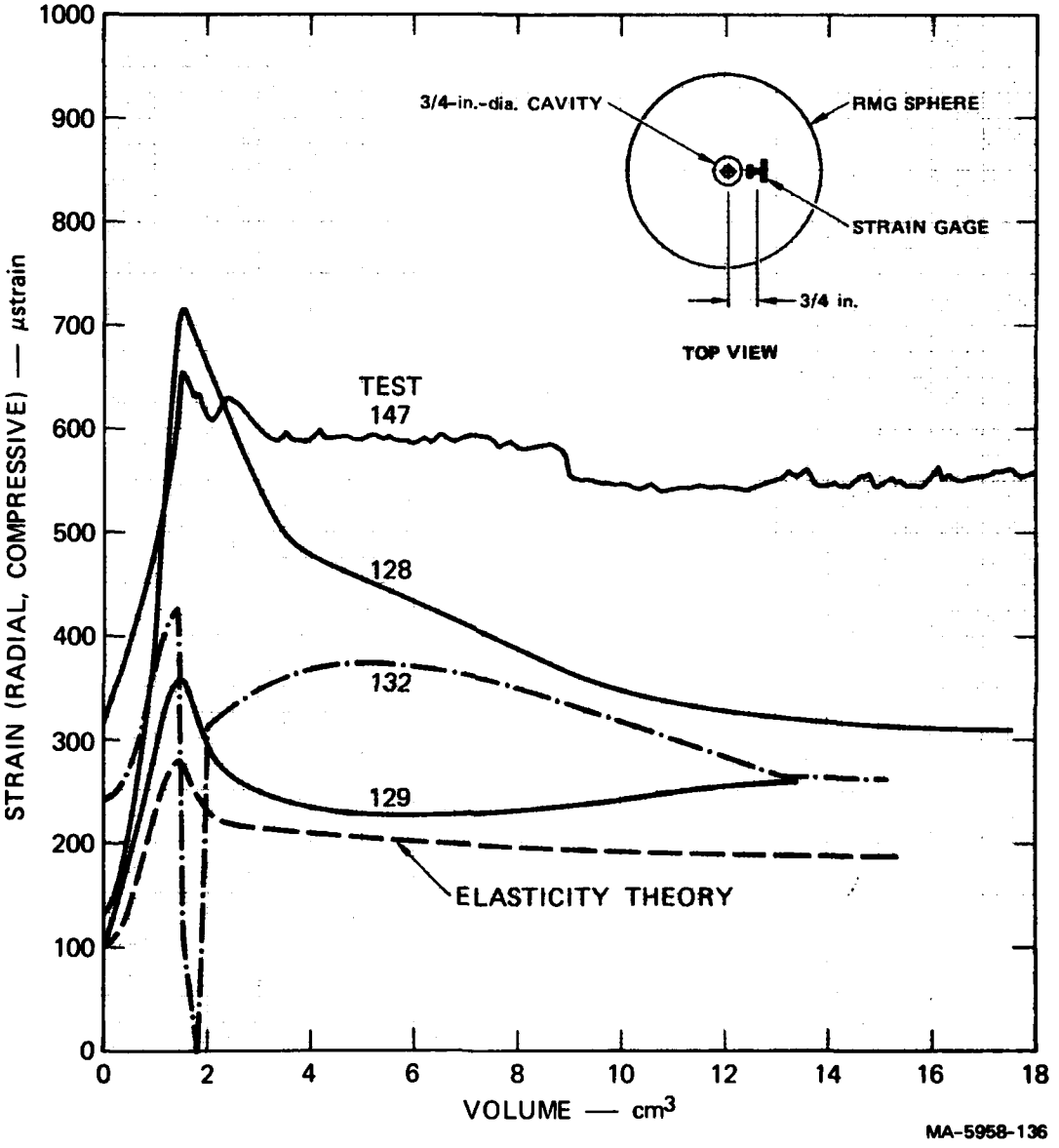

FIGURE 3.10 RADIAL STRAINS FOR UNEXPLODED CAVITY TESTS 128, 129, 132, AND 147

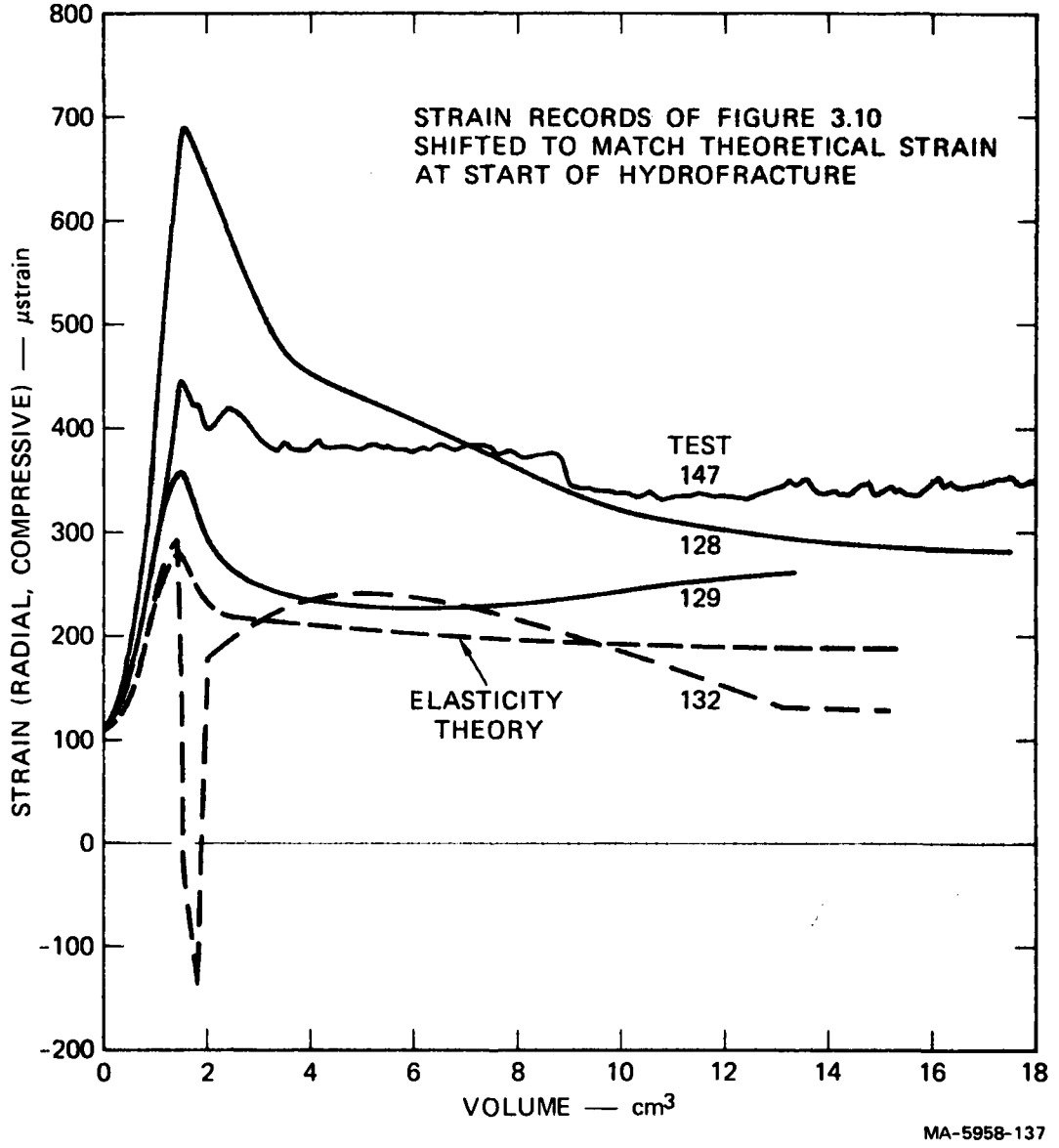

FIGURE 3.11 ADJUSTED RADIAL STRAINS FOR UNEXPLODED CAVITY TESTS 128, 129, 132, AND 147

Pressure records for the 1-inch-diameter (2.54-cm) lined cavity tests 126 and 127 are shown in Figure 3.12. Since the membrane was not fully expanded when pumping began, a large volume of fluid was required initially to fill the cavity. In each test the membrane developed a pinhole size leak that allowed fluid to escape. Hence only a partial lining was actually provided. The fluid loss is reflected in the spikes on the hydrofracture records near 1000 psi (6.9 MPa). With a restricted flow, pressures in excess of 3000 psi (20.7 MPa) were required to initiate fracture. The large steady-state pressures that followed are attributable, as least in part, to the flow restriction of the membrane. Figure 3.13 shows that the extent of cracking was comparable to that found in an unlined cavity. For an equivalent unlined cavity, fracture initiation occurred at 2750 psi (19.0 MPa). Hence, even with partial cavity lining, containment appears to be improved.

3.3 EXPLODED CAVITY TESTS

Series 9 - Reproducibility

Vented exploded cavity hydrofracture tests were performed to assess reproducibility of the experimental technique and to provide reference data for the parameter studies. The configuration for these tests centered on the vented explosive source described in Section 2.2. A 3/8-gram charge was chosen. The charge calibration tests described in Section 2.4 showed that reproducibility of the 3/8-gram charge is adequate for use in exploded cavity tests.

The basic hydrofracture system is described in Section 2.2. In the reproducibility tests described here, overburden was fixed at 1000 psi (6.9 MPa) and dyed glycerol was pumped into the vented exploded cavities at a rate of 4.26 cm^3/min. Pressure records for tests 117, 118, 119, and 120 are shown in Figure 3.14. The results are typical of exploded cavity tests in that pressure increased smoothly to a local maximum, decreased slightly, then increased to a maximum before decaying to a steady state. Previous tests[5] on exploded cavities have shown that fracture initiation occurs at the first pressure maximum and is followed

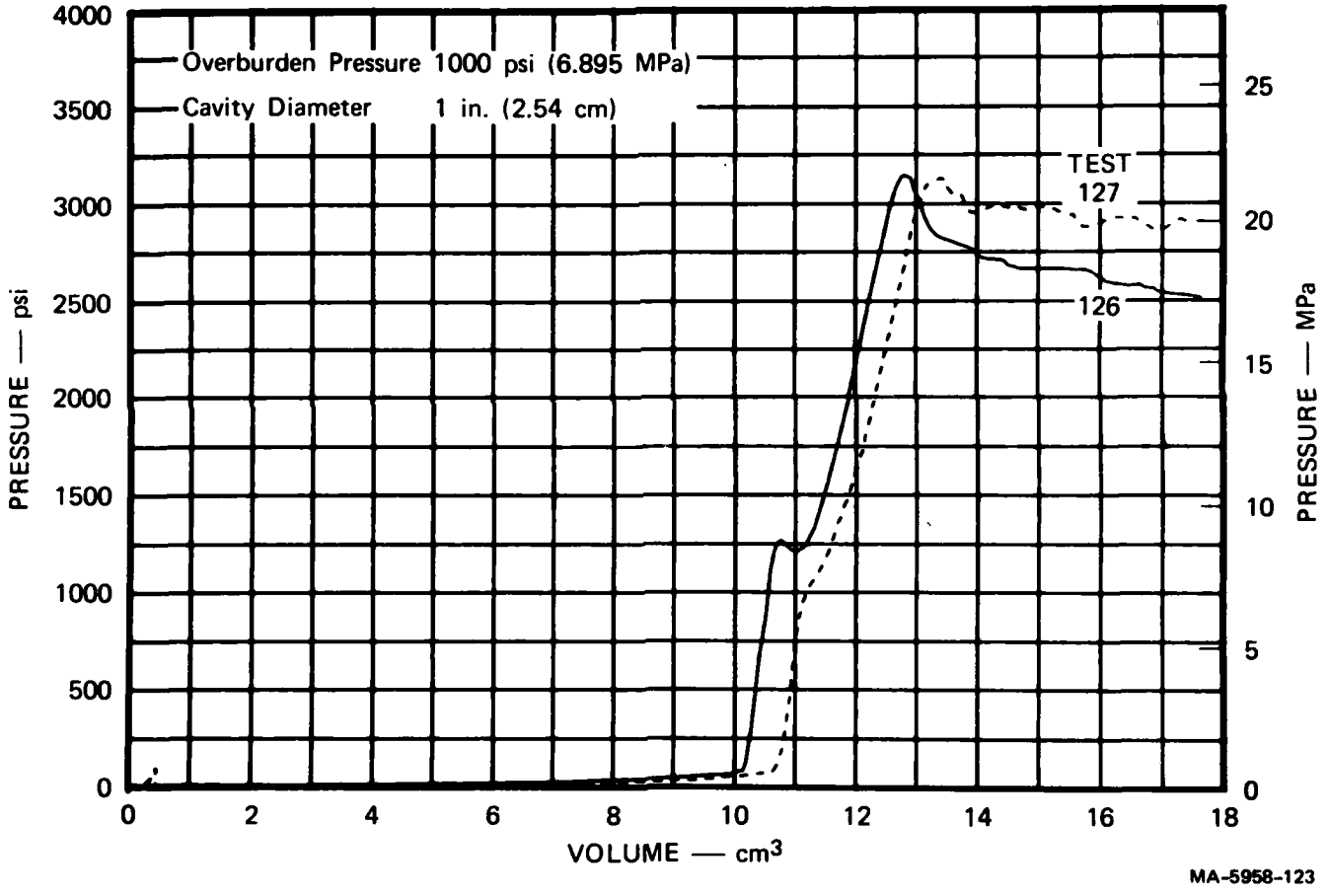

FIGURE 3.12 HYDROFRACTURE PRESSURES FOR UNEXPLODED CAVITY TESTS 126 AND 127—CAVITY LINING

MP-5958-105

FIGURE 3.13 HYDROFRACTURE FROM UNEXPLODED CAVITY TEST 127

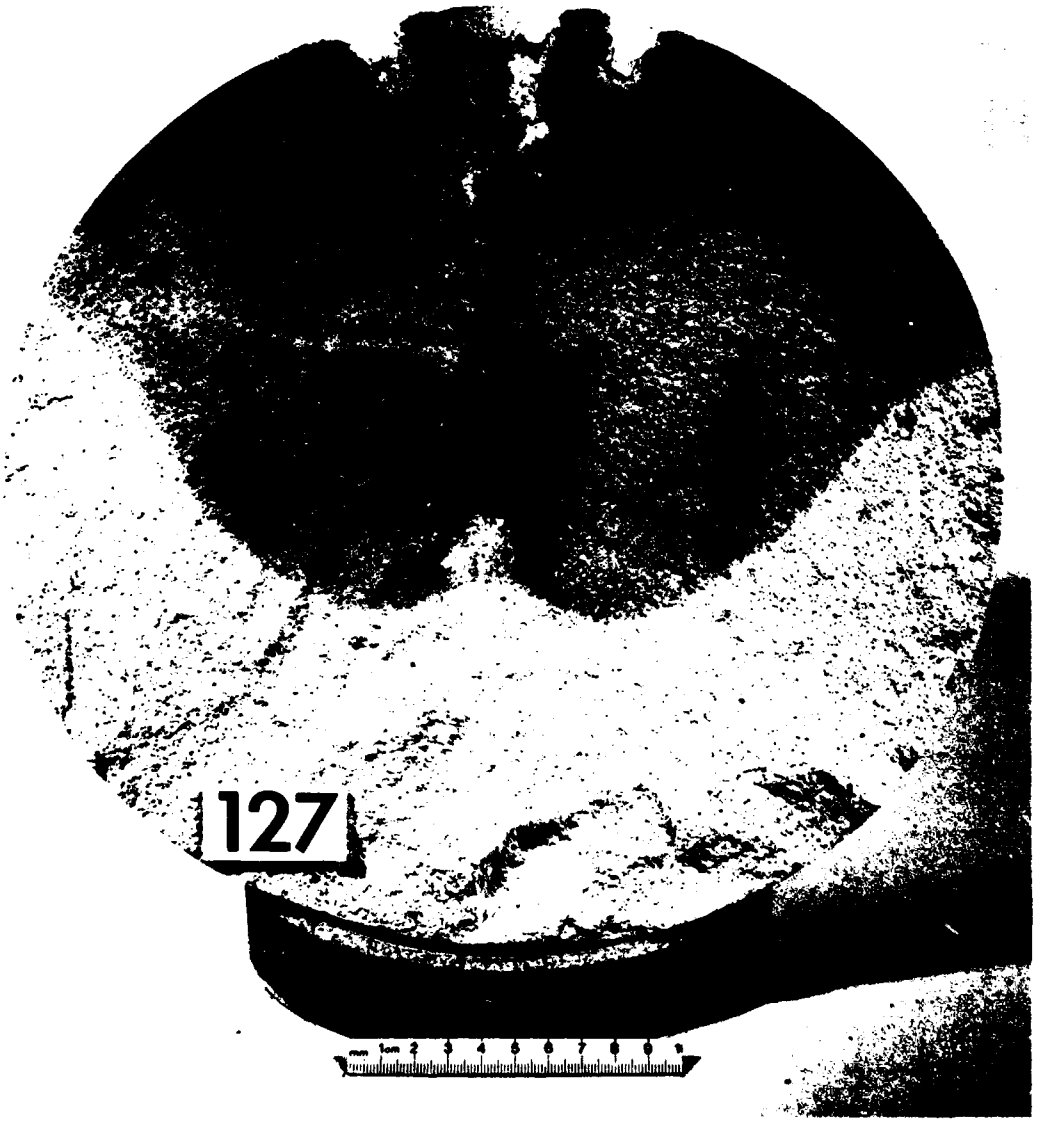

MP-5958-106

FIGURE 3.13 HYDROFRACTURE FROM UNEXPLODED CAVITY TEST 127 (Concluded)

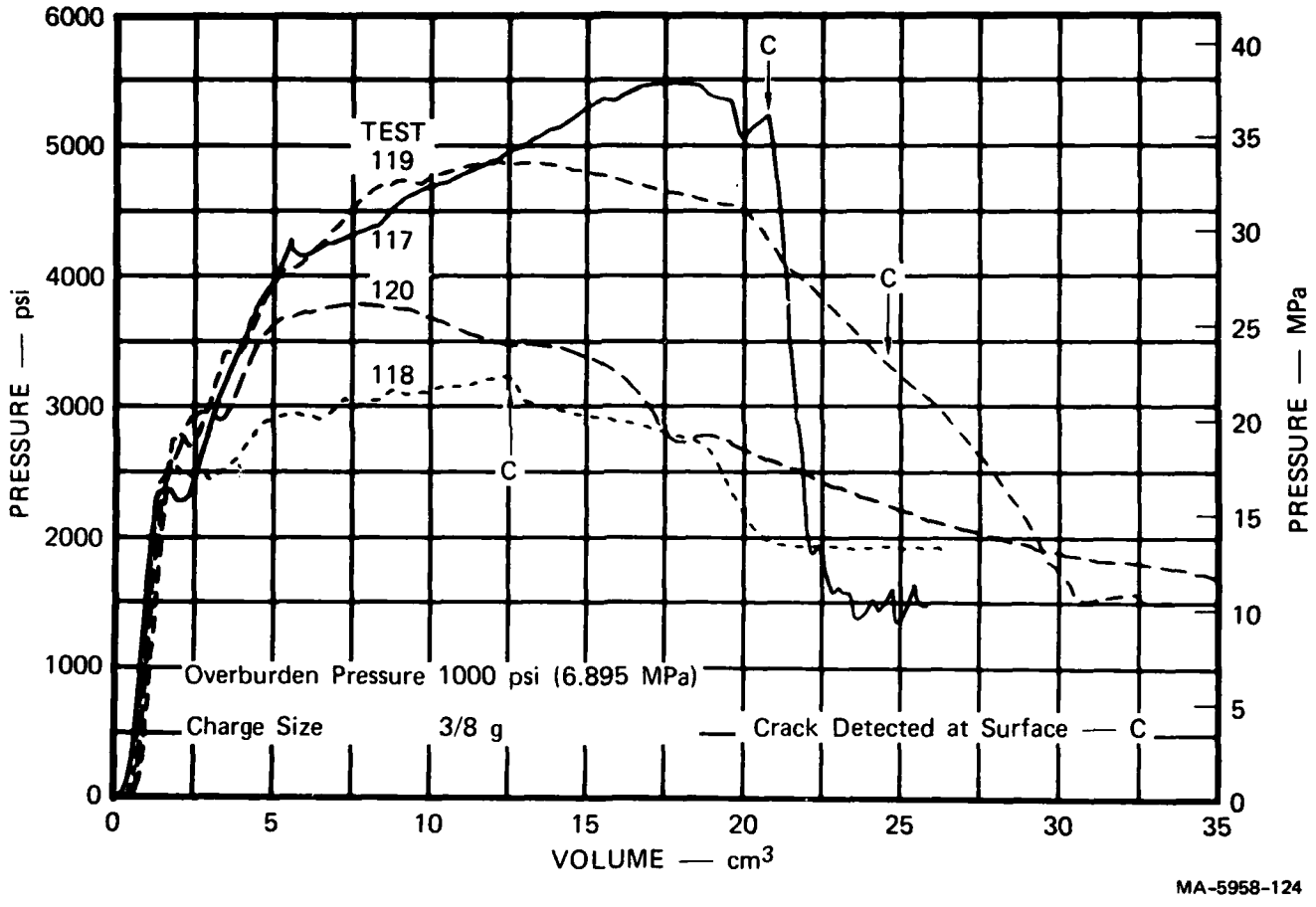

FIGURE 3.14 HYDROFRACTURE PRESSURES FOR VENTED EXPLODED CAVITY TESTS 117, 118, 119, AND 120—REPRODUCIBILITY

by rapid crack growth. Reproducibility of the fracture initiation pressure is good, with a maximum deviation of 12.3% from the 2690-psi (18.5-MPa) average. Also, steady-state pressures are consistent, with a value in the range 1500 to 1900 psi (10.3 to 13.1 MPa).

The most striking feature of the hydrofracture records is the spectrum of maximum pressures, which ranges from 3270 to 5480 psi (22.5 to 37.8 MPa). This spectrum is comparable to that found in the 1/4-gram charge tests. Since an increase in pressure following fracture initiation suggests an increase in flow resistance, a test at the higher end of the spectrum (test 118) should produce a more intensely dyed fracture surface than a test at the low end (test 117). A comparison of Figures 3.15 (test 117) and 3.16 (test 118) confirms this observation. Furthermore, flow resistance along one fracture surface may be influenced by the initiation and growth of others. Posttest sectioning of exploded cavity spheres reveals the presence of secondary fracture planes. Hence the spectrum of pressure records associated with exploded cavity tests may be the result of a random development of multiple fracture planes. Partial blockage of the fracture planes by crushed grout may also contribute to the spectrum by producing variations in pressure gradients near the cavity.

Series 10 - Unvented Cavity

The technique for constructing an unvented exploded cavity was described in Section 2.2. With this configuration, the cavity pressure resulting from charge detonation was measured. Also, the subsequent hydrofracture began soon after charge detonation so that stress relaxation due to loss of cavity pressure and material relaxation could be minimized. To allow for a comparison of vented and unvented cavity pressure records, a 3/8-gram charge, a 1000-psi (6.9-MPa) overburden, and a 4.26-cm^3/min flow rate were used in all exploded cavity tests.

Hydrofracture records for tests 135 and 142 are shown in Figure 3.17. Residual cavity gas pressure had decayed to approximately 1000 psi (6.9 MPa) when hydrofracture began. Compression of these cavity gases resulted in

MP-5958-99

FIGURE 3.15 HYDROFRACTURE FROM VENTED EXPLODED CAVITY TEST 117

MP-5958-100

FIGURE 3.15 HYDROFRACTURE FROM VENTED EXPLODED CAVITY TEST 117 (Concluded)

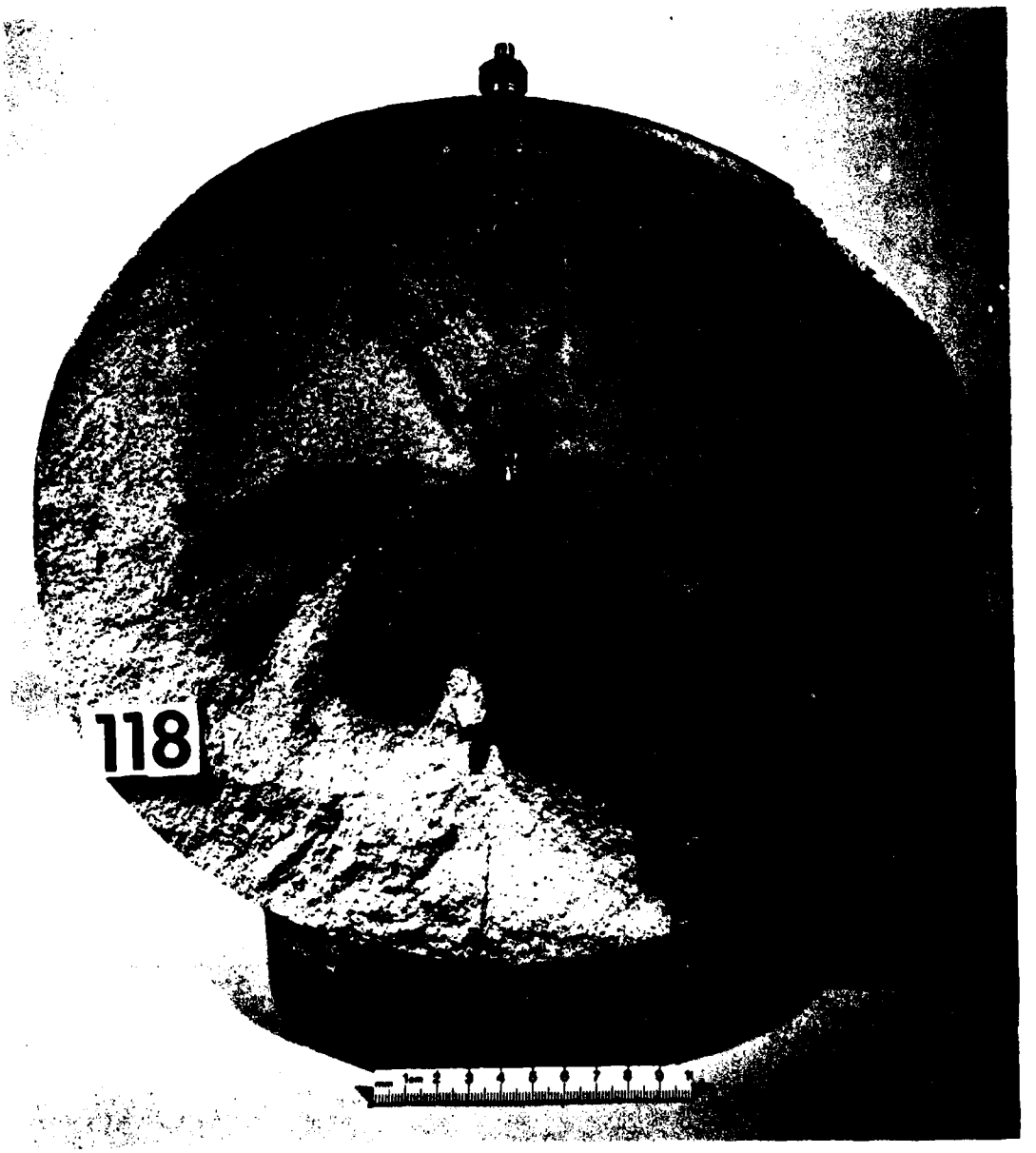

MP-5958-101

FIGURE 3.16 HYDROFRACTURE FROM VENTED EXPLODED CAVITY TEST 118

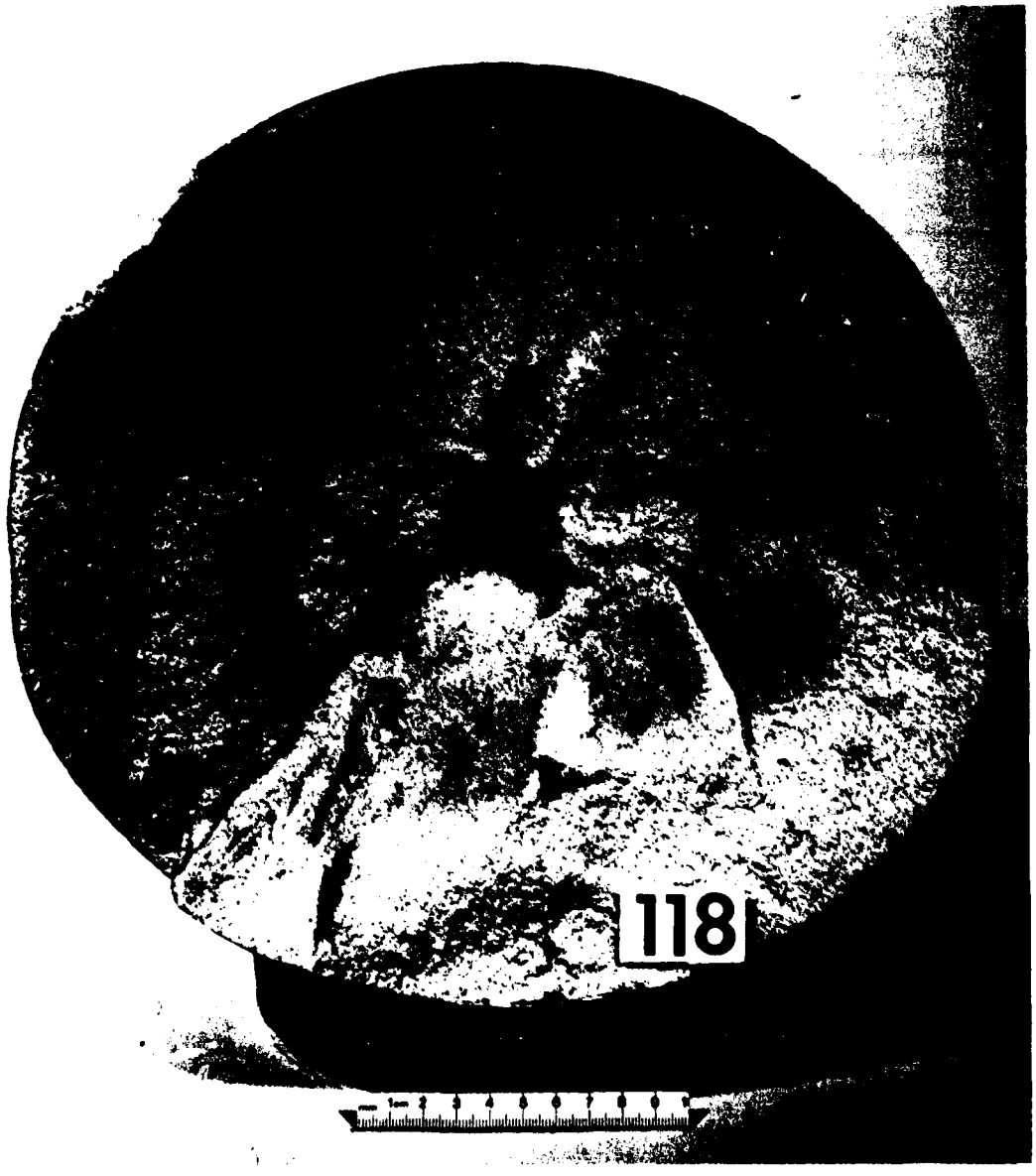

MP-5958-102

FIGURE 3.16 HYDROFRACTURE FROM VENTED EXPLODED CAVITY TEST 118 (Concluded)

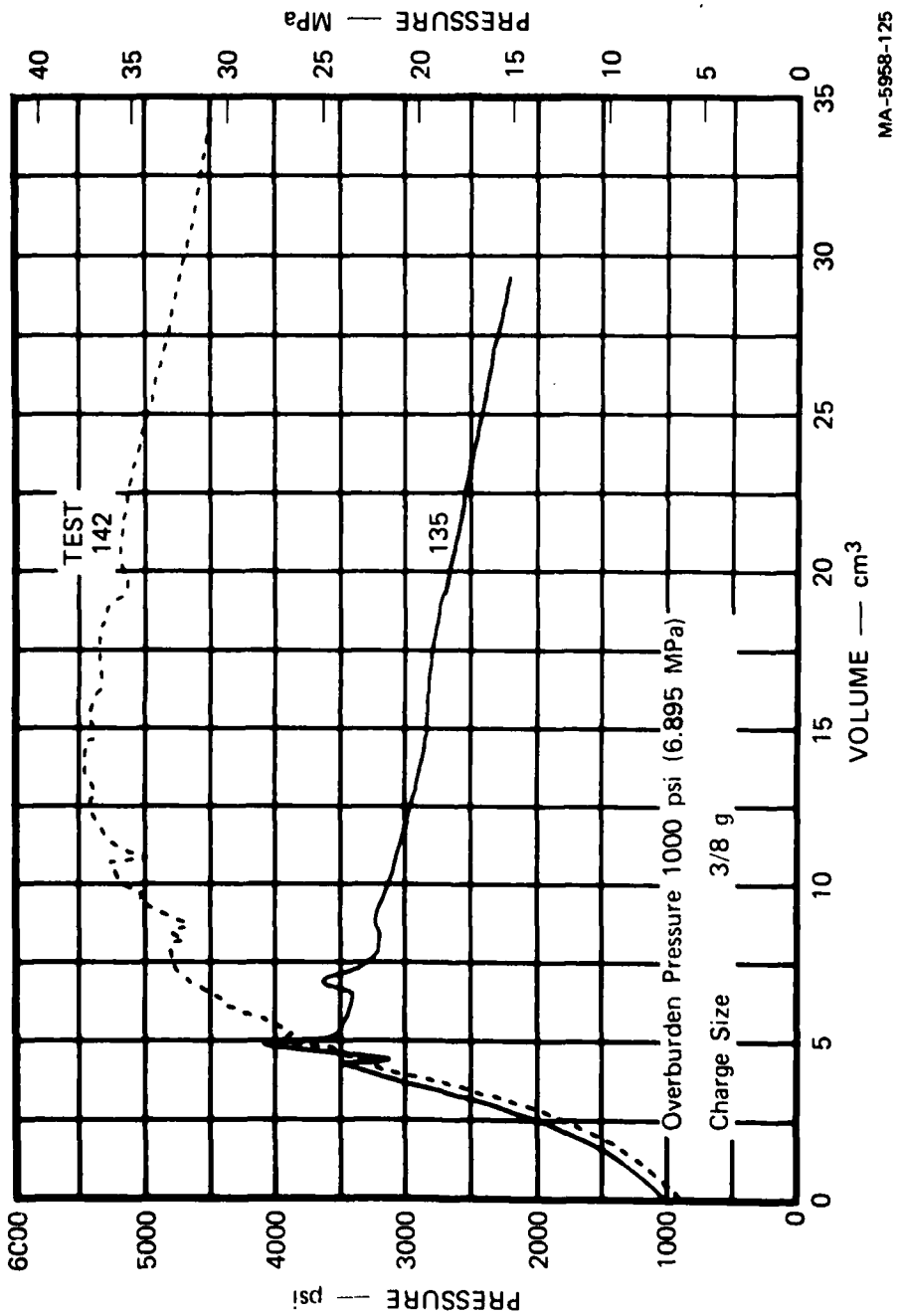

FIGURE 3.17 HYDROFRACTURE PRESSURES FOR UNVENTED EXPLODED CAVITY TESTS 135 AND 142

the initially slow pressure increase. Fracture initiation in test 135 was marked by a pronounced pressure peak at 3520 psi (24.3 MPa). In test 142, a change in slope at 3260 psi (22.5 MPa) was the first indication of a crack forming in the cavity wall. Both of these values represent an improvement in the 2690-psi (18.5-MPa) average fracture initiation pressure for vented cavities. Following fracture initiation, a spectrum of results similar to that of the vented cavities was generated. Maximum cavity pressures reached 4120 and 5490 psi (28.4 and 37.9 MPa). The subsequent rate of decay was the same for each unvented cavity, but generally less than the decay found in vented cavities. Overall, an unvented cavity represents an improvement in containment capability over a vented cavity.

Measurement of cavity gas pressure requires containment of the detonation products. Figure 3.18 shows the hydrofracture in test 131 where gases escaped from the cavity and vented along a tube that carried wires from the charge. Elimination of the tube resulted in the more uniform hydrofracture shown in Figure 3.19 for test 135. With the improved charge installation, cavity gas pressure following charge detonation decayed with time as shown in Figure 3.20. Delay in opening a valve accounts for each lapse in time between detonation and the start of measurement. This delay will be eliminated in future tests. Hydrofracture in tests 135 and 142 began 95 and 51 sec after detonation, respectively. The corresponding cavity pressures decayed to 1000 and 920 psi (6.9 and 6.3 MPa).

A theoretical estimate of the gas pressure in a dynamically expanding cavity is shown in Figure 3.21. The curve was derived from the pressure-volume data listed in Table 3.2. The explosive source used in the calculations was assumed to be a mixture of the PETN and Lucite. This assumption is based on the experimental observation that the Lucite charge holder is completely consumed in the explosion. Since the exploded cavity diameter is twice the initial cavity diameter, the theoretical estimate of cavity pressure immediately following detonation is found to be 11,000 psi (75.8 MPa). The pressure measured 1.5 sec after detonation was only 2040 psi (14.1 MPa). Hence significant decay in pressure occurs soon

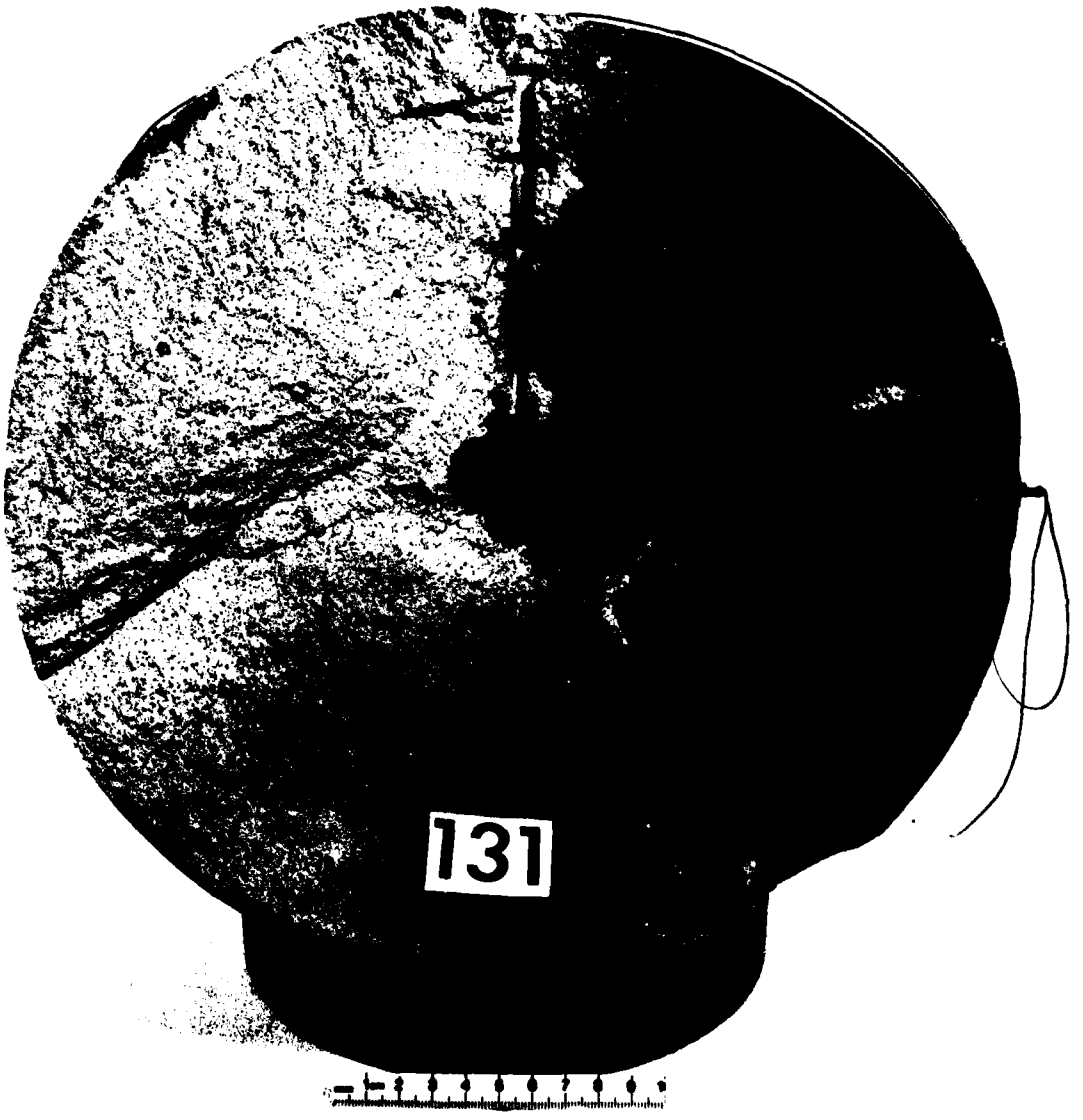

MP-5958-107

FIGURE 3.18 HYDROFRACTURE FROM UNVENTED CAVITY TEST 131

MP-5958-108

FIGURE 3.18 HYDROFRACTURE FROM UNVENTED CAVITY TEST 131 (Concluded)

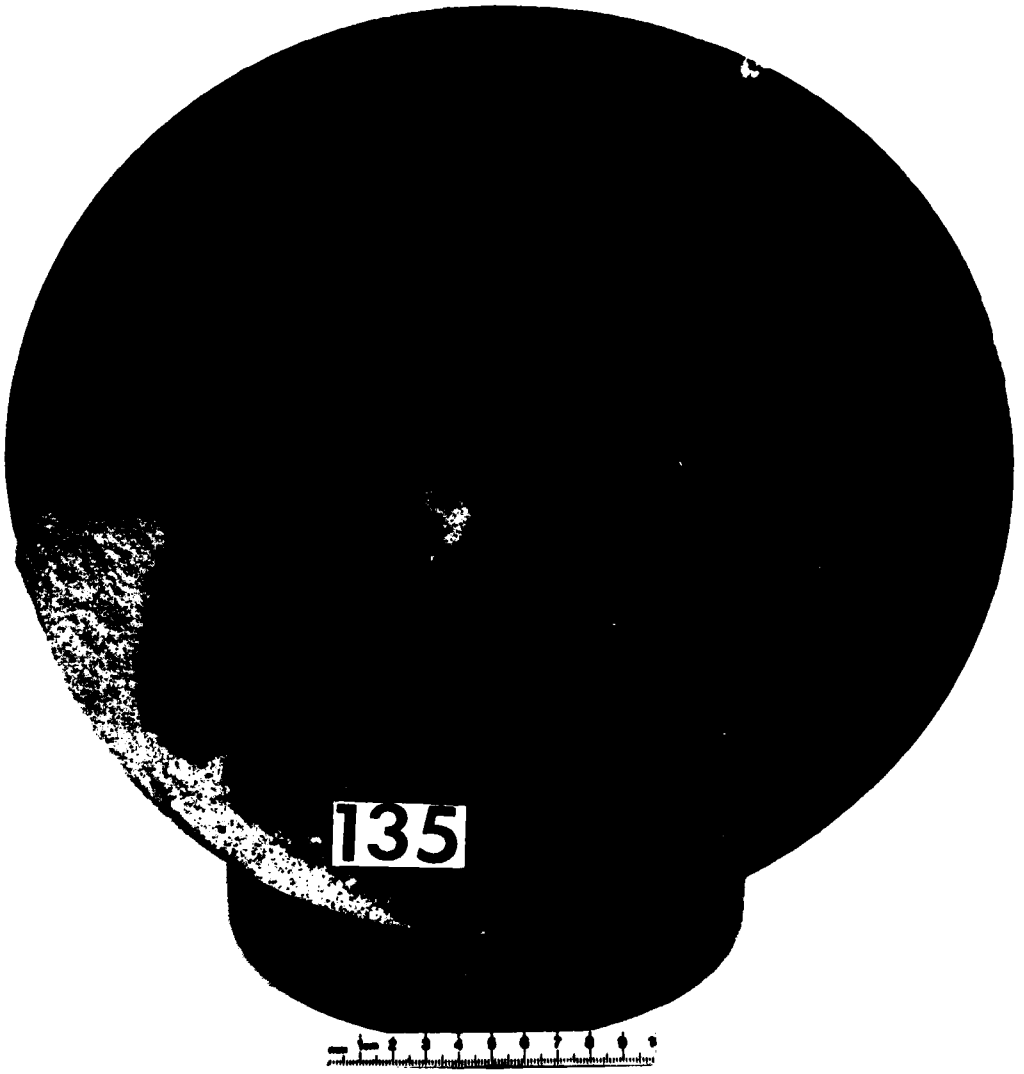

MP-5958-112

FIGURE 3.19 HYDROFRACTURE FROM UNVENTED CAVITY TEST 135

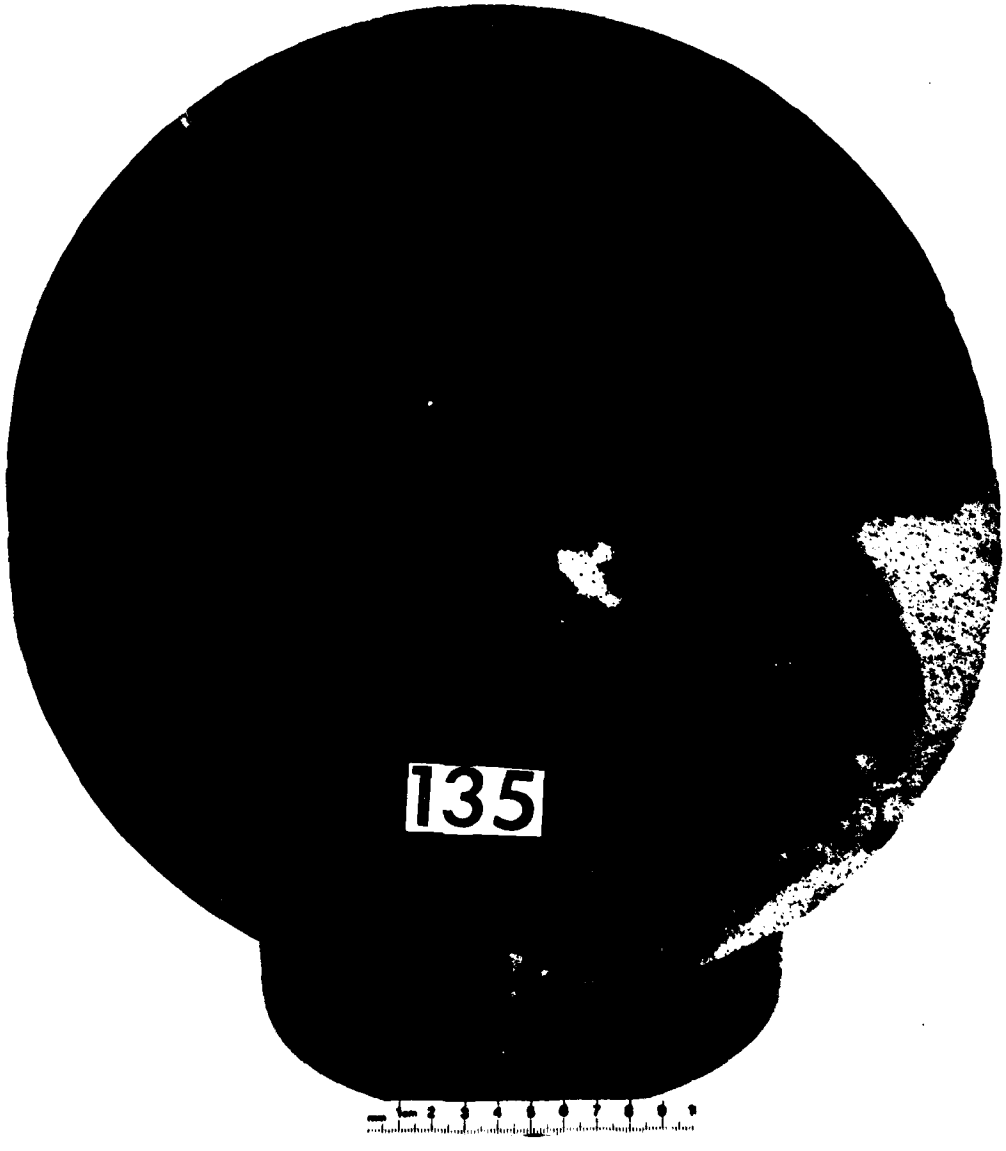

MP-5958-113

FIGURE 3.19 HYDROFRACTURE FROM UNVENTED CAVITY TEST 135 (Concluded)

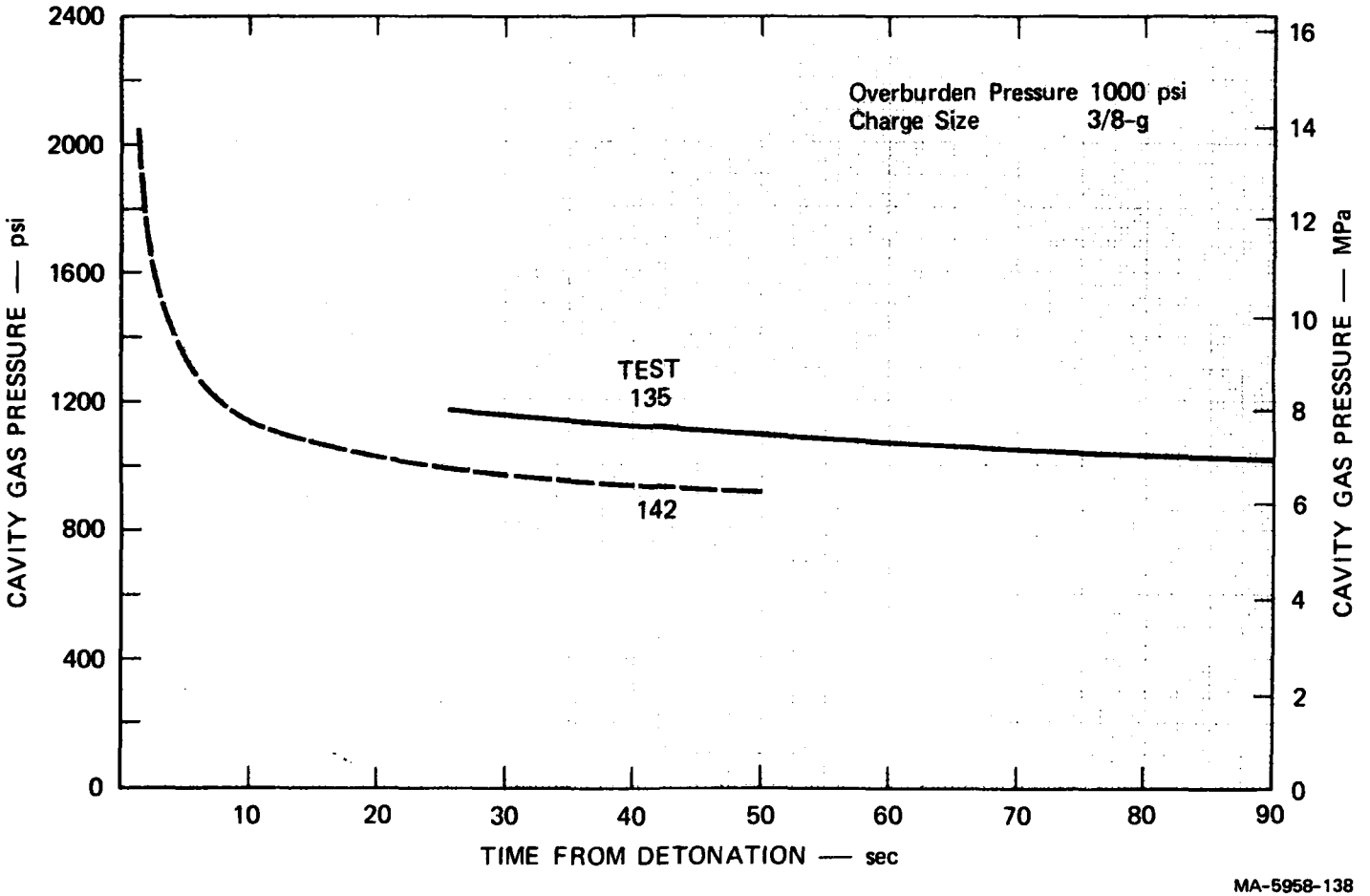

FIGURE 3.20 RESIDUAL CAVITY GAS PRESSURES FOR UNVENTED EXPLODED CAVITY TESTS 135 AND 142

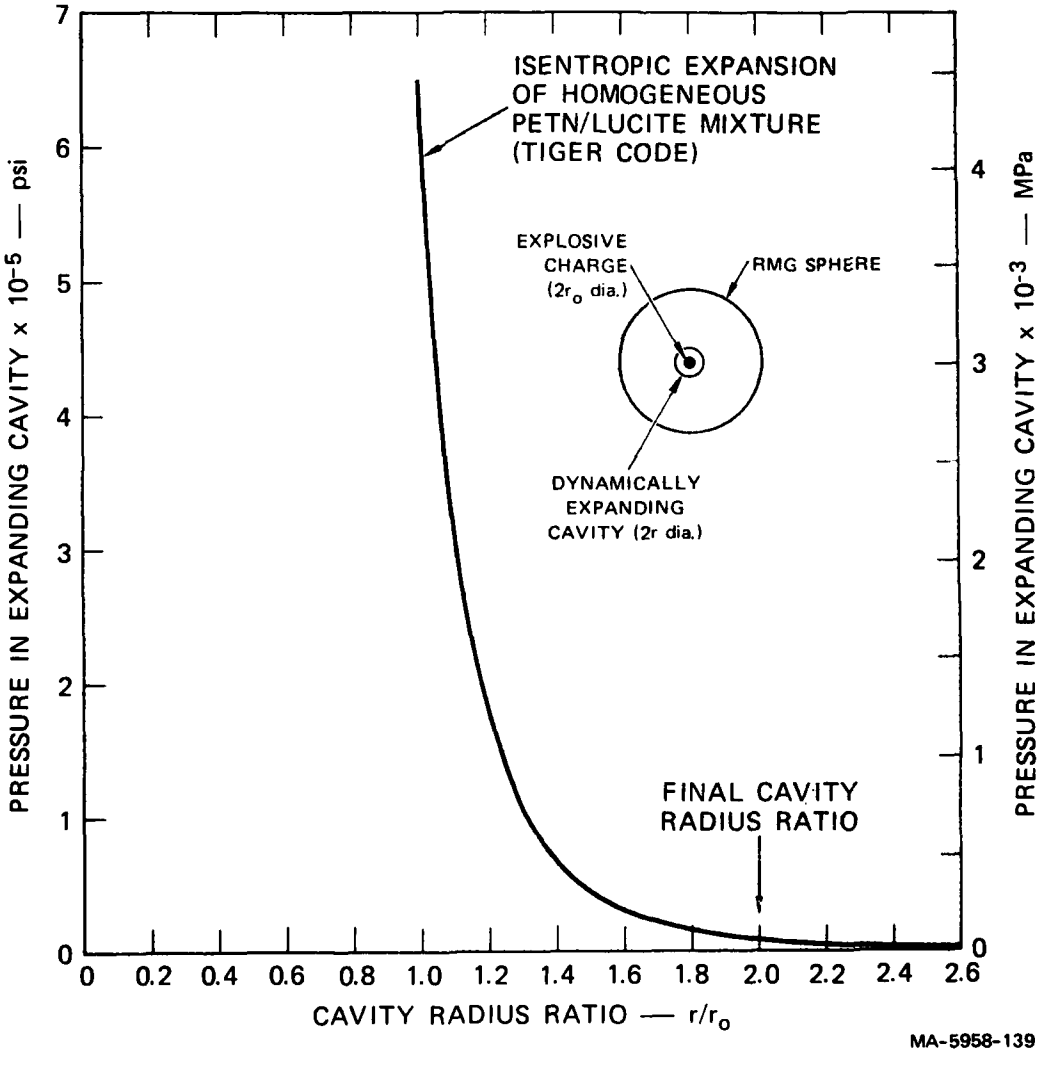

FIGURE 3.21 CALCULATED CAVITY GAS PRESSURE FOR A DYNAMICALLY EXPANDING CAVITY

Table 3.2

PRESSURE AND VOLUME FOR EXPLOSIVE PRODUCTS
OF PETN/LUCITE MIXTURE[a]

Pressure		Specific Volume	Radius Ratio
psi x 10^{-3}	MPa x 10^{-2}	(cm^3/gram)	(r/r_o)
643.0	44.38	0.9589	1.00
356.2	24.57	1.2246	1.08
203.8	13.99	1.5639	1.18
119.0	8.20	1.9972	1.28
71.5	4.93	2.5507	1.39
44.2	3.05	3.2574	1.50
28.0	1.93	4.1601	1.63
18.2	1.25	5.3128	1.77
12.0	0.83	6.7849	1.92
10.1	0.70	7.6712	2.00[b]
8.2	0.56	8.6650	2.08
5.6	0.39	11.0660	2.23
3.9	0.27	14.1324	2.45
2.0	0.19	18.0484	2.66

[a]P-V data from SRI TIGER Code
(PETN density 1 gram/cm^3).

[b]Final cavity radius ratio.

after charge detonation. The initially steep slope in the pressure-time curve for test 142 supports this conclusion.

Series 11 - Creep

Exploded and unexploded cavity spheres differ principally in the explosively generated residual stress field that surrounds an exploded cavity. Restrictions on crack growth and fluid flow through the compressively stressed region are believed to be responsible for the ability of an exploded cavity to withstand large pressures following fracture initiation. Hence any relaxation of the residual stress field by means of creep would reduce the containment capability of the sphere. The effects of creep were assessed by comparing the pressure records from a series of tests in which exploded cavities remained vented for various lengths of time before hydrofracture. In all creep tests, a 3/8-gram charge, a 1000-psi (6.9-MPa) overburden, and 4.26-cm^3/min flow rate were used. The reproducibility tests of series 9 provide data for a relaxation period of up to 1 hour.

Hydrofracture records for tests 121, 145, and 148 are shown in Figure 3.22. Relaxation periods were 3, 4, and 17 hours, respectively. The 2460, 2140, and 2080 psi (17.0, 14.8, and 14.3 MPa) fracture initiation pressures are all less than the 2690-psi (18.5-MPa) average for the reproducibility tests. Also, maximum cavity pressures are at the low end of the reproducibility test spectrum.

Steady-state pressures for the reproducibility tests ranged from 1500 to 1900 psi (10.3 to 13.1 MPa). In contrast, cavity pressure in test 121 had dropped to 1300 psi (9.0 MPa) before pumping was stopped. The 2400-psi (16.5-MPa) steady-state pressure in test 145 is high, but reflects the presence of embedded graphite rod fracture gages. Effects of these gages are described more fully in the following section.

In summary, the creep tests indicate that prolonged periods of stress relaxation generally result in a reduction of hydrofracture pressures.

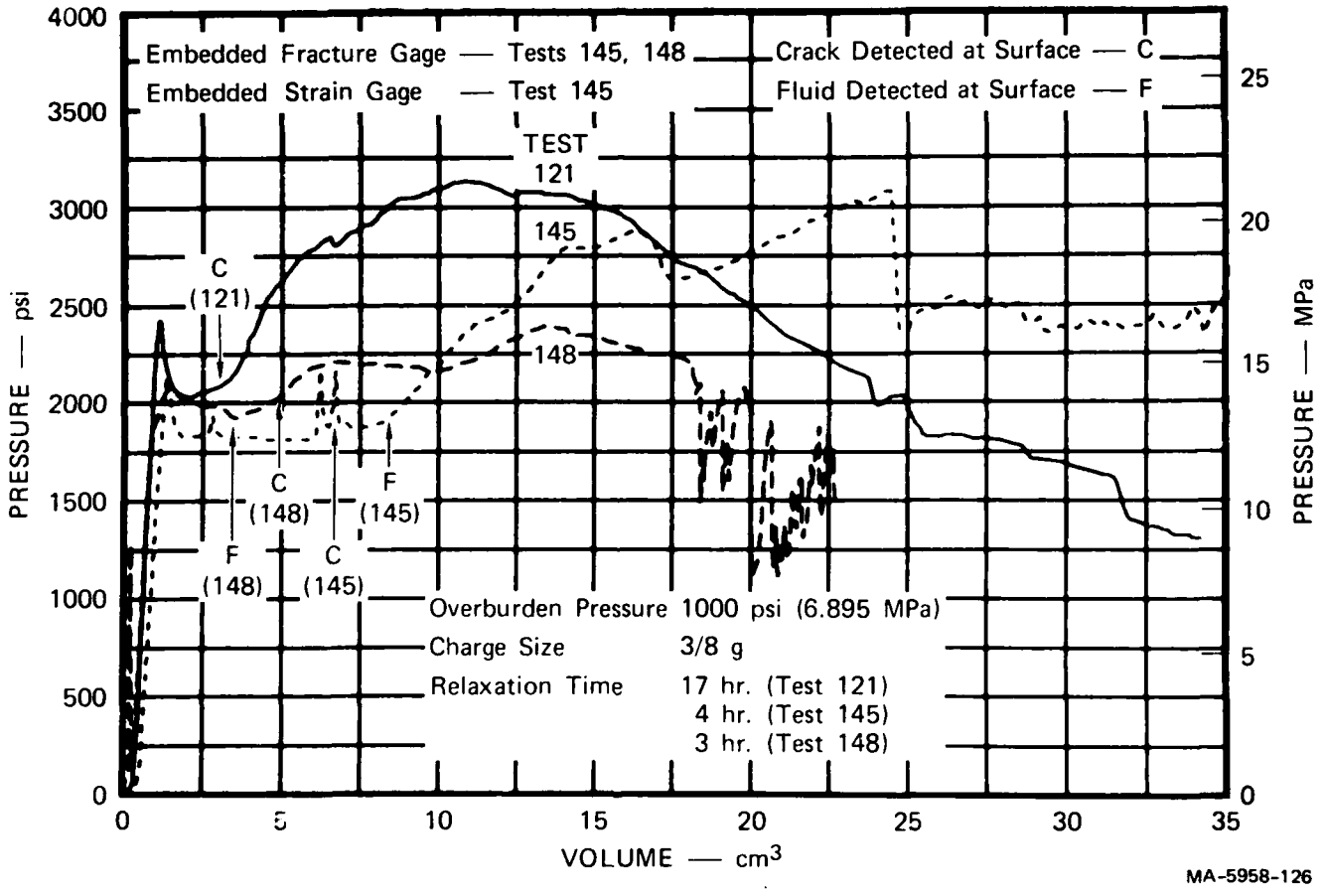

FIGURE 3.22 HYDROFRACTURE PRESSURES FOR VENTED EXPLODED CAVITY TESTS 121, 145, AND 148-CREEP

AD-A083 332 SRI INTERNATIONAL MENLO PARK CA F/G 18/3
LABORATORY STUDIES OF CONTAINMENT IN UNDERGROUND NUCLEAR TESTS,(U)
JAN 79 J C CIZEK, A L FLORENCE DNA001-77-C-0025
UNCLASSIFIED DNA-4847F NL

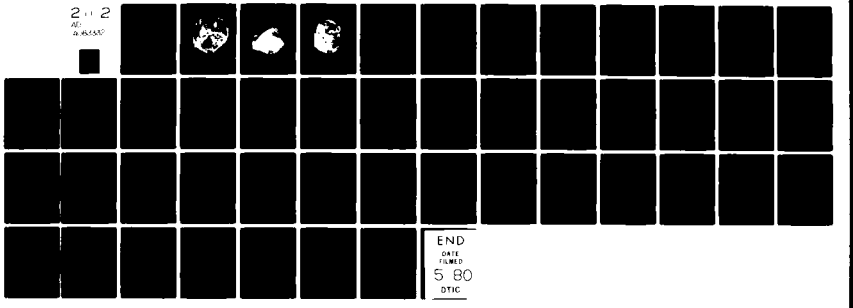

END
DATE FILMED
5 80
DTIC

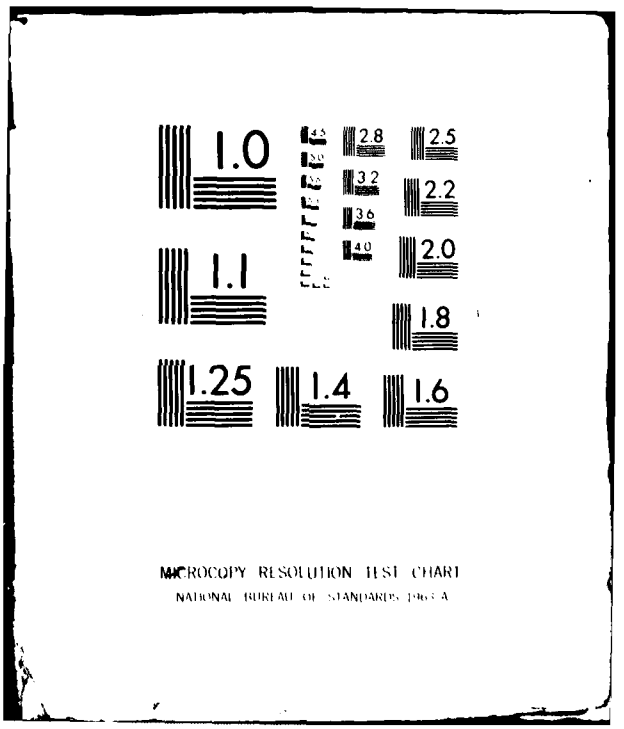
1.0
1.1
1.25
1.4
1.6
1.8
2.0
2.2
2.5
2.8
3.2
3.6
4.0
MICROCOPY RESOLUTION TEST CHART
NATIONAL BUREAU OF STANDARDS 1963-A

Series 12 - Internal Fracture

An array of the graphite fracture agaes described in Section 2.3 was embedded in exploded cavity spheres to provide data relative to the motion of a propagating crack tip during hydrofracture. The array consisted of three rods positioned vertically at distances of 1.5, 3, and 4.5 inches (3.81, 7.62, and 11.43 cm) from the center of the sphere.

Use of the gages in exploded cavity spheres was limited to the creep tests 145 and 148. Hydrofracture records are shown in Figure 3.22. The gages responded after surface fracture was detected and hence lacked the sensitivity to detect the leading edge of the crack. They influence steady-state flow, as evidenced by the high steady-state pressure in test 145. The same effect was observed in the hydrofracture records for unexploded cavity tests 144 and 147 shown in Figure 3.7. Figure 3.23 shows the multiple fracture planes developed in test 145. The intersection of two fracture planes at the embedded fracture gages suggests that the graphite rods may have influenced crack growth. Replacement of the graphite by a less perturbing fracture gage is planned in future tests.

Series 13 - Surface Fracture

Surface fracture of vented exploded cavity spheres due to hydrofracture was detected by means of the gages described in Section 2.3. Since only a small portion of surface could reasonably be monitored, the volume of hydrofracture fluid associated with the first detection of fracture is an upper bound estimate of the actual volume required to initiate a surface crack. The volumes quoted below were measured from the point of fracture initiation of the cavity.

Reference to Figure 3.14 shows that the minimum volume of fluid required to activate a gage in the exploded cavity reproducibility tests was 11.0 cm^3 in test 118 when the peak cavity pressure was developed. In test 117, where 19.3 cm^3 of flow was required, cracking was detected

MP-5958-114

FIGURE 3.23 HYDROFRACTURE FROM VENTED EXPLODED CAVITY TEST 145

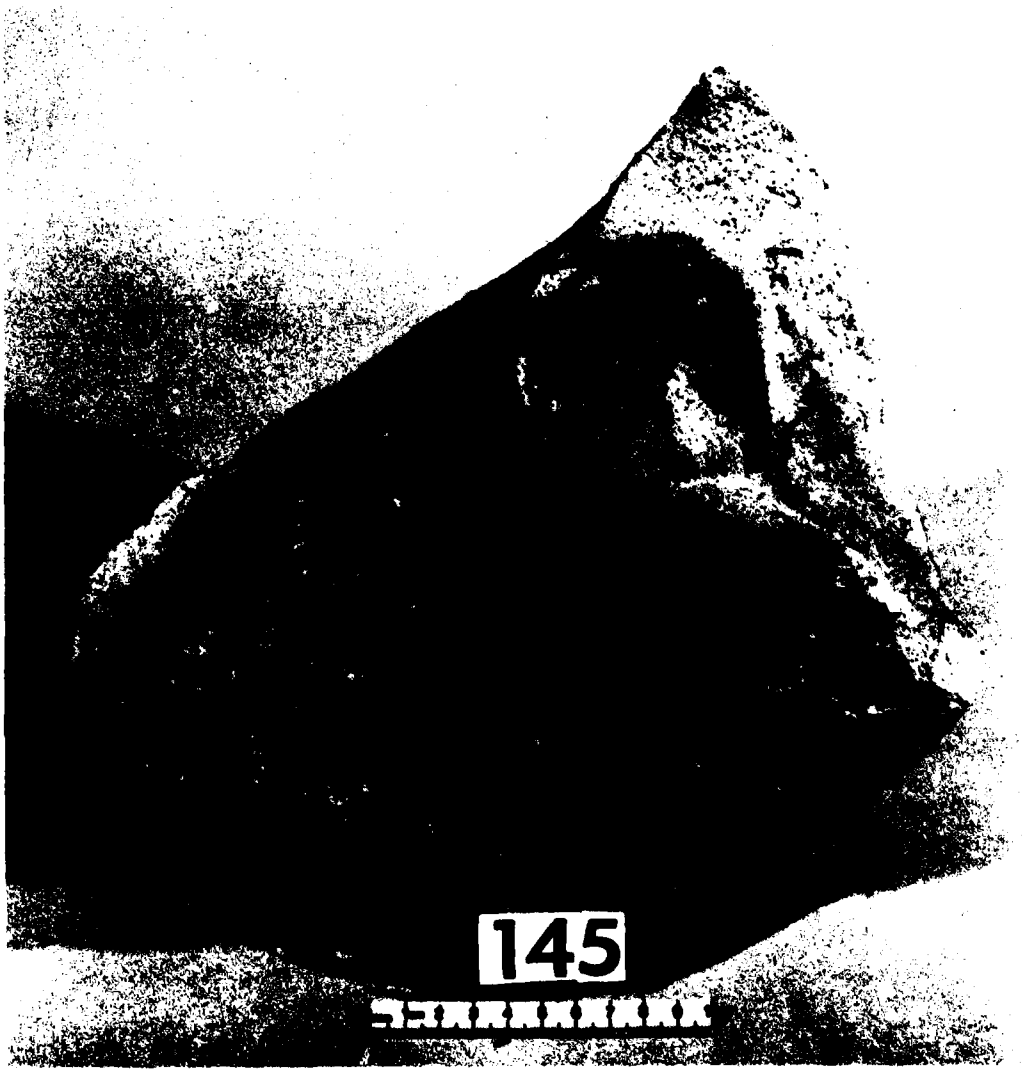

MP-5958-115

FIGURE 3.23 HYDROFRACTURE FROM VENTED EXPLODED CAVITY TEST 145 (Continued)

MP-5958-116

FIGURE 3.23 HYDROFRACTURE FROM VENTED EXPLODED CAVITY TEST 145 (Concluded)

soon after peak pressure was reached. The dramatic loss of pressure associated with crack detection in test 117 suggests the sudden formation of a widespread surface fracture. The subsequent development of steady-state flow supports this conclusion. In test 119, a similar pressure drop occurred and was followed by steady-state flow. Hence surface fracture in test 119 probably developed earlier than the point indicated on the pressure record.

For vented exploded cavities, the minimum volume of fluid required to activate a gage was 11.0 cm^3, compared with the minimum of 3.9 cm^3 in unexploded cavity tests. However, more extensive surface coverage is required to establish initial surface cracking and confirm these comparisons.

For the creep tests of series 11, Figure 3.22 shows that the volume corresponding to surface fracture detection was only 1.8 cm^3 in test 121. In addition, only 5.0 and 5.2 cm^3 were required in the other creep tests. These volumes are the minimum amounts for all exploded cavity tests instrumented with a surface fracture gage.

Series 14 - Internal Fluid Arrival

Motion of fluid along a fracture surface was monitored by means of the embedded copper rings described in Section 2.3. Except for these gages, the test configuration was the same as that for the exploded cavity reproducibility tests.

Hydrofracture records for tests 138, 139, and 143 are shown in Figure 3.24. In tests 138 and 139, a 6-inch-diameter (15.24-cm) ring was embedded symmetrically aobut the center of the sphere in the equatorial plane. With volume measured from fracture initiation, hydrofracture fluid was first detected after 0.5 and 2.1 cm^3 of flow. Hence, despite different fracture initiation pressures, 2240 and 3140 psi (15.4 and 21.7 MPa), the initial stages of hydrofracture were marked by rapid crack growth and fluid motion. In test 143, concentric 6- and 9-inch-diameter (15.24- and 22.86-cm) rings were embedded. Surprisingly, fluid was detected by both

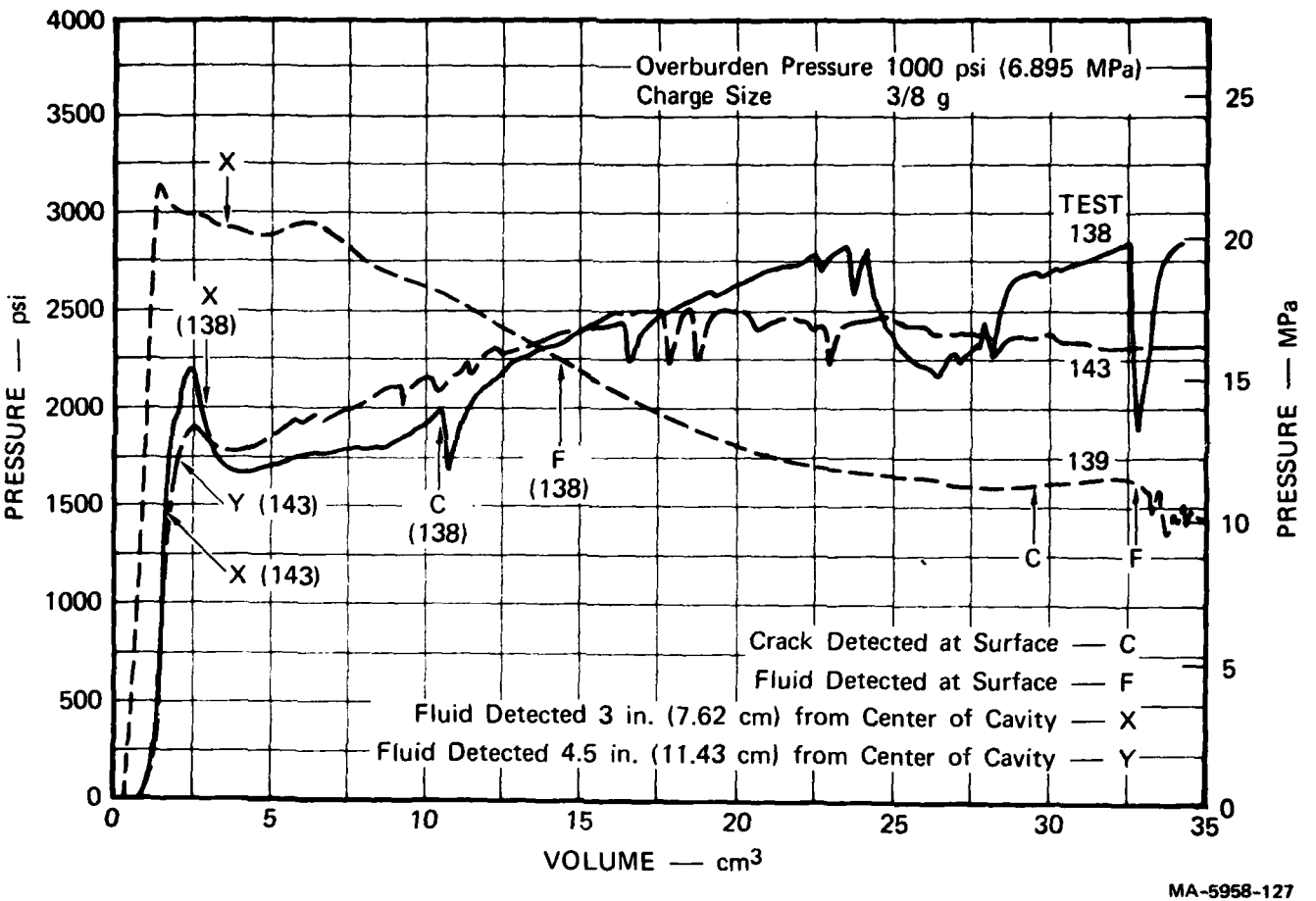

FIGURE 3.24 HYDROFRACTURE PRESSURES FOR VENTED EXPLODED CAVITY TESTS 138, *139, AND 143—INTERNAL AND SURFACE FLUID ARRIVAL*

gages while cavity pressure was still increasing to a relatively low pressure spike at 1900 psi (13.1 MPa). Close examination of the hydrofracture record reveals that loss of cavity fluid corresponds with a sudden change in slope of the curve instead of a small pressure drop. These observations suggest the formation of an extremely narrow crack extending to the gages. Hence the gages may have influenced the fracture initiation and growth process. The unusual character of the hydrofracture records in Figure 3.24 supports this conclusion. Development of a less perturbing internal fluid arrival gage is planned.

Series 15 - Surface Fluid Arrival

The copper wires described in Section 2.2 were used to detect the arrival of hydrofracture fluid at the surface of exploded cavity spheres. In general, each wire was positioned adjacent to a fracture gage so that the volumes of fluid required to initiate surface fracture and fluid arrival could be compared.

Figure 3.22 shows that arrival of surface fluid in test 148 required only 2.0 cm^3 of flow. Volume was measured from the pressure spike. Fracture was not detected until later because the surface gages were not adjacent in this test, so surface fracture actually required less than 2.0 cm^3. In test 145, where the gages were adjacent, 1.8 cm^3 of of fluid was pumped between the time of surface fracture and fluid arroval. Figure 3.24 shows that in tests 138 and 139, 3.8 and 3.2 cm^3 of flow occurred between the time of surface fracture and fluid arrival. Finally, Figure 3.7 shows that for unexploded cavity tests 137, 144, and 147 the flow between the time of surface fracture and fluid arrival ranged from 0.4 to 1.5 cm^3. Hence, when a crack reaches the surface of a sphere, fluid appears to be nearer the crack tip in unexploded cavity tests than in the corresponding exploded cavity tests.

Series 16 - Internal Strain Measurements

Dynamic strain associated with charge detonation and the subsequent quasi-static strain associated with hydrofracture were measured by means of the embedded strain gage described in Section 2.3. The gage was oriented to measure radial strain 1 inch (2.54 cm) from the center of a sphere containing a 3/8-gram charge.

The hydrofracture record for test 145 is shown in Figure 3.22. As shown in Figure 3.23, the gage was completely embedded in grout following the test and thus had no apparent effect on the pressure record or fracture pattern.

The dynamic response of the strain gage to charge detonation is shown in Figure 3.25. The record suggests that the first three cycles of cavity expansion and contraction are responsible for the formation of the residual stress field. The remaining oscillations appear to be within the known elastic limits of the grout. Posttest examination of the sphere revealed that the gage remained 1 inch (2.54 cm) from the center of the cavity, which had doubled in diameter. If the decay of radial strain was proportional to the elastic prediction of $1/r^3$ and the grout was incompressible, then doubling the initial cavity diameter would require a 5.0% strain at the gage. The 1.5% residual strain shown in Figure 3.25 then implies that crushing of the grout is significant in the formation of an exploded cavity.

The strain record resulting from hydrofracture pressures only is shown in Figure 3.26. Comparing this strain gage response with the pressure record of test 145 shown in Figure 3.22 reveals that the gage responded faithfully to fluctuations in cavity pressure. However, as in the unexploded cavity tests, hydrofracture strains were larger than the elasticity prediction. For the exploded cavity test, changes in material properties due to charge detonation could account for much of this difference.

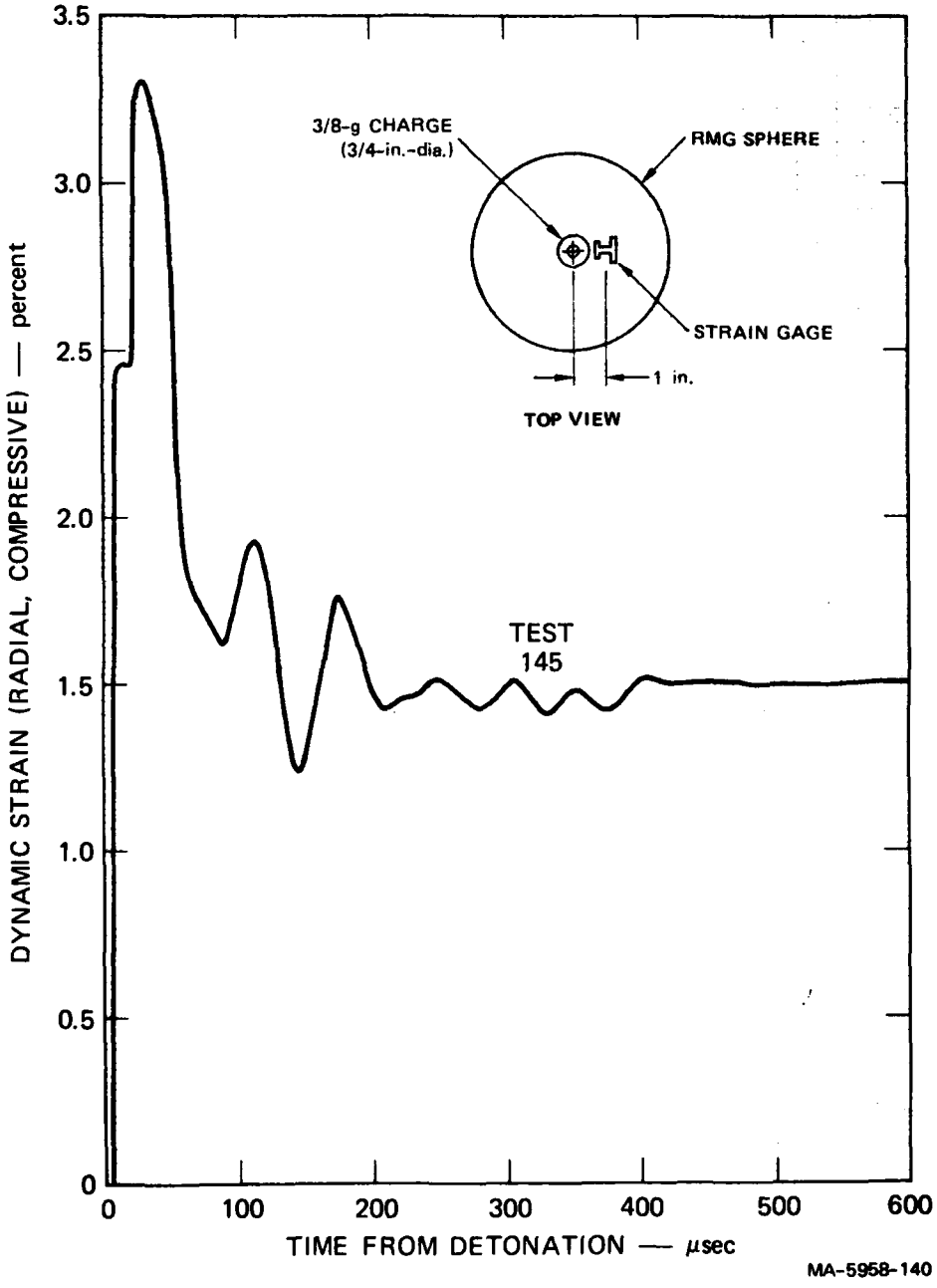

FIGURE 3.25 RADIAL DYNAMIC STRAINS FOR VENTED EXPLODED CAVITY TEST 145

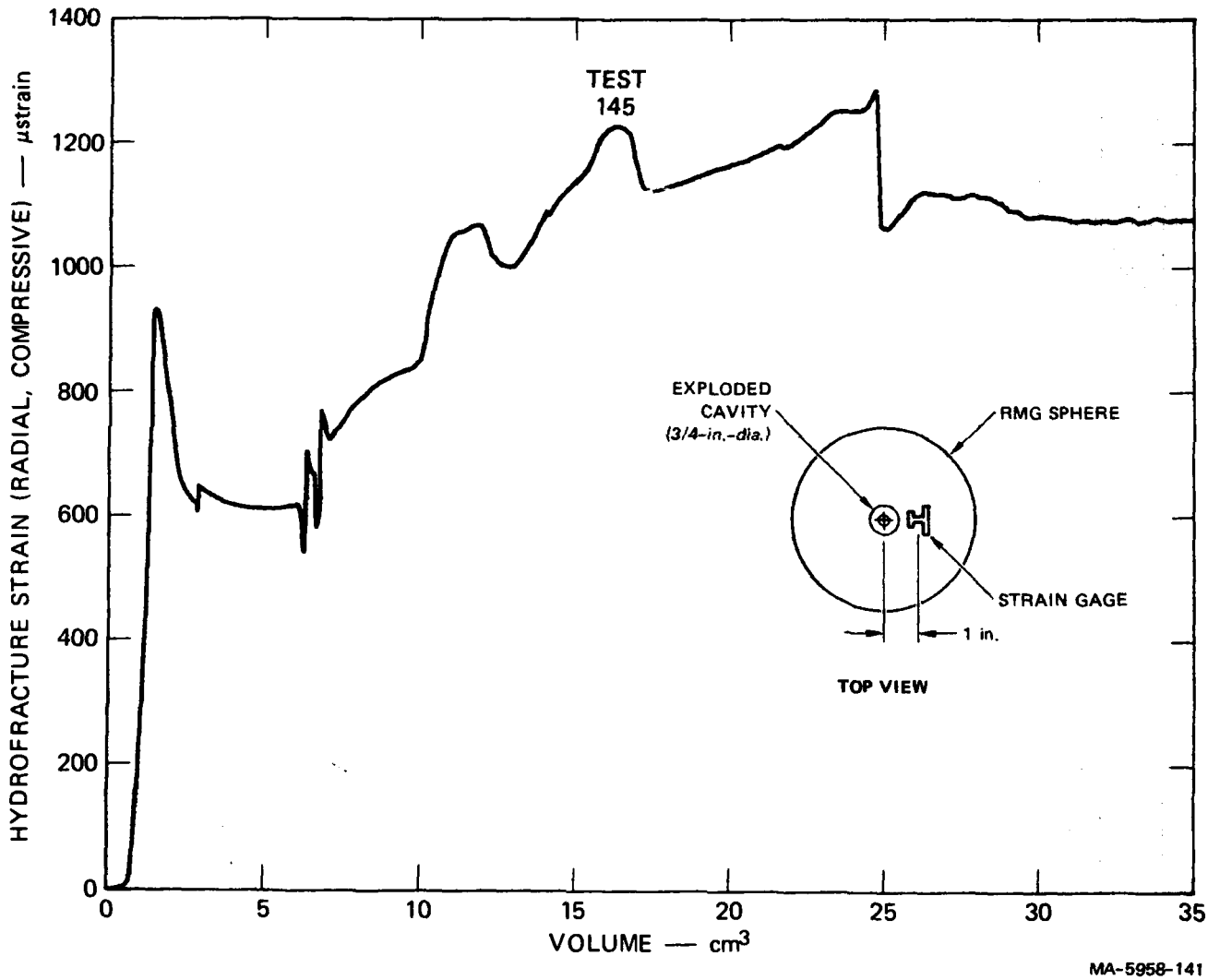

FIGURE 3.26 RADIAL HYDROFRACTURE STRAINS FOR VENTED EXPLODED CAVITY TEST 145

Series 17 - Internal Stress Measurement

The flat jack stress gage described in Section 2.3 was embedded 1 inch (2.54 cm) from the center of a sphere containing a 3/8-gram charge. The gage was oriented to measure changes in the radial component of stress due to overburden, dynamic cavity expansion, hydrofracture, and creep.

The hydrofracture record for test 148 is shown in Figure 3.22. The gage was completely embedded in grout following the test and thus had no apparent influence on the pressure record or fracture pattern. Response of the stress gage is shown in Figure 3.27. Before overburden was applied to the sphere, a pressure of 800 psi (5.5 MPa) in the gage supply line was required to open the gage, as shown by point A. Hence the pressure in excess of this value is the radial stress component acting on the gage caused by overburden and explosively generated residual stresses. As overburden was increased to 1000 psi (6.9 MPa), the gage responded by following path AB. Elasticity theory predicts the path AB' so a departure from linearity was observed. After charge detonation, an attempt was made to measure the radial component of the explosively generated residual stress field by following path BCD, but failure of the supply line fittings limited the gage opening pressure to 2000 psi (13.8 MPa). The difference in opening pressure at points B and C shows that the radial component of residual stress immediately following charge detonation was greater than 500 psi (3.5 MPa).

Although the gage was inoperative during hydrofracture and the subsequent release of overburden, residual stress measurements were made after a 94-hour period of stress relaxation. These measurements are shown by the path EFG in Figure 3.27. The residual stress, which is the difference between paths AB and EFG, varied with overburden from 200 psi (1.4 MPa) at zero overburden to 420 psi (2.9 MPa) at 1000 psi (6.9 MPa) overburden with a minimum of 110 psi (0.8 MPa) at about 400 psi (2.8 MPa) overburden.

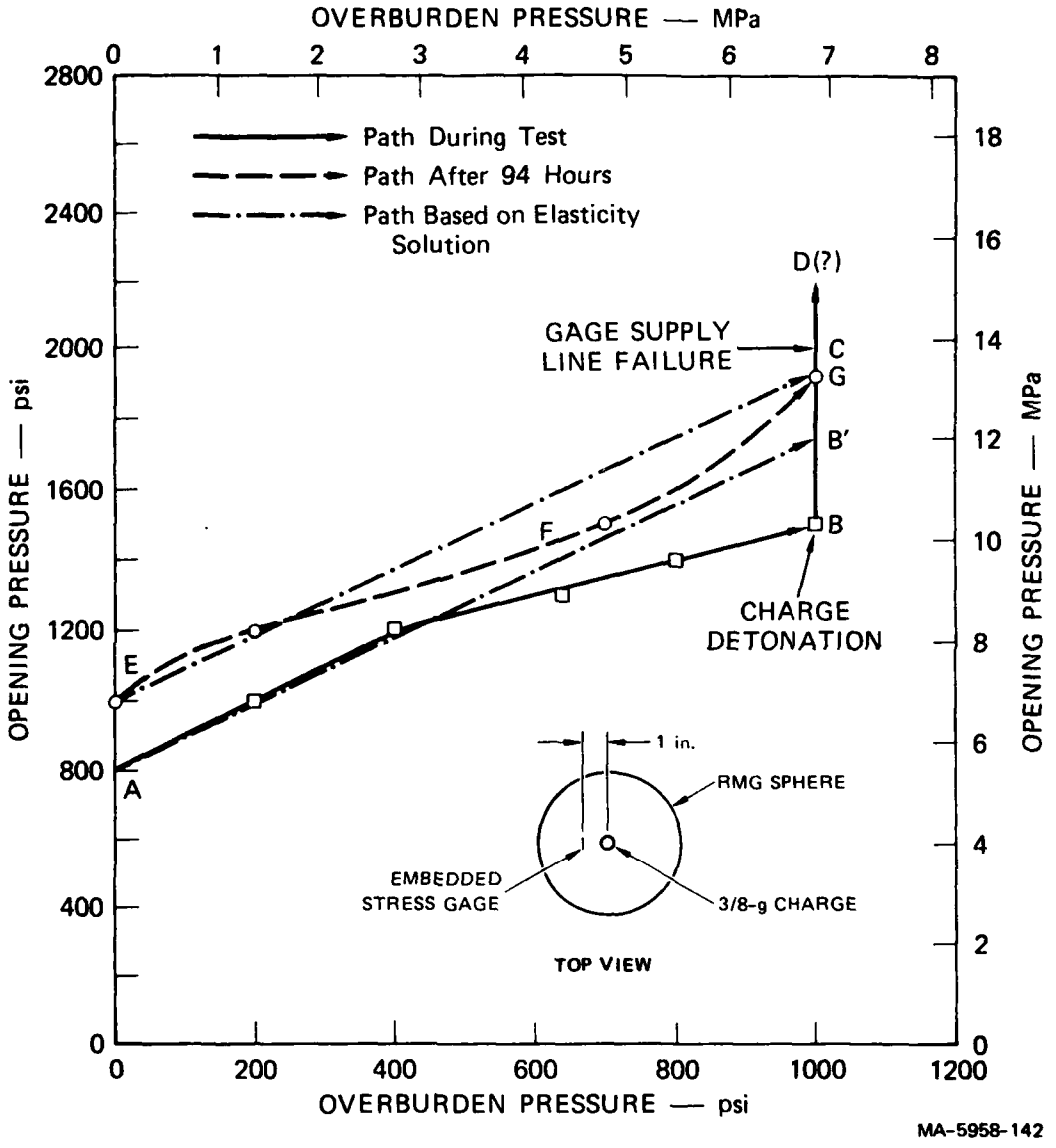

FIGURE 3.27 PRESSURE REQUIRED TO OPEN EMBEDDED STRESS GAGE DURING AND AFTER VENTED EXPLODED CAVITY TEST 148

SECTION 4

FRACTURE MECHANICS ANALYSIS

4.1 INTRODUCTION

A fracture mechanics analysis is presented here as an aid to interpreting the hydrofracture records of the exploded and unexploded cavity tests. The analytical results are formulas for the pressure in a penny-shaped crack that will cause crack propagation in an infinite elastic medium. The formulas are used to show the relationship between pressure distribution and crack stability. The pressure is taken as uniform over a constant central circular area that represents the unexploded cavity, and different pressure distributions are considered in the surrounding annular region that represents a crack propagating from a spherical cavity. Pressures required to start expansion of the circular crack from the constant central circular region are modified by predictions of the plate edge notch formulas that are presented.

A finite-element stress intensity code (SIC) was used to account for the inner and outer spherical boundaries and a residual stress field of the type generated by exploded cavity formation. For the case of a uniform pressure distribution in the annular crack and a constant overburden pressure, SIC was used to generate theoretical hydrofracture records for exploded and unexploded cavity tests.

Results for unexploded cavities indicate that:

- A uniform pressure throughout the crack causes unstable growth (less pressure required to sustain crack expansion).
- A uniform pressure confined to a central area of a penny-shaped crack, or in a spherical cavity that is surrounded by a planar annular crack (lined cavity), causes stable crack growth.

- A pressure that decreases linearly from the central region pressure to zero at the crack tip causes crack growth that is initially stable but finally unstable. A similar behavior is obtained when the outer annular region has a uniform pressure that is a constant fraction of the central region pressure.

- The shape of the hydrofracture record is the same as the experimental shape.

- Fracture initiation pressures based on reasonable flow or notch lengths are comparable to the experimental pressures.

- Fluid volumes in the crack are smaller than experimental values (later experiments with improved model fabrication and measuring techniques produced comparable volumes).

Results for exploded cavities indicate that:

- The overall shape of the hydrofracture record is similar to the experimental shape.

- Fluid volumes in the crack are similar to the experimental values; this result reinforces the observation that only the initial portion of the hydrofracture record is relevant to containment.

- Pressure rises occur if steep pressure gradients occur at the cavity wall in the crushed zone.

4.2 PENNY-SHAPED CRACKS

The stress intensity factor K_1 for a penny-shaped crack of radius a, subjected to an axisymmetric pressure distribution p(r) inside the crack is[9]

$$K_1 = \frac{2}{(\pi a)^{\frac{1}{2}}} \int_0^a \frac{rp(r)dr}{(a^2 - r^2)^{\frac{1}{2}}} \qquad (1)$$

A concentric region of radius b equal to that of the spherical cavity in the experiments is taken to be loaded by a uniform pressure distribution. The outer annular region is subjected to one of the three

loadings: (1) the same pressure as the central region so that the pressure is uniform throughout the crack, (2) a pressure that decreases linearly from the central region pressure to zero at the crack tip, and (3) zero pressure. Expressed mathematically, these three cases are

$$p(r) = P \qquad 0 < r < a \tag{2}$$

$$p(r) = \begin{cases} P & 0 < r < b \\ P\,\dfrac{a - r}{a - b} & b < r < a \end{cases} \tag{3}$$

$$p(r) = \begin{cases} P & 0 < r < a \\ 0 & a < r < b \end{cases} \tag{4}$$

Substituting pressure distributions (2), (3), and (4) into the integral in formula (1) and integrating provides the corresponding three stress intensity factors. As the pressure P is increased in each case the stress intensity factor is increased. When the pressure reaches the critical value P_c that makes the stress intensity factor equal to the fracture toughness, K_{Ic}, a material property, the crack is about to grow. If an incremental increase in P_c results in an incremental increase in the crack radius a, while imposing the same pressure distribution, the crack growth is stable. If an incrementally larger crack radius requires an incrementally smaller pressure to maintain $K_I = K_{Ic}$, the crack growth is unstable. For the above three loading cases substitution in (1), integration, and use of $K_I = K_{Ic}$ gives the critical pressures P_c in the form

$$\frac{2P_c}{K_{Ic}}\left(\frac{b}{\pi}\right)^{\frac{1}{2}} = \begin{cases} \dfrac{1}{F_1(\alpha)} & \text{(case 1-uniform)} \qquad (5) \\ \dfrac{1}{F_2(\alpha)} & \text{(case 2-linear)} \qquad (6) \\ \dfrac{1}{F_3(\alpha)} & \text{(case 3-zero)} \qquad (7) \end{cases}$$

In (5), (6), and (7),

$$F_1(\alpha) = \alpha^{\frac{1}{2}} \tag{8}$$

$$F_2(\alpha) = \frac{\alpha^{\frac{1}{2}}}{2\left(1 - \frac{1}{\alpha}\right)} \left[\left(2 - \frac{1}{\alpha}\right)\left(1 - \frac{1}{\alpha^2}\right)^{\frac{1}{2}} - \frac{\pi}{2} + \sin^{-1}\left(\frac{1}{\alpha}\right)\right] + F_3(\alpha) \tag{9}$$

$$F_3(\alpha) = \alpha^{\frac{1}{2}}\left[1 - \left(1 - \frac{1}{\alpha^2}\right)^{\frac{1}{2}}\right] \tag{10}$$

where $\alpha = a/b$. According to the model, b is a constant equal to the spherical cavity radius, so an increase of α from its initial value of unity means an increase of the crack radius a. When a = b, that is, when $\alpha = 1$, the crack has a radius b and is subjected to a uniform pressure over its entire surface so the starting critical pressure is given by the classical result

$$\frac{2P_c}{K_{Ic}}\left(\frac{b}{\pi}\right)^{\frac{1}{2}} = 1 \tag{11}$$

When $\alpha = 1$, each of the functions (8), (9), and (10) have the value unity, which makes formulas (5), (6), and (7) initially consistent with formula (11).

Figure 4.1 shows the variation of critical pressure with crack radius. In case 1, a uniform pressure always acts over the entire crack surface. Such a condition may be realized approximately by pressurizing fluid of very low viscosity or by using a very slow pumping rate. The crack growth is unstable in that larger cracks require less pressure just to keep them stationary. In case 2, the pressure applied in the crack decreases linearly from the uniform pressure in the initial penny-shape to zero at the crack tip. Such a condition may be realized approximately by pressurizing a very viscous fluid. The crack growth is initially stable until the crack radius is about 2-1/2 times the initial radius.

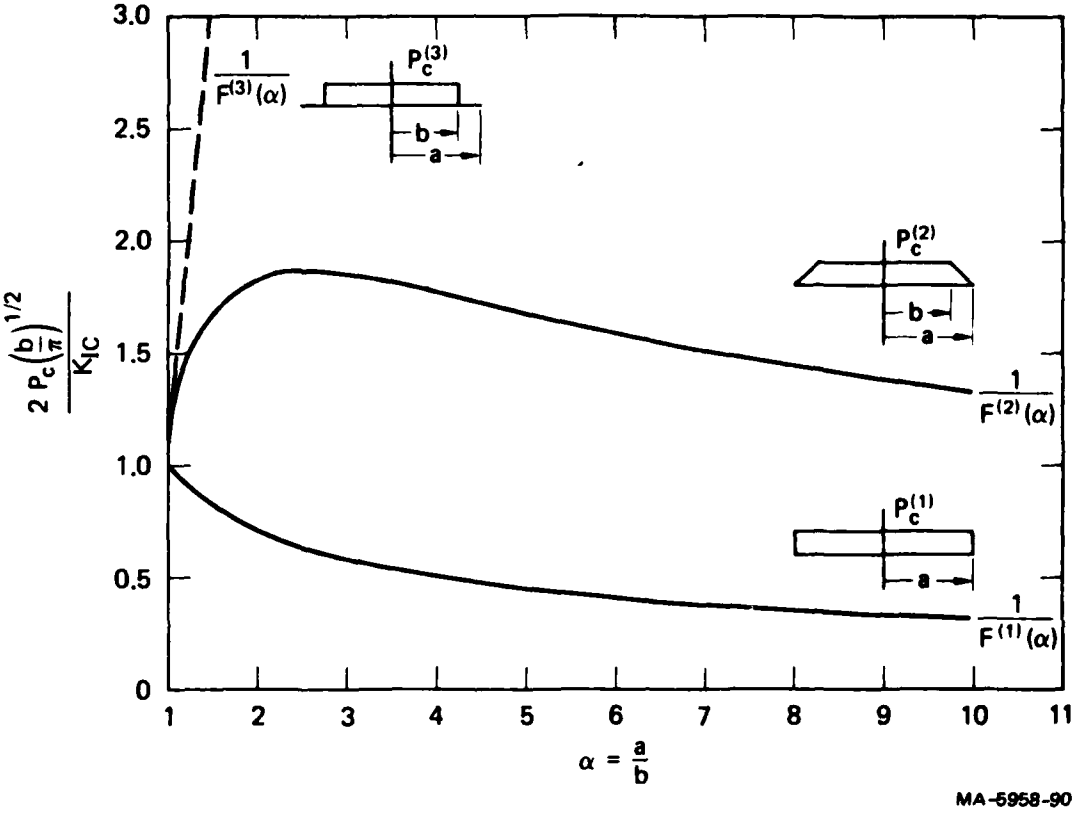

FIGURE 4.1 CRITICAL PRESSURE CURVES FOR A PRESSURIZED PENNY-SHAPED CRACK

Further growth is unstable. In case 3, the pressure is confined to the initial crack surface. Such a condition may be obtained by not allowing pressurized fluid into the extended annular region of the crack. The crack growth is stable throughout. Because of the difficulty of clearly showing this curve at a scale suitable for cases 1 and 2, it is shown again in Figure 4.2.

For crack radii that are many times the initial crack radius the behaviors of the critical pressures are given by

$$\frac{2P_c}{K_{Ic}}\left(\frac{b}{\pi}\right)^{\frac{1}{2}} \sim \begin{cases} \dfrac{1}{\alpha^{\frac{1}{2}}} & \text{(case 1)} \quad (12) \\ \dfrac{1}{(1 - \pi/4)\alpha^{\frac{1}{2}}} & \text{(case 2)} \quad (13) \\ 2\alpha^{3/2} & \text{(case 3)} \quad (14) \end{cases}$$

Formulas (12), (13), and (14) are obtained by letting $\alpha \to \infty$ in (8), (9), and (10) for use in (5), (6), and (7). Hence, in cases 1 and 2, the pressures tend to zero, but in case 3 the pressure tends to infinity.

Figures 4.3 and 4.4 show the variations of critical pressure with crack radius when the initial crack radius is b = 3/8 inch and the fracture toughness is K_{Ic} = 1000 psi $\sqrt{\text{inch}}$. The initial radius is the same as the spherical cavity radius in the hydrofracture experiments; the fracture toughness value is an estimate for 2C4 RMG. The overall shapes of the curves are the same as those in Figures 4.1 and 4.2. The initial fracture pressure in each case is 1450 psi, and the maximum pressure required for crack growth in case 2 is 2700 psi. Superposition of a hydrostatic stress state of 1000 psi throughout the material, which corresponds to the overburden pressure most commonly used in the experiments, increases the fracture initiation pressure to 2450 psi and gives a maximum pressure for crack growth in case 2 of 3700 psi. In Figures 4.3 and 4.4, the critical pressure P_c may be interpreted as the difference between the pressure in the crack and the hydrostatic overburden pressure. The

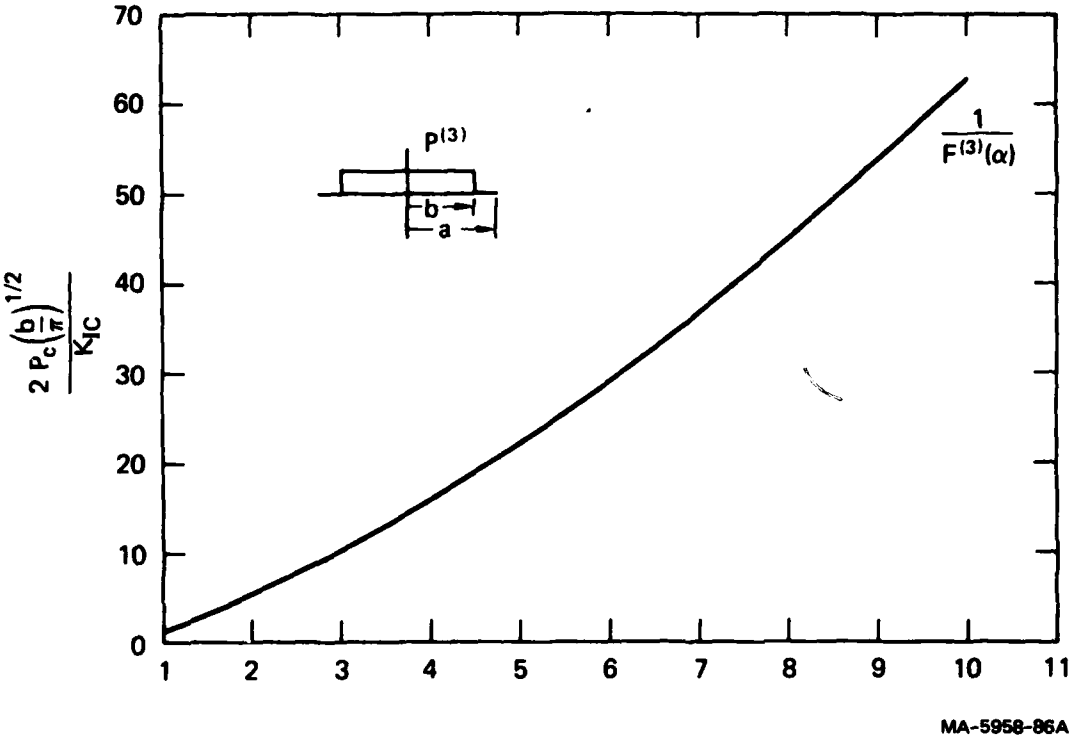

FIGURE 4.2 A CRITICAL PRESSURE CURVE FOR A PRESSURIZED PENNY-SHAPED CRACK

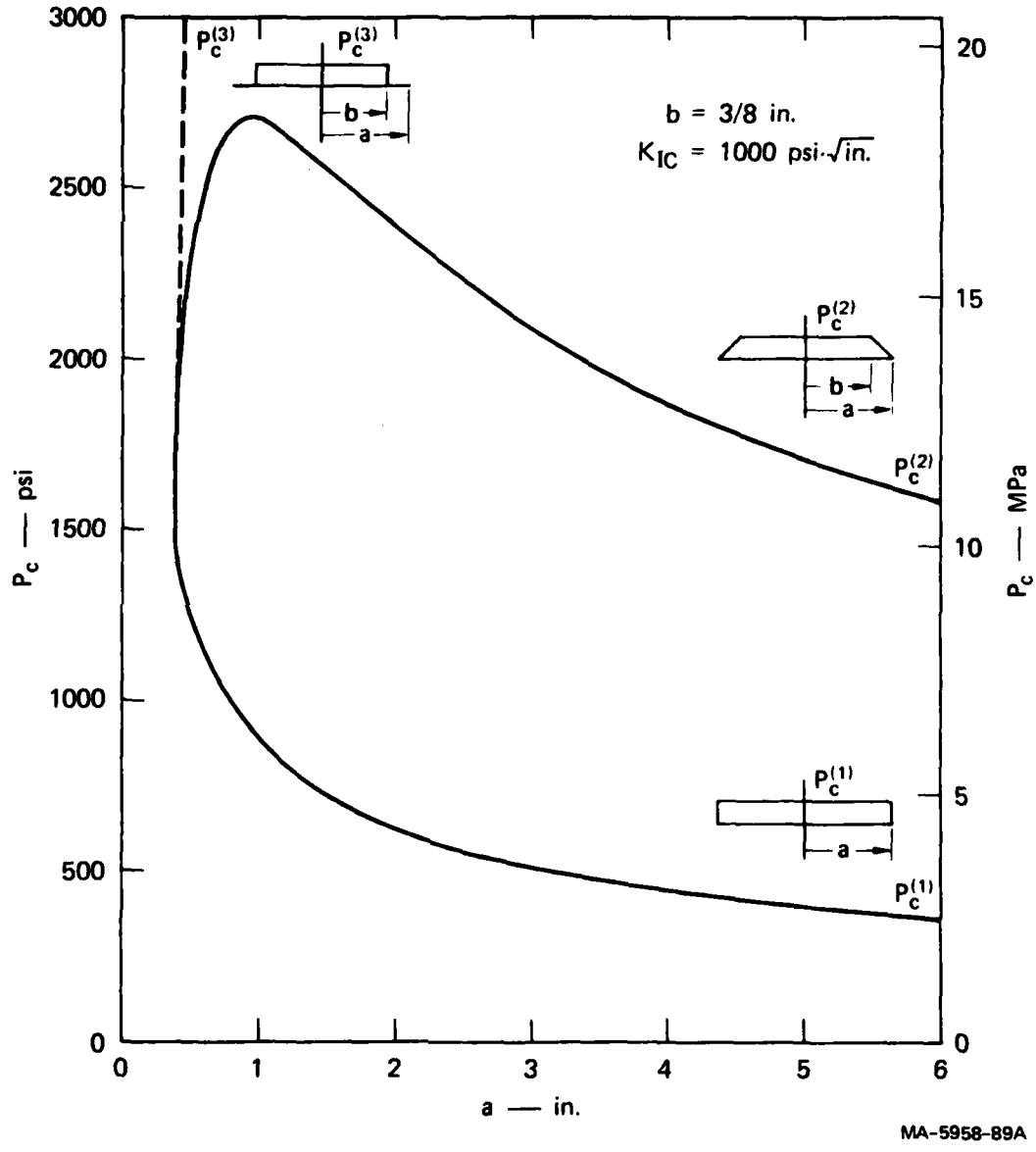

FIGURE 4.3 VARIATIONS OF CRITICAL PRESSURE WITH CRACK RADIUS FOR PRESSURIZED PENNY-SHAPED CRACKS

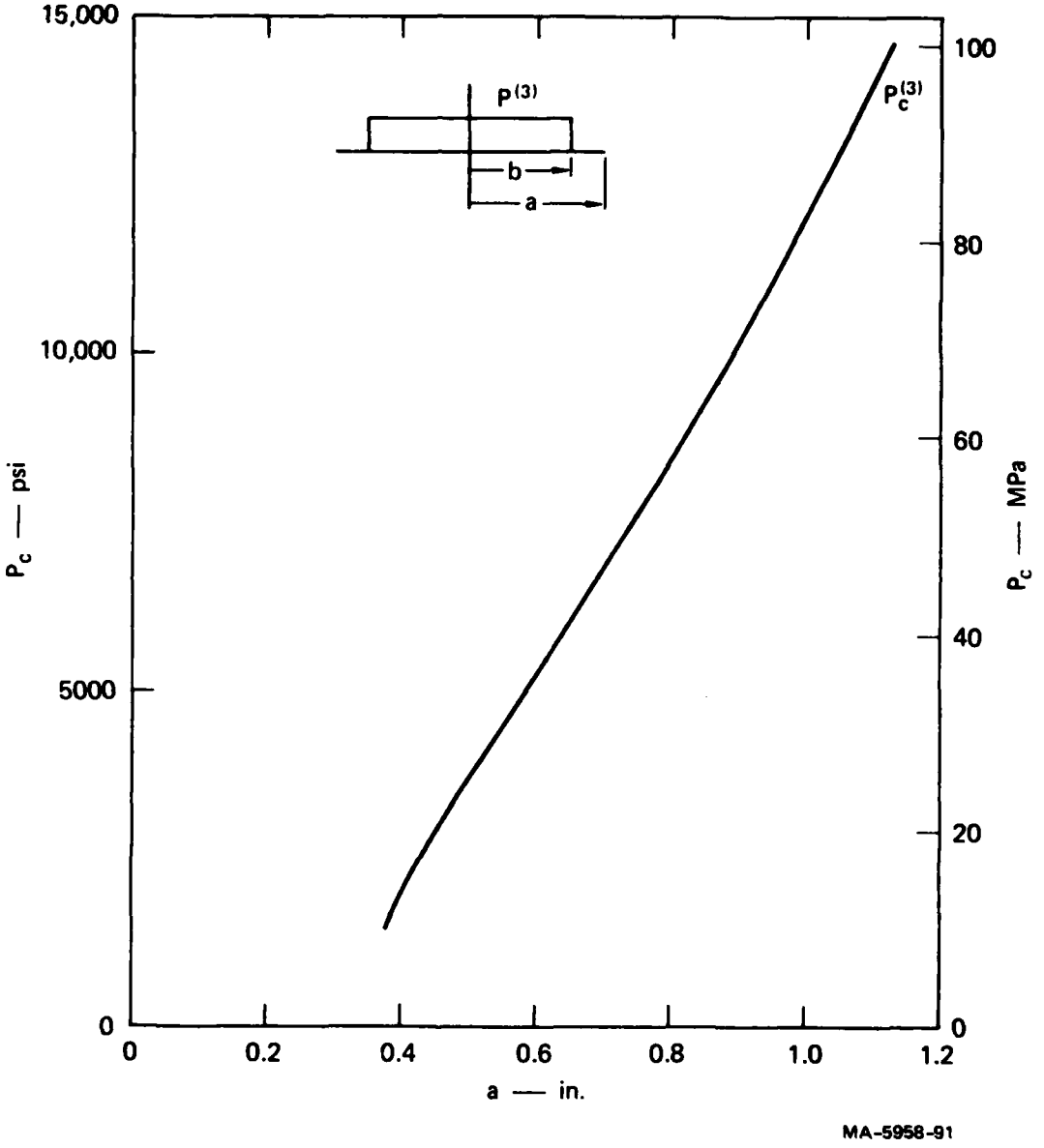

FIGURE 4.4 VARIATION OF CRITICAL PRESSURE WITH CRACK RADIUS FOR A PRESSURIZED PENNY-SHAPED CRACK

unexploded cavity experiments produced pressure-volume records that after fracture initiation resemble the pressure-crack radius curve of case 1.

It has been shown[9] that the displacement normal to the face of a penny-shaped crack that is internally pressurized is

$$w(r) = \frac{4(1 - \nu^2)a}{\pi E} \int_{r/a}^{1} \frac{\mu d\mu}{(\mu^2 - r^2/a^2)} \int_{o}^{1} \frac{xp(\mu a x)dx}{(1 - x^2)} \qquad (15)$$

where E and ν are Young's modulus and Poisson's ratio for the elastic medium. For a uniform pressure of case 1, formula (15) reduces to

$$w(r) = \frac{4(1 - \nu^2)aP}{\pi E} \left(1 - \frac{r^2}{a^2}\right)^{\frac{1}{2}} \qquad (16)$$

which gives a crack volume of

$$V = 16(1 - \nu^2)a^3P/3E \qquad (17)$$

The critical pressure-crack radius relationship is given by (5) and (8), so elimination of the radius in (17) leads to the pressure-volume relationship

$$V = \frac{(1 - \nu^2)\pi^3 K_{Ic}^6}{12EP_c^5} \qquad (18)$$

This relationship, modified to give approximate volume change, is shown in Figure 4.5. The curve resembles the hydrofracture curves obtained for the unexploded cavities. A comparison of experimental and theoretical hydrofracture curves is discussed later.

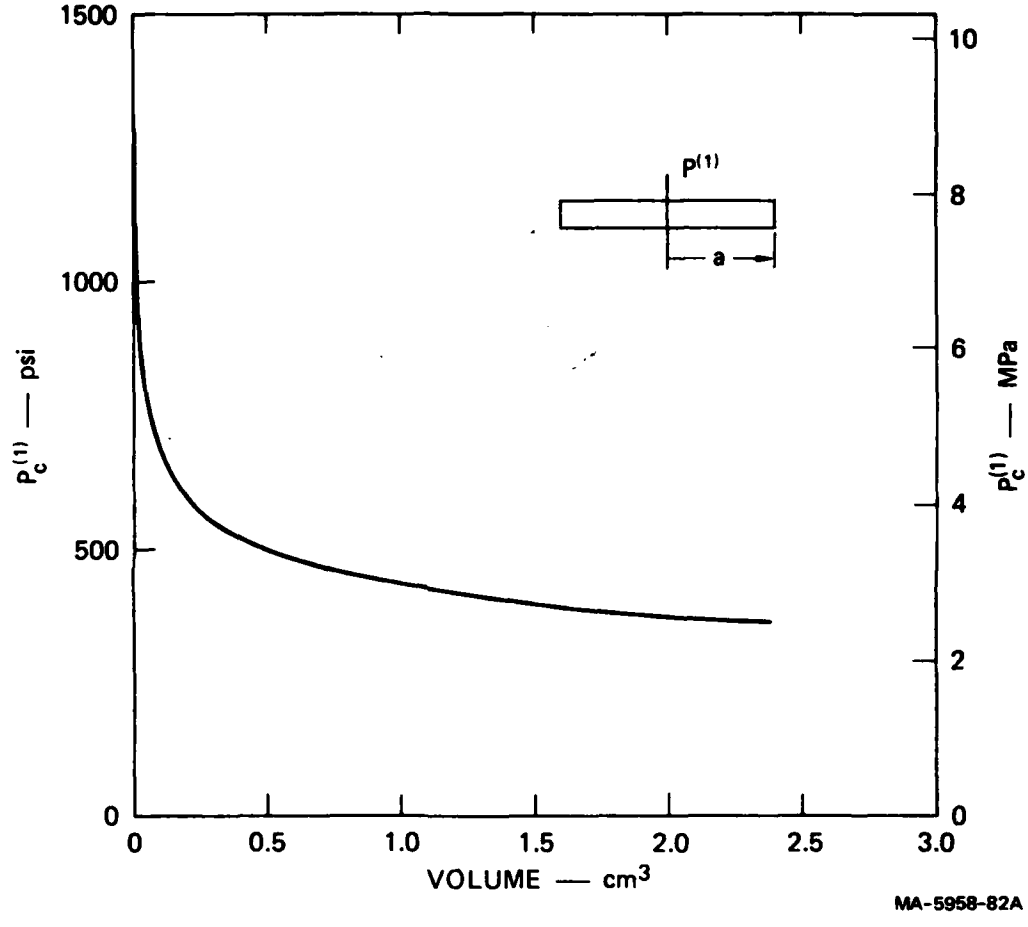

FIGURE 4.5 PRESSURE-VOLUME RELATIONSHIP FOR A UNIFORMLY PRESSURIZED CRACK

The penny-shaped crack solutions are useful for illustrating the effect on crack stability of a very steep pressure drop at the spherical cavity wall caused by a partial blockage. If this state is modeled by the pressure distribution

$$p(r) = \begin{cases} P & 0 < r < b \\ \gamma P & b < r < a \end{cases} \tag{19}$$

where $0 < \gamma < 1$, the critical crack pressure is

$$\frac{2P_c}{K_{Ic}} \left(\frac{b}{\pi}\right)^{\frac{1}{2}} = \frac{1}{F_4(\alpha\ ;\ \gamma)} \quad \text{(case 4-step)} \tag{20}$$

with

$$F_4(\alpha\ ;\ \gamma) = \alpha^{\frac{1}{2}} \left[1 - (1 - \gamma)\left(1 - \frac{1}{\alpha^2}\right)^{\frac{1}{2}}\right] \tag{21}$$

The extreme values of $\gamma = 1$ and $\gamma = 0$ give cases 1 and 3. Figure 4.6 shows critical pressure curves for several values of γ, including the extreme values. The general shape of the curves for $0 < \gamma < 1$ is similar to that for case 2 (Figure 4.1), which shows that the crack growth is initially stable and ultimately unstable; case 2 corresponds approximately to the $\gamma = 0.3$ curve. As expected, increasing effectiveness of blockage, denoted by decreasing values of γ, gives rise to increasing critical pressures and increasing crack radii before unstable growth. These crack radii are given by

$$\alpha_m^2 = \frac{\lambda + 2 + (\lambda^2 + 8\lambda)^{\frac{1}{2}}}{2(\lambda - 1)} \qquad \lambda = \frac{1}{(1 - \gamma)^2} \tag{22}$$

4.3 SIC CODE RESULTS FOR A SPHERICAL MEDIUM: UNEXPLODED CAVITY

The finite-element stress intensity code, SIC, was applied to the experimental RMG sphere having internal and external radii of 3/8 inch and 6 inches. The fracture toughness was again taken as

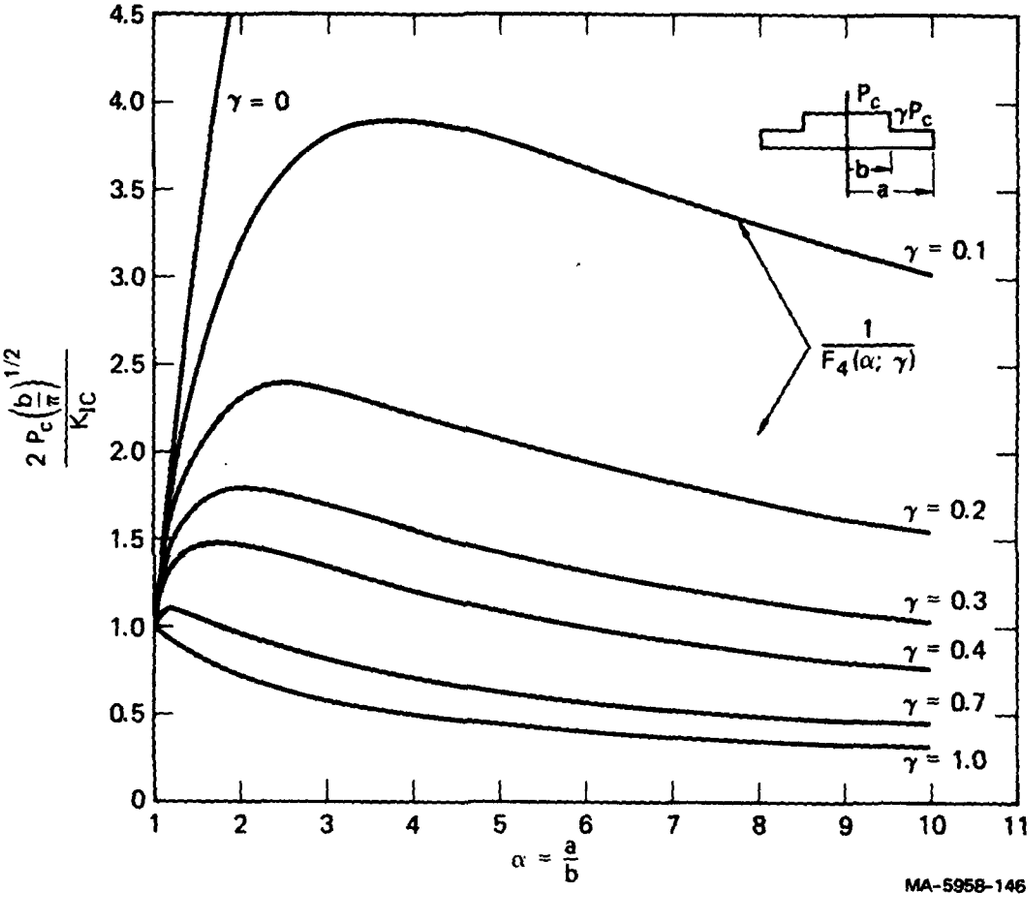

FIGURE 4.6 CRITICAL PRESSURE CURVES FOR A PENNY-SHAPED CRACK UNDER AN INTERNAL STEP PRESSURE

K_{Ic} = 1000 psi $\sqrt{\text{inch}}$. Figure 4.7 shows the relationship between the resulting critical pressure and the circular crack radius. Also shown for comparison in Figure 4.7 are two critical pressure curves for a penny-shaped crack, one in an infinite medium (Figure 4.3) and the other in a cylindrical medium[10] of 6 inches radius. In all cases the pressure distribution is uniform throughout the crack.

When the crack is less than about 1-1/2 inches in radius, the penny-shaped crack curves 1 and 2 agree with each other. When the crack is greater than about 1-1/2 inches in radius, the influence of the outer boundary of the medium causes a divergence by reducing to zero the pressures for curve 2 as the crack approaches the boundary. The SIC pressures agree with the analytical pressures for curve 2 except for crack radii between 3/8 and about 5/8 inch. These comparisons serve as a code verification. Other verifications were performed, but they are not reported here.

Overburden is included by superposing a hydrostatic state throughout the sphere. In this case the critical pressure is the difference between the pressure in the spherical cavity and the external overburden pressure, $P_a - P_b$ in Figure 4.8.

The fracture initiation pressure requires an assumption on the initial size of the crack, that is, the initial flaw size inherent in the material or caused by the manufacturing process. If the flaw is idealized to a circular notch around the cavity and if the depth of the notch is small relative to the cavity radius, an approximation to the stress intensity factor may be taken as that for an edge notch. The tensile stress acting on the notch is the circumferential stress at the cavity caused by internal and external pressures, p_a and p_b. As shown in Figure 4.9(a), this stress is $p_a/2 - 3p_b/2$, and the stress intensity factor is[10]

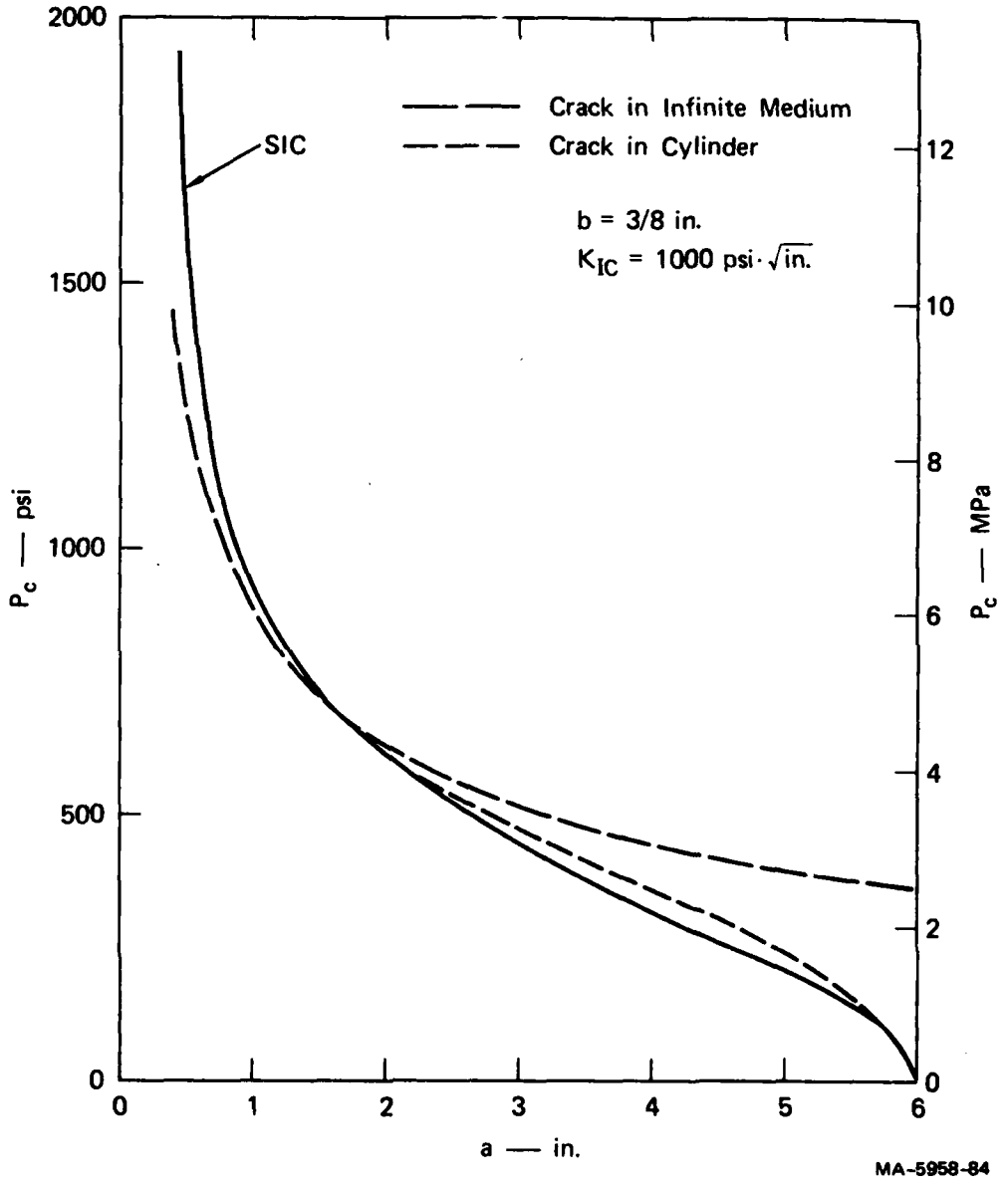

FIGURE 4.7 COMPARISONS OF PRESSURE-CRACK RADIUS CURVES

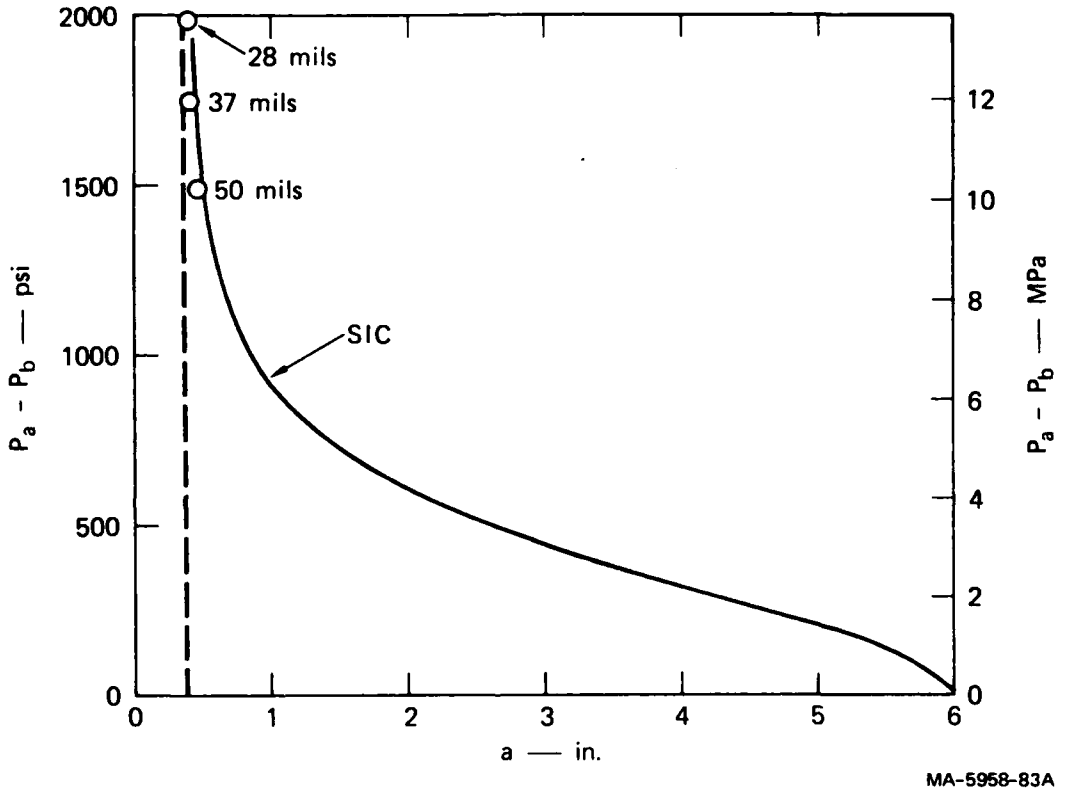

FIGURE 4.8 PRESSURE DIFFERENCE REQUIRED TO ADVANCE CRACK
K_{IC} = 1000 psi·$\sqrt{\text{in.}}$ b = 3/8 in.

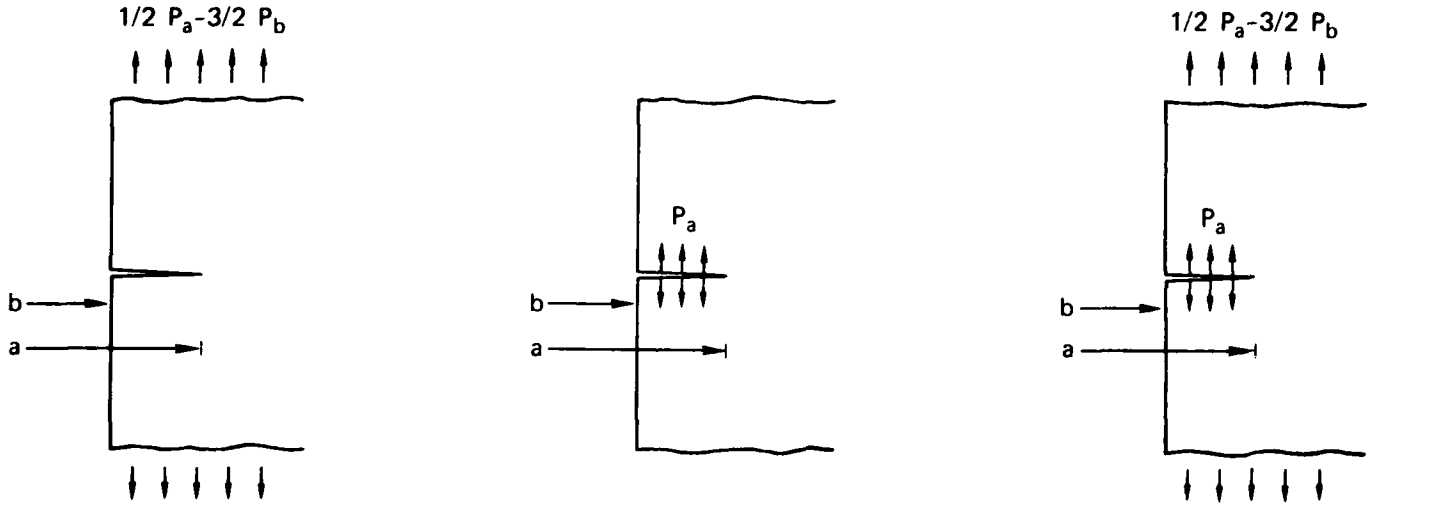

(a) $K_1 = 1.12\ (1/2\ P_a - 3/2\ P_b)[\pi(a-b)]^{1/2}$ (b) $K_1 = 1.12\ P_a[\pi(a-b)]^{1/2}$ (c) $K_1 = 1.12 \times 3/2\ (P_a - P_b)[\pi(a-b)]^{1/2}$

MA-5958-147

FIGURE 4.9 STRESS INTENSITY FACTORS FOR EDGE NOTCH

$$K_1 = 1.12 \left(\frac{1}{2} p_a - \frac{3}{2} p_b\right) [\pi(a - b)]^{\frac{1}{2}} \qquad (23)$$

For a constant fluid pressure p_a in an edge notch, as shown in Figure 4.9(b), the stress intensity factor is[10]

$$K_1 = 1.12\, p_a\, [\pi(a - b)]^{\frac{1}{2}} \qquad (24)$$

Superposition of the loading states, as shown in Figure 4.9(c), gives the stress intensity factor that is the sum of (23) and (24), namely,

$$K_I = 1.12 \left\{\frac{3}{2} (p_a - p_b)[\pi(a - b)]^{\frac{1}{2}}\right\} \qquad (25)$$

The critical pressure difference is therefore, from (25),

$$P_a - P_b = \frac{K_{Ic}}{1.68[\pi(a - b)]^{\frac{1}{2}}} \qquad (26)$$

For a material with a fracture toughness of K_{Ic} = 1000 psi $\sqrt{\text{inch}}$, formula (26) gives fracture initiation pressures of $P_a - P_b$ = 1500, 1750, and 2000 psi for initial notch flaws with depths 50, 37, and 28 mils, respectively. These data, shown in Figure 4.8, fall close to the SIC curve. For an overburden of p_b = 1000 psi, the corresponding critical pressures are 2500, 2750, and 3000 psi. These values are comparable to the fracture initiation pressures obtained in the unexploded cavity experiments. It is not known, however, how realistic the associated notch sizes are.

Figure 4.10 shows the SIC hydrofracture record when the overburden pressure is 1000 psi. Also shown is an experimental hydrofracture record (test 137). Cracking was first detected at the outside of the sphere after

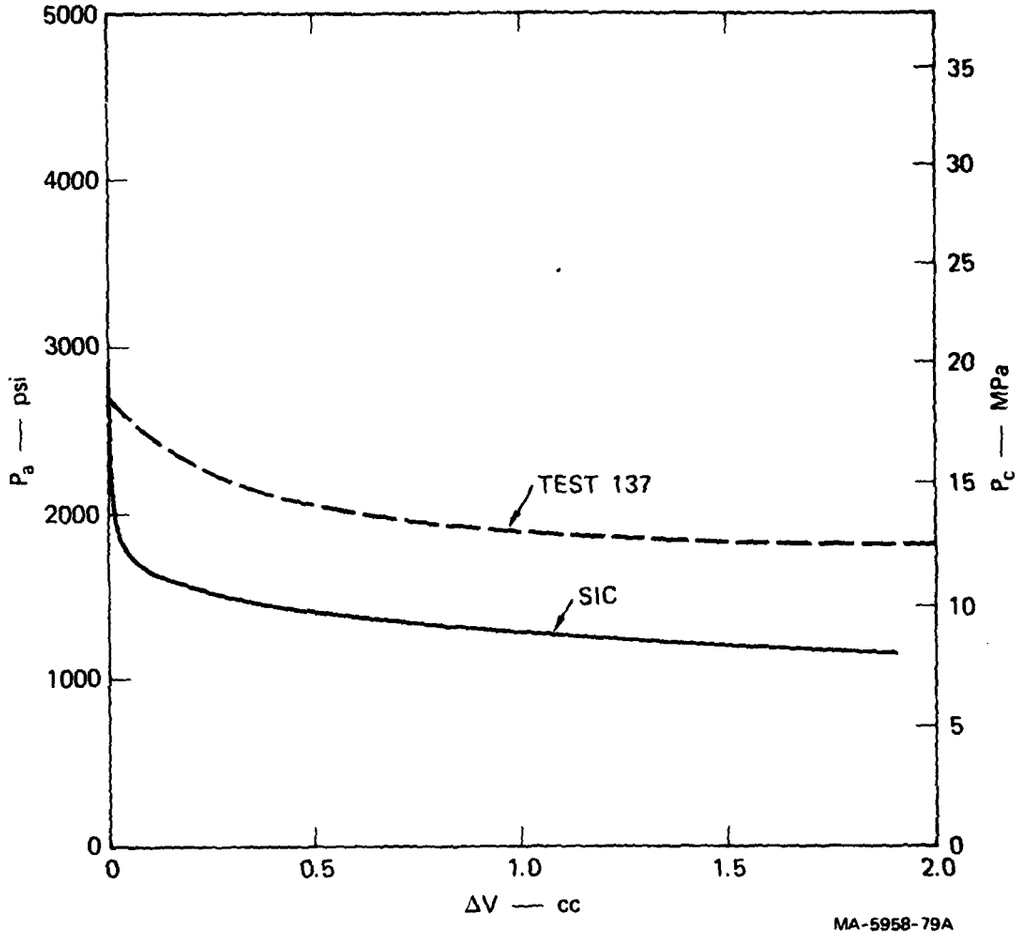

FIGURE 4.10 PREDICTED AND EXPERIMENTAL HYDROFRACTURE RECORDS FOR UNEXPLODED CAVITY

P_b = 1000 psi. K_{IC} = 1000 psi·$\sqrt{in.}$

3.8 cm^3 of fluid had been pumped in after fracture initiation at the spherical cavity. The experimental pressures are higher than the predicted pressures, which may be due to a combination of the glycerol viscosity and flow rate causing radial pressure gradients along the crack; the experimental pressure is approximately that measured in the spherical cavity. A better comparison will be made in the next phase of the program by using water and a slower flow rate.

4.4 SIC CODE RESULTS FOR A SPHERICAL MEDIUM: EXPLODED CAVITY

Before the exploded cavity experiments can be examined by means of the SIC code, a residual stress field has to be included in the analysis. At the time of the fracture mechanics study, the SIC code was entirely elastic; therefore, the residual stress field was included by applying artificial body forces. The overall form of the residual stress field is similar to that caused by the spherical cavity expansion.

The stresses and strains in spherical coordinates are σ_r, σ_θ and $\varepsilon_r, \varepsilon_\theta$, and the compatibility equation and Hooke's law are

$$r \frac{d\varepsilon_\theta}{dr} + \varepsilon_\theta - \varepsilon_r = 0 \tag{27}$$

$$E\varepsilon_r = \sigma_r - 2\nu\sigma_\theta \tag{28}$$

$$E\varepsilon_\theta = (1 - \nu)\sigma_\theta - \nu\sigma_r \tag{29}$$

The compatibility equation (27) in terms of stress can be put in the form

$$(1 - \nu)\, r \frac{d\sigma_\theta}{dr} + (1 + \nu)\sigma_\theta = \nu r \frac{d\sigma_r}{dr} + (1 + \nu)\sigma_r \tag{30}$$

If $\sigma_r(r)$ is given, the compatibility equation (30) requires that σ_θ satisfies

$$r \frac{d\sigma_\theta}{dr} + \frac{1 + \nu}{1 - \nu} \sigma_\theta = f(r) \tag{31}$$

A solution of (31) is

$$\sigma_\theta = \frac{1}{r^\alpha} \int f(r) r^{\alpha-1} \, dr \tag{32}$$

where $\alpha = (1 + \nu)/(1 - \nu)$.

The equilibrium equation is

$$\frac{d\sigma_r}{dr} + \frac{2}{r} (\sigma_\theta - \sigma_r) = -F \tag{33}$$

This equation now determines the body force F.

The example used in this study is

$$\sigma_r = \sigma(r - a)(r - b)(1 + \beta r) \tag{34}$$

where again a and b are the inner and outer radii of the spherical medium. In (34), σ and β are constants that determine the magnitude and skew of the function. Substitution of (34) in (32) gives the circumferential stress, and (34) gives the body force distribution. The field is shown in Figure 4.11 for one value of β. For SIC calculations, σ = 1000 psi was chosen so that the maximum compressive stresses are about 4000 psi, a value comparable to the static crush strength of the RMG. For an overburden of 1000 psi, the internal pressure as a function of crack radius is shown in Figure 4.12. The corresponding pressure-volume relationship is shown in Figure 4.13. The pressures are higher

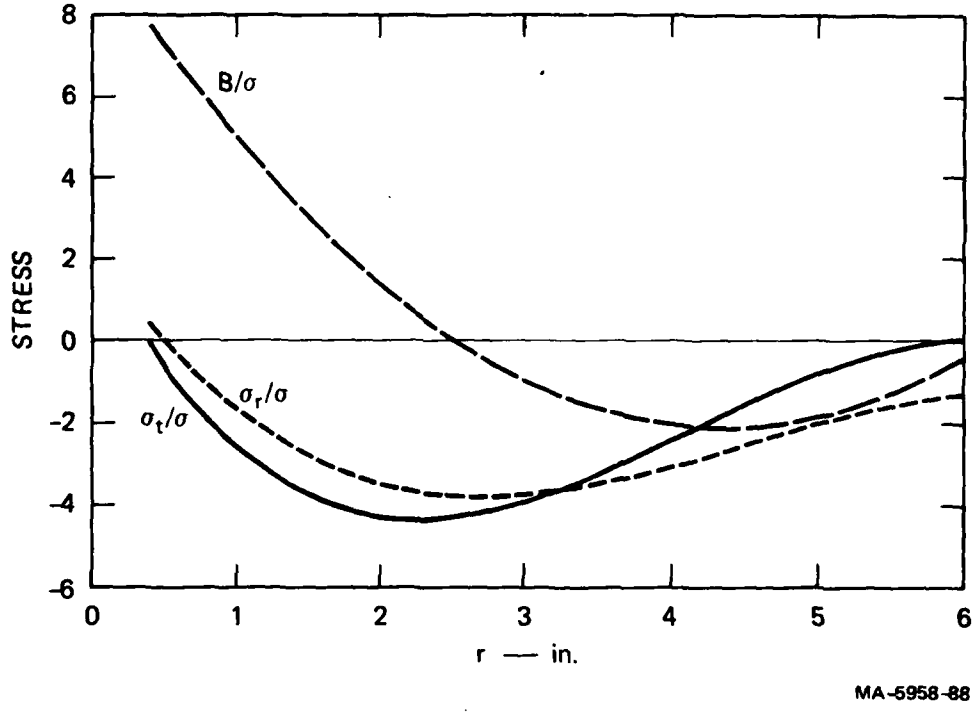

FIGURE 4.11 RESIDUAL STRESS FIELD GENERATED BY BODY FORCES

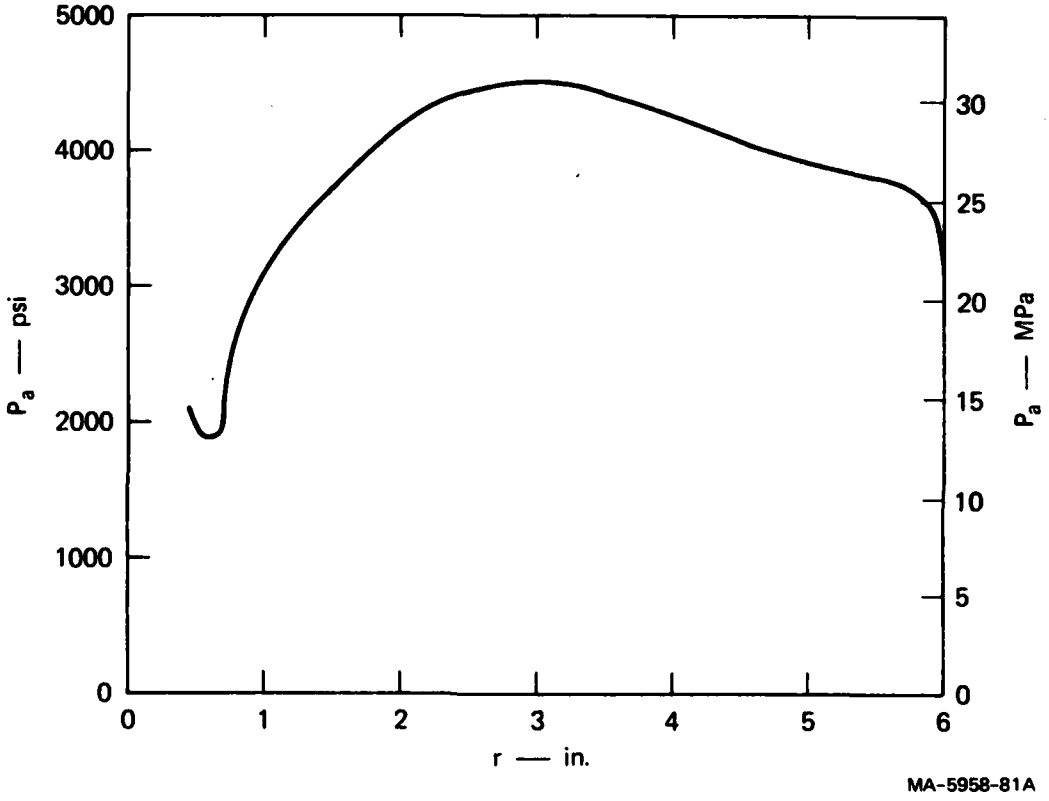

FIGURE 4.12 INTERNAL PRESSURE REQUIRED TO ADVANCE CRACK
P_b = 1000 psi. σ = 1000 psi. K_{IC} = 1000 psi·$\sqrt{in.}$

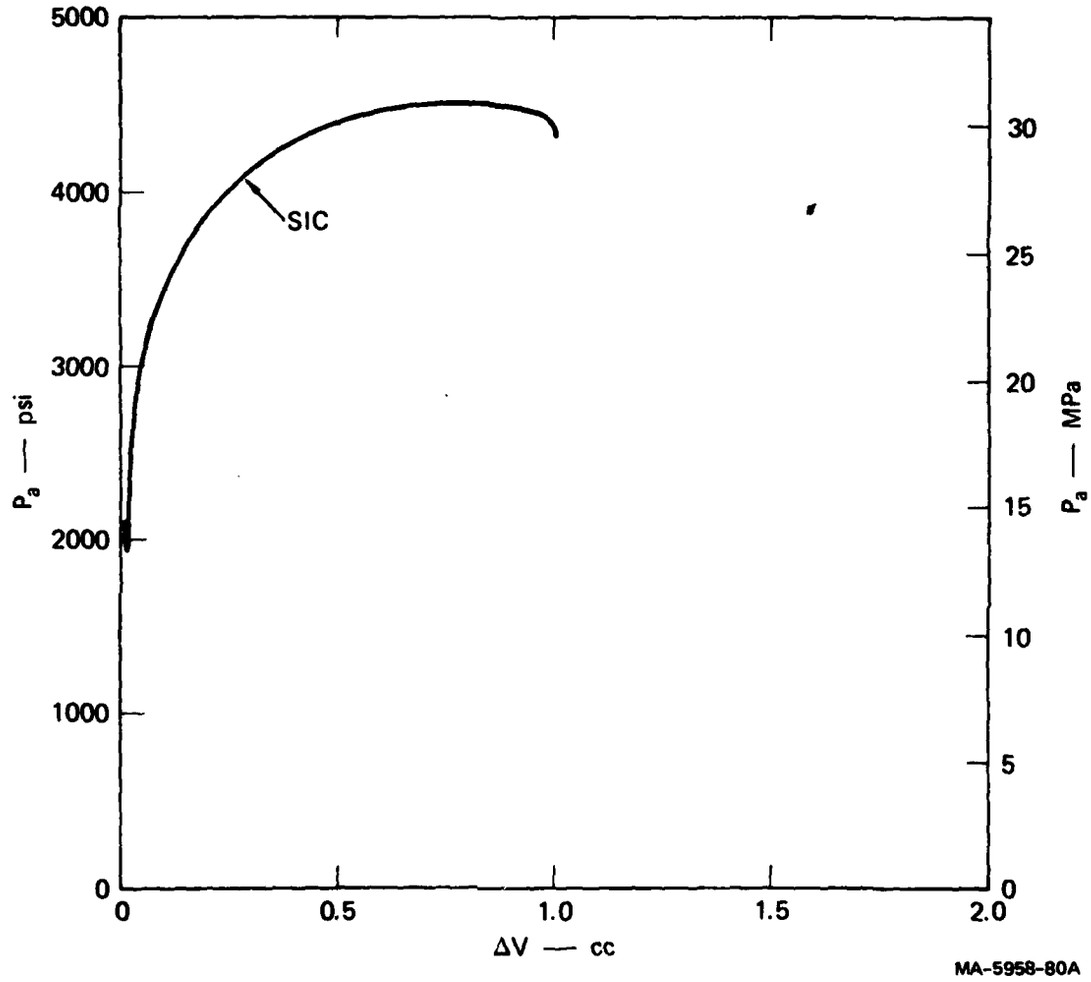

FIGURE 4.13 PREDICTED HYDROFRACTURE RECORD FOR EXPLODED CAVITY
P_b = 1000 psi. σ = 1000 psi. K_{IC} = 1000 psi·$\sqrt{in.}$

than the experimental pressures recorded during hydrofracture to the outside of the sphere although the fluid volumes are comparable. The observed initially stable crack growth is predicted.

Before the predicted hydrofracture record can confidently be compared with the experimental hydrofracture record, a more realistic model of the residual stress and strain field must be incorporatedin the SIC code. Since plasticity has now been incorporated in the code, this required improvement will be made during the next phase of the program.

REFERENCES

1. R. W. Gates and C. F. Petersen, "A Laboratory Method for Studying Stemming of Line-of-Sight Tunnels in Underground Nuclear Tests," SRI Final Report DNA 3058Z, Contract DNA001-72-C-0047 (November 1972).

2. R. W. Gates, C. F. Petersen, and A. L. Florence, "Laboratory Method for Studying Stemming of Line-of-Sight Tunnels in Underground Nuclear Tests," SRI Final Repoet DNA 3592F, Contract DNA001-73-C-0122 (December 1973).

3. A. L. Florence, "Laboratory Investigation of Stemming of Horizontal Line-of-Sight (HLOS) Underground Nuclear Tests," SRI Final Report DNA 3684F, Contract DNA001-74-C-0101 (February 1975).

4. A. L. Florence, "Laboratory Investigation of Stemming and Containment in Underground Nuclear Tests," SRI Final Report DNA 4149F, Contract DNA001-75-C-0083 (October 1976).

5. J. C. Cizek and A. L. Florence, "Laboratory Investigation of Containment in Underground Nuclear Tests," SRI Final Report (Draft), Contract DNA001-77-C-0025 (January 1978).

6. A. L. Florence and T. C. Kennedy, "A Simple Analysis for Containment Studies," SRI Topical Report 76-3702-2, Contract DNA001-75-C-0083 (August 1976).

7. L. Seaman, "SRI PUFF 3 Computer Code for Stress Wave Propagation," prepared for Air Force Weapons Laboratory, Air Force Systems Command, Kirtland AFB, New Mexico, Technical Report No. AFWL-TR-70-51, SRI International, Menlo Park, California (September 1970).

8. N. Rimer and K. Lie, "Spherically Symmetric Numerical Simulation of the SRI Grout Spheres Containment Experiments," Systems, Science and Software Topical Report SSS-R-79-3831, Contract DNA001-77-C-0099 (October 1978).

9. I. N. Sneddon, Fourier Transforms (McGraw Hill, New York, NY 1951).

10. H. Tada, P. Paris, and G. Irwin, The Stress Analysis of Cracks Handbook (Del Research Corporation, 226 Woodburne Drive, St. Louis, Missouri 63105).

Appendix

MATERIAL PROPERTIES

Table A.1 provides the mixture and heat curing cycle for the rock-matching grout 2C4. Table A.2 provides a summary of the commonly used physical and mechanical properties.

The scatter in crush strength and tensile strength associated with the testing of a large number of 2-inch-diameter (5.08-cm) cylinders is shown in Figures A.1 and A.2, respectively. These figures show that, in general, close tolerances are maintained on grout strength.

Additional strength properties of 2C4 are shown in Figures A.3 and A.4. For comparison, strength properties of the granite simulant, GS3, are included.

The stress-strain curve corresponding to the cyclic loading and unloading of a 4-inch-diameter (10.16-cm) cylinder of 2C4 in uniaxial compression is shown in Figure A.5. Axial strain measurements were made with an embedded strain gage. A surface extensometer was used to monitor the axial strain during the initial loading. The loading, creep, and unloading portions of a cycle each required the same amount of time to complete.

Table A.1

MIXTURE[a] FOR THE ROCK-MATCHING GROUT SRI RMG 2C4

Component	RMG 2C4
Type I-II Portland cement	32.691%
Sand (20-40 Monterey)	21.896%
Barite (barium sulfate)	20.848%
Bentonite (gel)	2.837%
CFR 2 (concrete friction reducing compound)	0.078%
Water	21.650%

[a]28-day aging procedure: Sealed in plastic and submerged in water with the following temperature sequence: raise to 54°C over 48-hour period, hold at 54°C for 48 hours, lower to 25°C over 36-hour period.

Table A.2

PROPERTIES OF THE ROCK-MATCHING GROUT SRI RMG 2C4

PHYSICAL PROPERTIES		MECHANICAL PROPERTIES	
Density (g/cm^3)			
Aged	2.15	Modulus in compression (psi)	2.64×10^6
Dry	1.75	Shear modulus (psi)	1.03×10^6
Grain	2.87	Poisson's ratio	0.28
Water by wet weight (%)	18.6	Compressive strength (psi)	3990
Porosity (%)	39	Tensile strength (psi)	530
Saturation (%)	100	Crush strain	1.50×10^{-3}
Air voids (%)	0		
Longitudinal velocity (km/sec)	3.29		
Shear velocity (km/sec)	1.82		

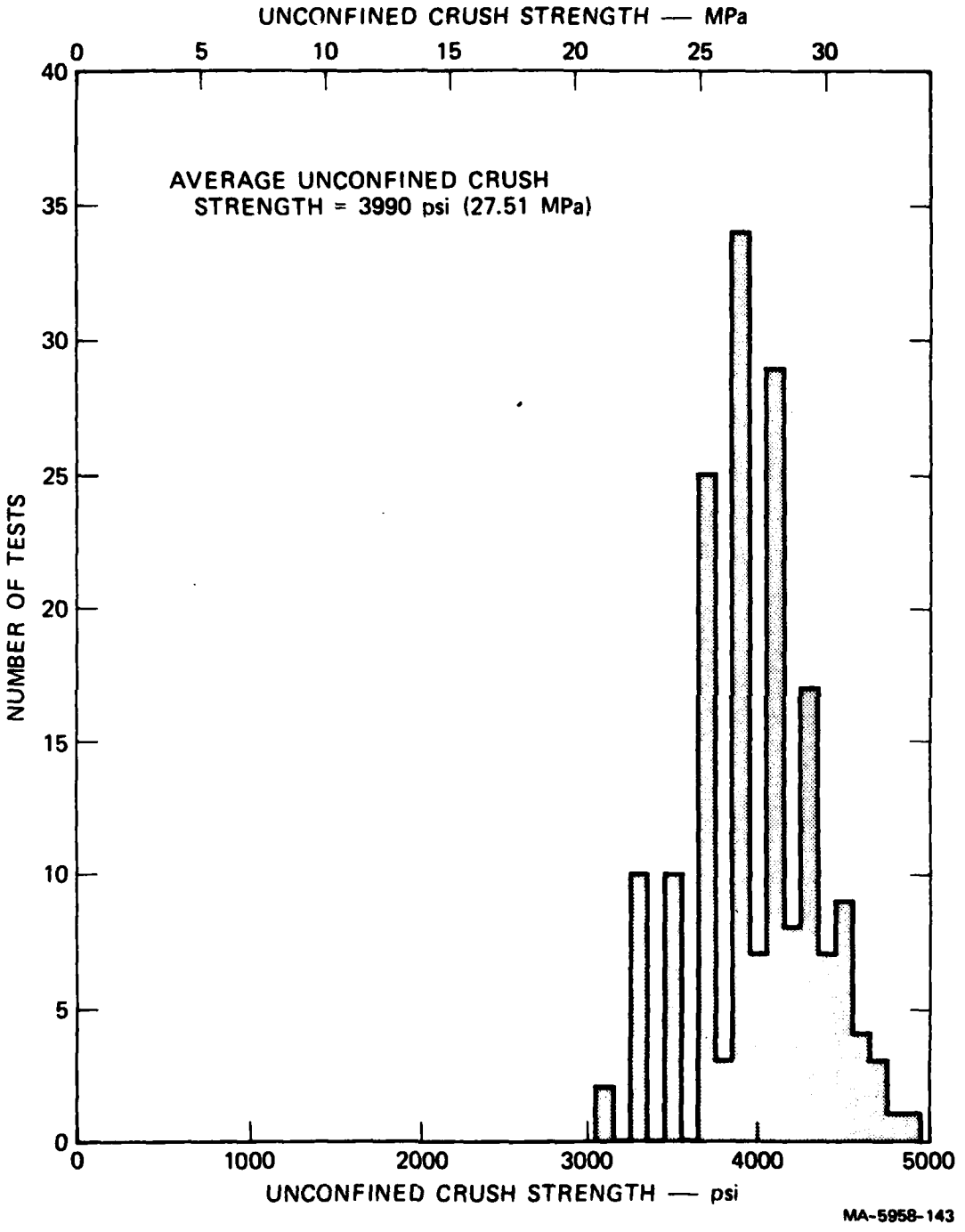

FIGURE A.1 UNCONFINED CRUSH STRENGTH OF THE ROCK-MATCHING GROUT SRI RMG 2C4

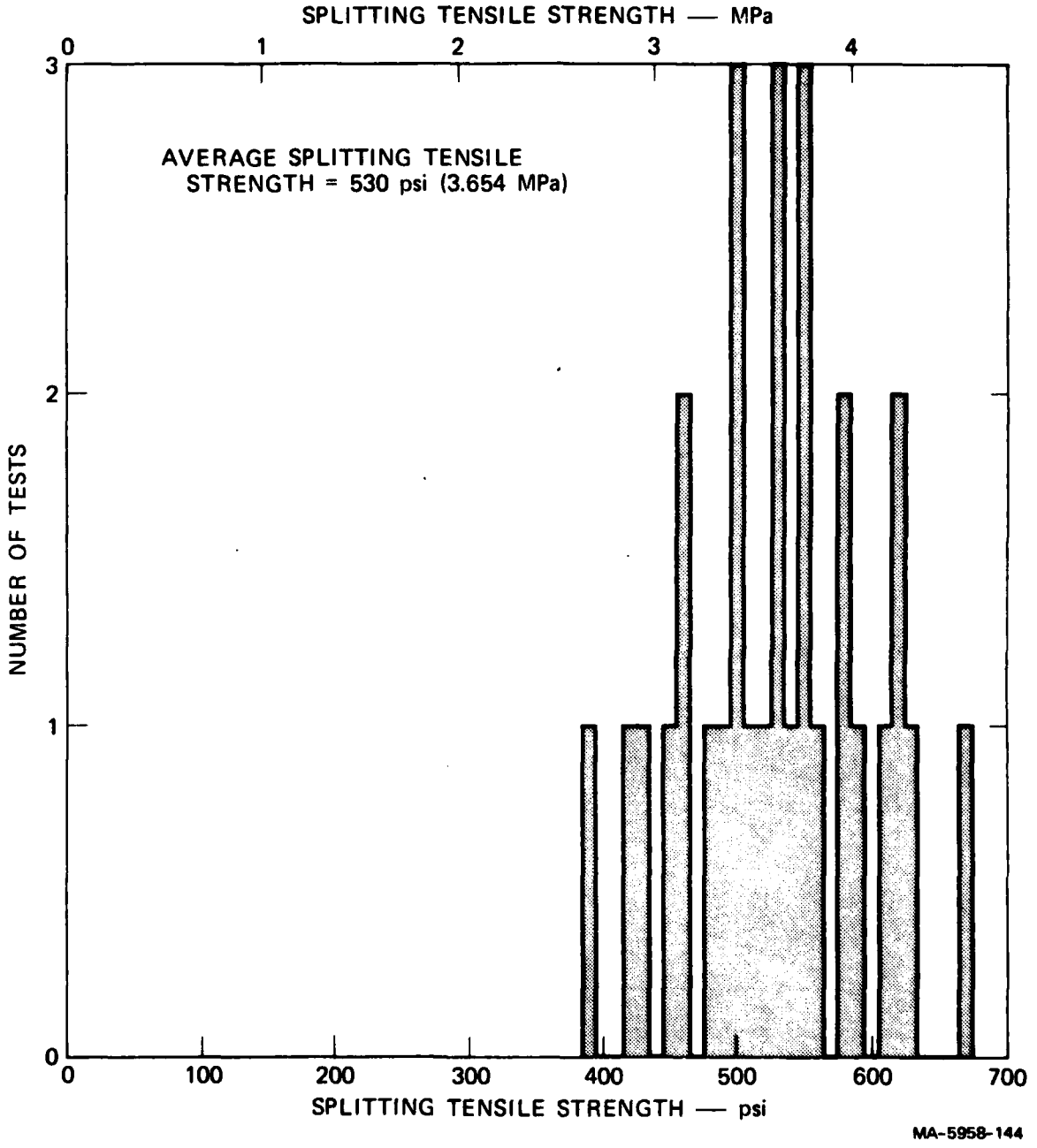

FIGURE A.2 SPLITTING TENSILE STRENGTH OF THE ROCK-MATCHING GROUT SRI RMG 2C4

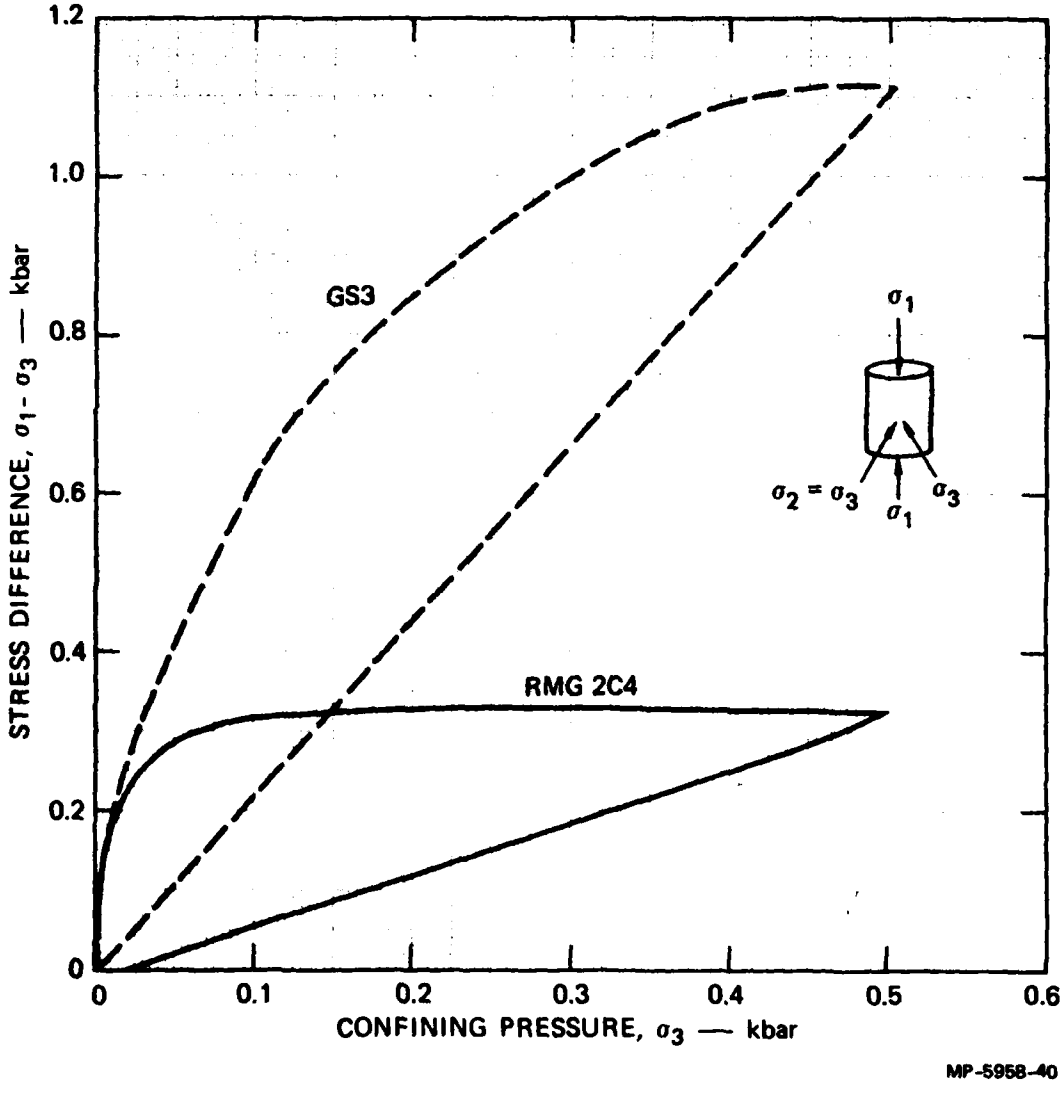

FIGURE A.3 STRENGTH PROPERTIES OF THE ROCK-MATCHING GROUT SRI RMG 2C4 AND THE MODIFIED GRANITE SIMULANT GS3: STRESS DIFFERENCE VERSUS CONFINING PRESSURE

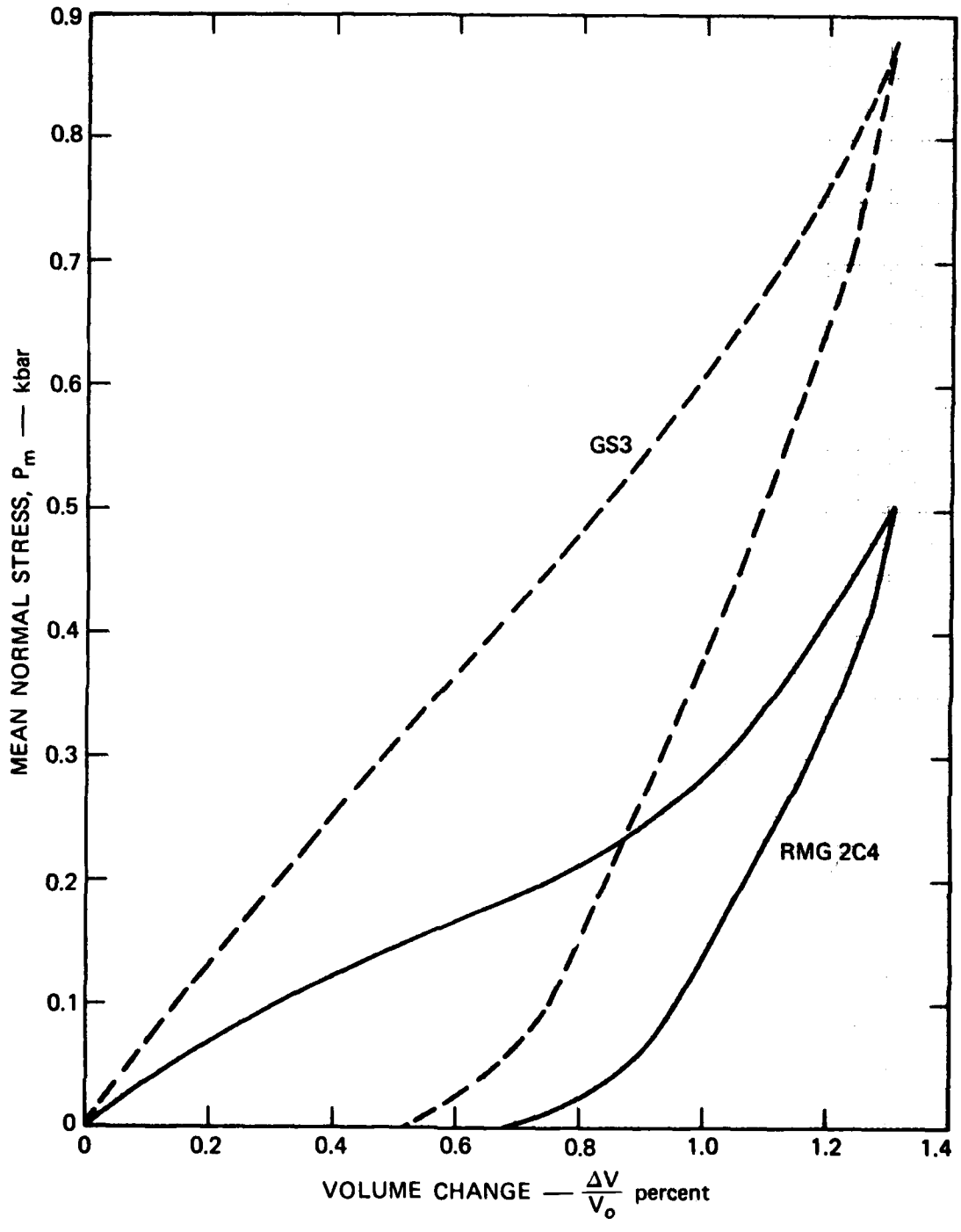

FIGURE A.4 STRENGTH PROPERTIES OF THE ROCK-MATCHING GROUT SRI RMG 2C4 AND THE MODIFIED GRANITE SIMULANT GS3: MEAN NORMAL STRESS VERSUS VOLUME CHANGE

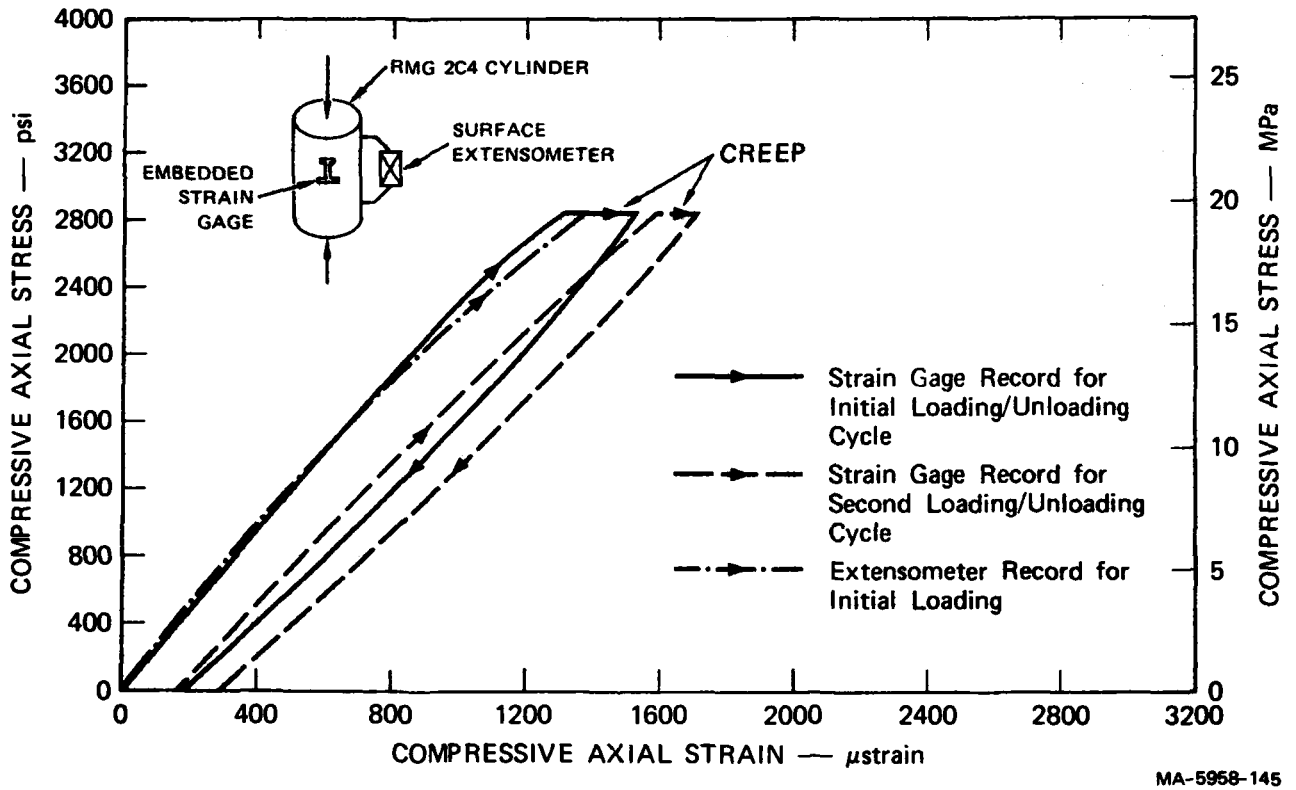

FIGURE A.5 STRESS-STRAIN CURVE FOR THE UNIAXIAL LOADING AND UNLOADING OF THE ROCK-MATCHING GROUT SRI RMG 2C4

DISTRIBUTION LIST

DEPARTMENT OF DEFENSE

Assistant to the Secretary of Defense
Atomic Energy
ATTN: Executive Assistant

Defense Nuclear Agency
ATTN: DDST
ATTN: SPTD, T. Kennedy
4 cy ATTN: TITL

Defense Technical Information Center
12 cy ATTN: DD

Field Command
Defense Nuclear Agency
ATTN: FCPR
ATTN: FCTK, C. Keller
ATTN: FCTMD, W. Summa

Field Command
Defense Nuclear Agency
Livermore Division
ATTN: FCPRL

Field Command Test Directorate
Test Construction Division
Defense Nuclear Agency
ATTN: FCTC, J. LaComb

Undersecretary of Def. for Rsch. & Engrg.
ATTN: Strategic & Space Systems (OS)

DEPARTMENT OF THE ARMY

Harry Diamond Laboratories
Department of the Army
ATTN: DELHD-N-P

DEPARTMENT OF THE NAVY

Naval Surface Weapons Center
ATTN: Code F-31

DEPARTMENT OF THE AIR FORCE

Air Force Weapons Laboratory
ATTN: SUL

OTHER GOVERNMENT AGENCY

Department of Interior
U.S. Geological Survey
Special Project Center
ATTN: R. Carroll

DEPARTMENT OF ENERGY

Department of Energy
Nevada Operations Office
ATTN: R. Newman

DEPARTMENT OF ENERGY CONTRACTORS

Lawrence Livermore Laboratory
ATTN: Document Control for D. Oakley
ATTN: Document Control for B. Hudson
ATTN: Document Control for B. Terhune
ATTN: Document Control for J. Shearer

Los Alamos Scientific Laboratory
ATTN: Document Control for R. Brownlee
ATTN: Document Control for E. Jones
ATTN: Document Control for F. App
ATTN: Document Control for A. Davis

Sandia Laboratories
ATTN: C. Mehl
ATTN: C. Smith

DEPARTMENT OF DEFENSE CONTRACTORS

General Electric Company-TEMPO
ATTN: DASIAC

Pacifica Technology
ATTN: G. Kent

Physics International
ATTN: E. Moore

R & D Associates
ATTN: C. MacDonald

SRI International
ATTN: A. Florence

Systems, Science & Software, Inc.
ATTN: R. Duff

Terra Tek, Inc.
ATTN: S. Green